Alma Mater Studiorum - Università di Bologna

DOTTORATO DI RICERCA IN

SCIENZE BIOMEDICHE E NEUROMOTORIE

Ciclo 34

Settore Concorsuale: 06/D6 - NEUROLOGIA

Settore Scientifico Disciplinare: MED/26 - NEUROLOGIA

WHOLE EXOME SEQUENCING WIDENS THE GENETIC LANDSCAPE OF HEREDITARY OPTIC NEUROPATHIES

Presentata da: Claudio Fiorini

Coordinatore Dottorato

Matilde Yung Follo

Supervisore

Valerio Carelli

Esame finale anno 2022

Summary

Abstract 5
Introduction 7
1. Clinical manifestation of ON 7
2. Mitochondrial HON genetics 9
2.1. Leber's Hereditary Optic Neuropathy 9
2.2. Autosomal Dominant Optic Atrophy 10
2.3 ON related to mitochondrial network dynamics and morphology 12
2.4 ON related to MAMs function 14
2.5 ON related to mitochondrial bioenergetics 16
2.6 ON related to other mitochondrial functions 19
3. ON from different pathogenic mechanisms 24
4. Next-Generation Sequencing 26
4.1. Technical principles of NGS 27
4.2. NGS bioinformatic pipeline fundamentals 29
4.3. Potential and pitfalls of WES 30
5. Rare diseases genetics and molecular diagnostics 31
5.1. Sequencing strategy for pathogenic variants discovery 31
5.2. Genetic variants filtering and classification criteria 34
5.3. Case phenotyping and phenotype-driven gene variant prioritization 35
Aim of thesis 37
Materials and Methods 39
1. Cohort description 39
2. Sample collection 40
3. Targeted sequencing 40
4. Bioinformatic analysis of NGS data 41
5. Manual WES data analysis and classification 43
6. Automated prioritization tools 43
6.1. The Exomiser 44
6.2. MutationDistiller 44
7. Sanger sequencing 44

8. Targeted *OPA1* and *UCHL1* cDNA sequencing 45
9. Cell cultures 45
10. Protein levels analysis 46
10.1. Protein extraction and quantification 46
10.2. SDS-PAGE and Western Blotting 46
10.3. BN-PAGE of respiratory complexes 47
11. Statistical analysis 47
Results 49
1. WES metrics and diagnostic rate 49
1.1 Coverage metrics 49
1.2 Diagnostic rate 50
1.3. Identified genes inheritance 51
1.4. Gene function in positive results cases 52
2. WES results in Optic Neuropathies 53
2.1. Autosomal Dominant solved ON cases 54
2.2. Autosomal and X-linked Recessive solved ON cases 58
2.2. VUS and GUS cases in ON cohort 62
3. WES results in syndromic Optic Neuropathies 64
3.1. Autosomal Dominant solved sON cases 64
3.2. Autosomal and X-linked Recessive solved sON cases 65
3.2. VUS and GUS cases in sON cohort 71
4. *In vitro* validation for *SDHA* variants in ON_10 and sON_15 77
4.1. *SDHA* variants yeast modelling 77
4.2. Protein levels and activity on skeletal muscle 78
4.3. Protein levels on fibroblast cell lines 79
5. *In vitro* validation for *UCHL1* variant in ON_23 81
4.1. *UCHL1* transcript analysis 81
4.1. Protein levels and activity on fibroblast lines 82
Discussion 85
1. WES general results 85
1.1. WES metrics comparison 85
1.2. Diagnostic yield in study cohorts 85

1.3. Inheritance in WES with positive results 87
1.4. Mitochondrial cases in study cohort 88
2. Solved ON and sON cases 88
2.1. Mitochondrial ON with AD inheritance 88
2.2. Mitochondrial ON with AR/XLR inheritance 90
2.3. Non-mitochondrial ON cases 91
2.4. Mitochondrial sON with AD inheritance 92
2.5. Mitochondrial sON with AR/XLR inheritance 92
2.6. Non-mitochondrial sON cases 94
3. VUS ON and sON cases 95
3.1. Mitochondrial VUS cases 95
3.2. Non-mitochondrial VUS cases 96
4. GUS ON and sON cases 98
4.1. Non-mitochondrial GUS cases 98
5. Validation studies of *SDHA* variants 100
5.1. Yeast modelling studies 100
5.2. Studies on skeletal muscle and fibroblasts 101
6. Validation studies of *UCHL1* variant 102
6.1. Studies on fibroblasts protein levels 102
Conclusions 103
References 107
Appendix 118

Abstract

Hereditary optic neuropathies (HON) are genetic cause of visual impairment characterized by degeneration of retinal ganglion cells. The most common HON forms are caused by pathogenic variants in mtDNA genes or in genes coding for mitochondrial proteins, like *OPA1*. However, several genes can cause optic atrophy, also acting on non-mitochondrial pathways, and can only be identified by high throughput genetic analysis. Whole Exome Sequencing (WES) is becoming the primary choice in rare disease molecular diagnosis, being both cost effective and informative. To date, a few studies applied WES to heterogenous cohorts with mitochondrial disorders, but no work specifically addressed optic neuropathy patients.

We performed WES on a cohort of 106 cases, of which 74 isolated ON patients (ON) and 32 syndromic ON patients (sON). The cumulative solved cases rate amounts to 27%, slightly higher for syndromic ON (31%) than for isolated ON (26%). Considering variants of unknown significance identified in a disease-gene or in a gene of unknown significance with candidate role in optic atrophy, a positive result was then obtained for 63% of sON and 32% of ON cases.

The majority of genes found are related to mitochondrial function and already reported for harbouring HON pathogenic variants: *ACO2*, *AFG3L2*, *C19orf12*, *DNAJC30*, *FDXR*, *MECR*, *MTFMT*, *NDUFAF2*, *NDUFB11*, *NDUFV2*, *OPA1*, *PDSS1*, *SDHA*, *SSBP1*, and *WFS1*. Among these *OPA1*, *ACO2*, and *WFS1* were confirmed as the most relevant genetic causes of ON and in particular of DOA. Moreover, several non-mitochondrial genes were also identified, especially in sON patients, with direct impairment of different molecular pathways: from autophagy and ubiquitin system *(LYST*, *SNF8*, *WDR45*, *UCHL1*), to neural cells development and function (*KIF1A*, *GFAP*, *EPHB2*, *CACNA1A*, *CACNA1F*), but also vitamin metabolism (*SLC52A2*, *BTD*), cilia structure (*USH2A*), and nuclear pore shuttling (*NUTF2*).

Functional validation on yeast model was performed for pathogenic variants detected in *MECR*, *MTFMT*, *SDHA*, and *UCHL1* genes. For *SDHA* and *UCHL1* also muscle biopsy and fibroblast cell lines from patients were analysed, detecting a reduction in these proteins' levels and pointing to possible pathogenic mechanisms that will be investigated in further studies.

In conclusion, WES proved to be an efficient tool when applied to our ON cohort, for both common disease-genes identification and novel genes discovery. It is therefore recommended to consider WES in ON molecular diagnostic pipeline, as for other rare genetic diseases.

Introduction

Optic Neuropathies (ON) comprise a group of human disorders, which lead to visual impairment of variable severity by affecting the optic nerve. The main clinical feature of ON is a selective degeneration of retinal ganglion cells (RGCs), the innermost layer of the retina, whose axons form the optic nerve. Optic atrophy is linked to several pathogenic mechanisms, from a toxic/nutritional origin to a compressive or traumatic origin, as well as to an inflammatory/autoimmune one. In its most common form, however, ON is inherited and appears as both isolated and syndromic disorder (ON plus). Mitochondrial involvement in the disease is also common, considering that the main genetic causes of ON are mutations in the mitochondrial genome (mtDNA) and in the *OPA1* gene. Moreover, several other genes have now been identified as rarer cause of ON and are often related to mitochondrial function (1).
The heterogenous genetic background of ON requires flexible methods for molecular diagnosis, thus Whole Exome Sequencing (WES) is becoming the primary choice in this context, being both cost effective and informative.

1. Clinical manifestation of ON

A typical case of hereditary optic neuropathy (HON) presents a bilateral visual loss related to optic nerve degeneration, with demyelination and loss of RGC axons. Fundus examination usually shows a pallid optic disc and central scotoma is evident at visual field perimetry. Optical coherence tomography (OCT) allows the evaluation of thickness of the retinal nerve fiber layer (RNFL) at a fixed distance from the edge of the optic nerve head and is nowadays the golden standard for optic atrophy diagnosis. Here a reduction of RNFL thickness is observed, often more marked in the temporal quadrant, the side of the optic nerve head receiving the small axons originated from the macula, defining the so-called papillo-macular bundle (**Fig. 1**). The severity of the disease in terms of visual acuity is extremely variable, from patients seeing 20/20 to others having only light perception (2). Great variability in optic atrophy onset, childhood to late, and disease course, subacute or progressive, is expected as different pathogenic genes are involved giving specific phenotypes (3).

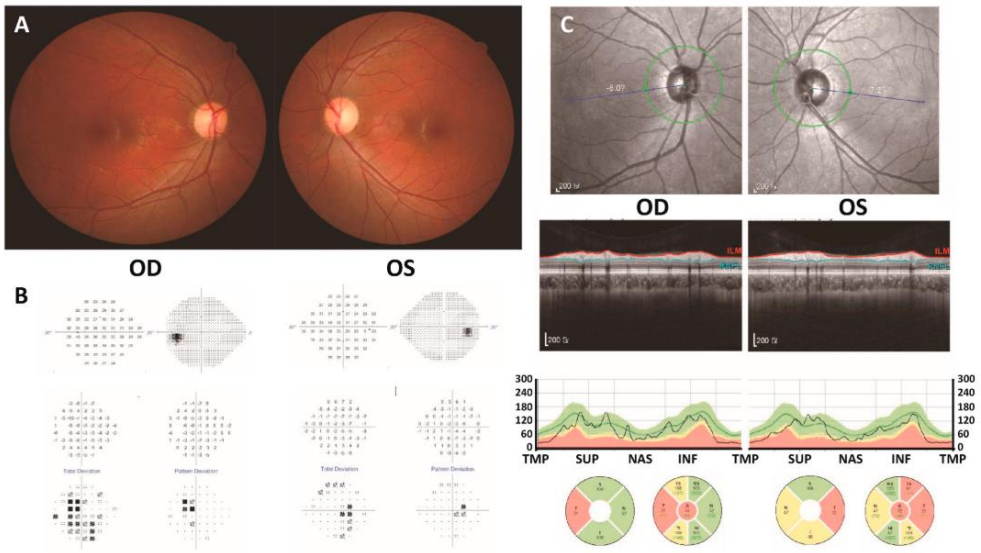

Figure 1. *Typical ophthalmological phenotype of DOA male patient caused by OPA1 variant. (A) Fundus photography shows pallor of optic discs, due to diffuse atrophy of optic nerve. (B) Visual field with bilateral central scotoma present as limited darker area in the field. (C) OCT imaging shows RNFL thinning especially in temporal quadrant (TMP), where below-average values in nerve fibers thickness is indicated by red colour. Image from (2).*

RGCs degeneration is the marking feature of ON, traditionally associated with mitochondrial impairment observed in many ON cases. In fact, RGCs axons are unmyelinated along their intraocular length, and here they rely completely on mitochondria for the high energy demand of electric potential generation. Once out of the lamina cribrosa, the optic nerve axons become myelinated and are then less dependent on mitochondrial function, needed for the more energy-efficient "saltatory" conduction of the action potentials (**Fig. 2**) (4). The abundance in mitochondria in constant activity, as well as the skewed distribution in the cell, makes RGCs one of the first tissues targeted by mitochondrial impairment.

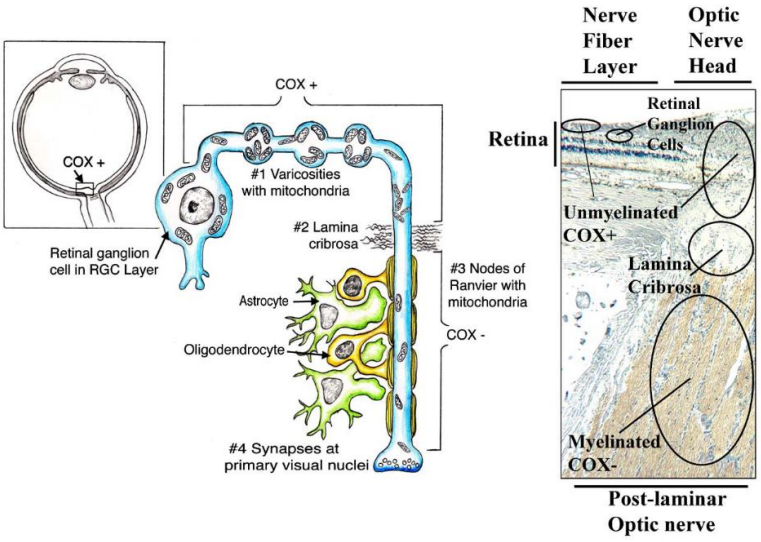

Figure 2. *RGCs schematic representation with mitochondria mainly located in the first section of the axon (left) and histology of human retina and optic nerve (right), stained for COX activity indicative of mitochondrial abundance. Image from (4).*

2. Mitochondrial HON genetics

The main genetic causes for ON point to mitochondrial dysfunction as a key process in its pathophysiology. Leber's Hereditary Optic Neuropathy (LHON) and Dominant Optic Atrophy (DOA) account for most of the diagnosed ON cases, underlying a close connection between mitochondria and optic atrophy.

- **2.1. Leber's Hereditary Optic Neuropathy**

LHON (MIM#535000) represents a distinctive form of ON, and the first disorder to be associated with a point mutation in mtDNA in 1988 (5). LHON is typically a non-syndromic ON with subacute onset in a single eye, then followed by the second one within days/months (**Fig. 3**). Moreover, it shows incomplete penetrance in both genders, but with different percentage of affected mutation carriers, translating into a striking male prevalence (4).

This is the most common disease caused by mtDNA mutation, with a reported minimum prevalence reaching 3.22 per 100 000 in North-East of England, that reflects an estimated prevalence of the main LHON mutations of 11.82 per 100 000 (6).

The genetic cause of LHON is usually a homoplasmic mtDNA mutation affecting NADH:ubiquinone oxidoreductase (complex I) subunits, essential components of this electron transport chain complex. Three common mutations m.3460G>A/*MT-ND1*, m.11778G>A/*MT-ND4*, and m.14484T>C/*MT-ND6* account for 90% of cases, the remaining 10% being attributed to several rare mtDNA point mutations or even combinations of rare polymorphisms (7,8). The three common mutations differ in severity and penetrance, going from biochemically stronger m.3460G>A/*MT-ND1* to milder m.14484T>C/*MT-ND6*. There are rarer reported cases showing additional symptoms to optic neuropathy (often referred as "LHON plus") and a variable percentage of patients experience spontaneous recovery.

The pathogenic mechanism of LHON is still not fully elucidated; it probably originates from an interplay between different mitochondrial processes, altered by complex I dysfunction. According to literature, LHON affected carriers show ATP production and bioenergetics slight defect, higher levels of reactive oxygen species (ROS) and increased apoptosis rate of RGCs (1). Various studies also demonstrated environmental triggers of the disease, like tobacco smoke or alcohol consumption, that however act together with genetic background from mtDNA and nuclear DNA (nDNA). No recurrent nDNA variants have been identified to explain incomplete

penetrance nor male prevalence, but mitochondrial biogenesis activation is seen as a protective factor for unaffected carriers (9).

In recent years, a LHON-like phenotype with autosomal recessive inheritance has also been documented in pedigrees with variants in nuclear genes mainly linked to complex I activity. The most relevant of such genes appears to be *DNAJC30*, encoding a newly characterized mitochondrial chaperone that promotes complex I turnover. Several pedigrees with a few pathogenic variants in *DNAJC30* were described, all presenting with a mostly mild, recessive LHON (LHONAR, MIM#619382), except for one case with Leigh syndrome (10). Then, a single case of isolated recessive LHON was reported bearing compound heterozygous variants in *NDUFS2* gene; while biallelic variants in this core subunit of complex I usually associates with syndromic CI deficiency (MC1DN6, MIM#618228 (11,12). Finally, a LHON-like phenotype has been proposed for one pedigree with pathogenic variants in *MCAT*, gene also known for another single pedigree with double homozygous variants leading to ROA phenotype. *MCAT* encodes the mitochondrial malonyl-CoA-acyl carrier protein transacylase. This is a key enzyme in fatty acid synthesis, that transfers malonyl-CoA to the mitochondrial acyl carrier protein NDUFAB1 (also an accessory subunit of complex I), (13–15).

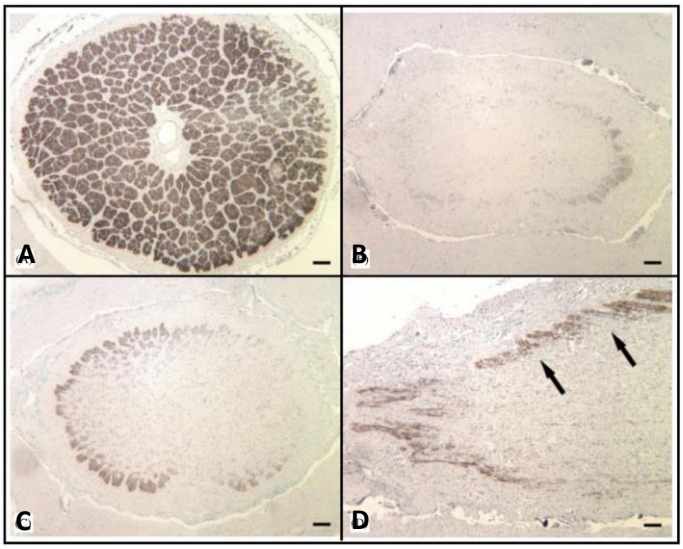

Figure 3. *Human optic nerves histopathology, with staining for myelin basic protein: (A) healthy control cross-section, (B) LHON/3460 cross-section, (C) LHON/11778 cross-section and (D) longitudinal section. Bar 100 µm. Image from (4).*

- **2.2. Autosomal Dominant Optic Atrophy**

DOA (MIM#165500), also described as Kjer's type Optic Atrophy, is another common cause of visual impairment, characterized by autosomal dominant transmission and usually non-

syndromic form. Typically, from a clinical aspect it is a slowly progressive optic nerve degeneration with childhood-onset, leading to a bilateral loss of central vision (16).

DOA estimated prevalence in the North-East of England is 4.07 per 100 000, but the figure was even higher in Danish population from earlier studies, possibly due to a founder effect (17,18).

The first gene discovered as causative for DOA is *OPA1* (19,20), and soon it was recognized as the predominant gene, accounting for as much as 60-70% of DOA cases (21,22). *OPA1* gene is composed of 30 exons, of which exon 4, 4b, and 5b are alternatively spliced giving rise to eight mRNA transcript and peptide isoforms, differentially expressed in the body. OPA1 protein is a dynamin-related GTPase targeted to inner mitochondrial membrane (IMM), that regulates IMM fusion during mitochondrial network conformational changes. The enzyme in its "long" form is attached to IMM but can be further cleaved by proteases YME1L and OMA1, generating the "short" forms that localize in the intermembrane space (IMS). The levels of different isoforms, as well as long and short forms, are finely balanced in order to maintain the right mitochondrial network and *cristae* architecture (**Fig. 4**) (23).

Through its action on inter- and intramitochondrial remodelling, OPA1 act as a key regulator for several other functions, like respiratory chain integrity, mtDNA maintenance, apoptosis via cytochrome *c* release and calcium homeostasis (2). Thus, OPA1 impairment primarily cause mitochondrial network fragmentation and abnormal *cristae* morphology, that secondarily affect all these processes leading to RGCs degeneration. Finally, in DOA patients and *in vitro* models an alteration of the metabolomic and lipidomic profiles has been observed, highlighting the complex pathophysiology of the disease (1).

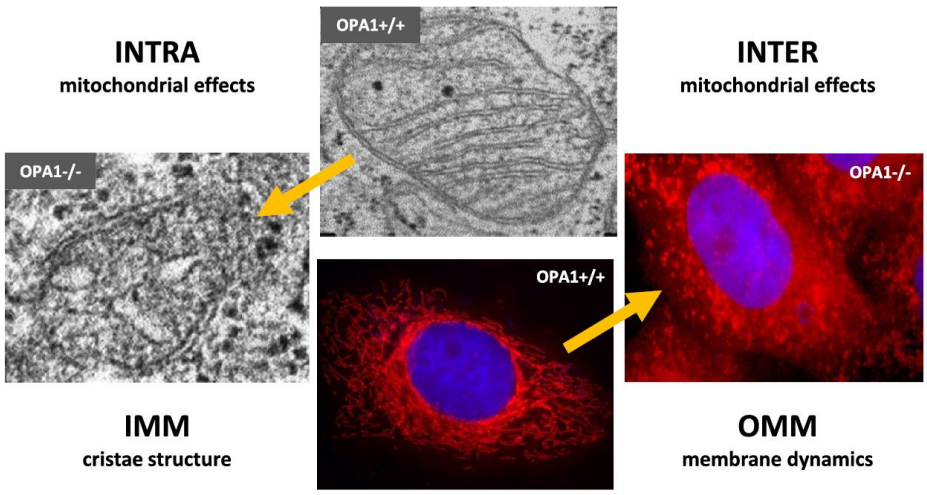

Figure 4. *Mitochondrial network fragmentation and cristae disorganization characteristic of OPA1 mutants. Image from (2).*

OPA1 currently lists more than 400 reported pathogenic mutations (Leiden Open Variant Database at https://www.lovd.nl/OPA1) (24). Those mutations include missense as well as loss-of-function variants, which often lead to a null allele. They are distributed along the entire coding region and even UTRs, with the majority of missense variants located in the GTPase domain (exon 8-16) (25).

While haploinsufficiency is thus the default genetic mechanism for OPA1 pathogenic mutations, a dominant negative mechanism has been proposed for some mutations in the GTPase domain often linked to "DOA plus" phenotype (26,27). The more complex DOA plus phenotypes are restricted to about 20% of pedigrees, and can include sensorineural hearing loss, myopathy with chronic progressive external ophthalmoplegia (CPEO), peripheral neuropathy, ataxia, Parkinsonism and dementia (1). As with most mitochondrial disorders, also DOA exhibit variable penetrance and clinical severity inside each family and between different families, even harbouring the same mutations (9). Besides, rare *OPA1* biallelic variants are associated with a syndromic phenotype known as Behr Syndrome (MIM#210000), featuring childhood-onset optic atrophy and progressive neurological symptoms like spinocerebellar ataxia, spasticity, peripheral neuropathy, intellectual disability and neurodevelopmental delay (2,28). However, the phenotypic spectrum of biallelic OPA1 patients is wide, and even more severe forms have been described where optic atrophy is not a relevant symptom, instead resembling Leigh syndrome with infantile lethal encephalopathy and cardiomyopathy (29,30).

- **2.3 ON related to mitochondrial network dynamics and morphology**

Optic neuropathies pathogenesis has been attributed to with several more nuclear genes other than *OPA1*, especially components of the mitochondrial dynamics machinery, that cause both syndromic phenotypes with ON and isolated DOA-like phenotypes (**Fig. 5**) (31).

In this category we find some enzymes directly or indirectly involved in OPA1 processing, like YME1L and the complex AFG3L2/SPG7 (Figure 5). The gene *YME1L* is only reported with homozygous mutations in a consanguineous family presenting a mitochondrial encephalopathy with optic atrophy (OPA11, MIM#617302) (32). The subunits AFG3L2 and SPG7/paraplegin assemble into the m-AAA protease on the IMM, and act in protein homeostasis and quality control, also having OMA1 and YME1L as cleavage targets. *AFG3L2* and *SPG7* mono- and biallelic variants have been associated with syndromic disorders often involving OA, like spinocerebellar ataxia type 28 (SCA28, MIM#610246) and spastic ataxia type 5 (SPAX5,

MIM#614487), and hereditary spastic paraplegia type-7 (HSP7, MIM#607259), respectively (33). More recent reports, however, identify AFG3L2 and SPG7 as relevant cause of DOA and DOA plus phenotypes as a result of OPA1 dysregulation (34–37).

While OPA1 operates in IMM fusion, for the outer mitochondrial membrane (OMM) combined action of mitofusins, MFN1 and 2, is required. *MFN2* mutations cause Charcot-Marie-Tooth neuropathy type 2A in both dominant (CMT2A2A, MIM#609260) and recessive form (CMT2A2B, MIM#617087) (38,39), accounting for up to 20% of all CMT2 and thus being the most important axonal CMT gene. Phenotype severity is variable, but many cases are severe and progressive, and optic atrophy is a common feature in about 10–20% labelled as hereditary motor and sensory neuropathy VI (HMSN6/CMT6, MIM#601152) (40,41). The exact pathogenic mechanism is complex and still debated, but there is evidence, besides mitochondrial fusion impairment, for a dysregulation of mitochondria-associated endoplasmic reticulum membranes (MAMs), where MFN2 also localizes (42).

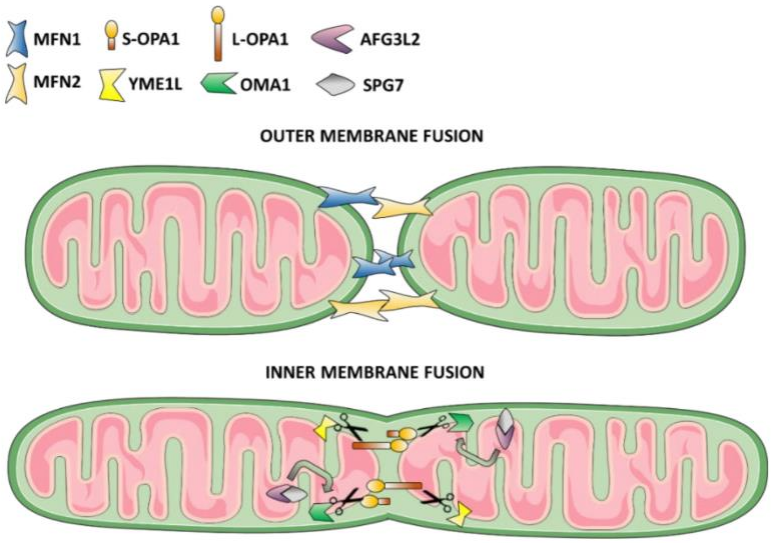

Figure 5. *Main proteins acting in mitochondrial fusion and involved in ON pathogenesis. Image from (1).*

Mitochondrial network fission proteins are involved in ON as well (**Fig. 6**). For this process, the endoplasmic reticulum (ER) firstly makes contact with mitochondria in pre-constriction sites, where then the fission dynamin-related GTPase DRP1 assembles on the OMM thanks to the adaptors MFF, MID49, MID51 and FIS1 (43,44). Mutation of gene *DNM1L*, encoding for DRP1, has initially been associated with a lethal infantile phenotype including optic nerve atrophy and hypoplasia, microcephaly, abnormal brain development, and lactic acidemia (45). The disease was then described as dominant lethal encephalopathy due to defective mitochondrial and

peroxisomal fission (EMPF1, MIM#614388), grouping different complex phenotypes of encephalopathy and refractory epilepsy (46). Interestingly, heterozygous mutations in *DNM1L* can also lead to DOA-like isolated ON (OPA5, MIM#610708) as a result of hyper-filamentous mitochondrial network, the opposite effect than in OPA1 patients (47).

Similarly to *DNM1L*, syndromic phenotype of encephalopathy with optic atrophy is also reported for biallelic mutation in the adaptor *MFF* (EMPF2, MIM#617086) (48). The gene *MIEF1*, encoding another adaptor for DRP1, MID51, has recently been identified as cause of a peculiar dominant form of ON, characterized by adult subacute onset and slowly progressive peripheral loss of visual field (49).

Besides, optic atrophy is rarely found in different forms of Charcot-Marie-Tooth disease linked to gene *GDAP1* (CMT4A, MIM#214400 and CMT2K, MIM#607831) (50), with both dominant and recessive inheritance, and similar pathogenic features to MFN2 patients (51). GDAP1 is mostly expressed in neurons, it regulates mitochondrial functions and especially the fission process, but its function is not fully elucidated and requires further study (52).

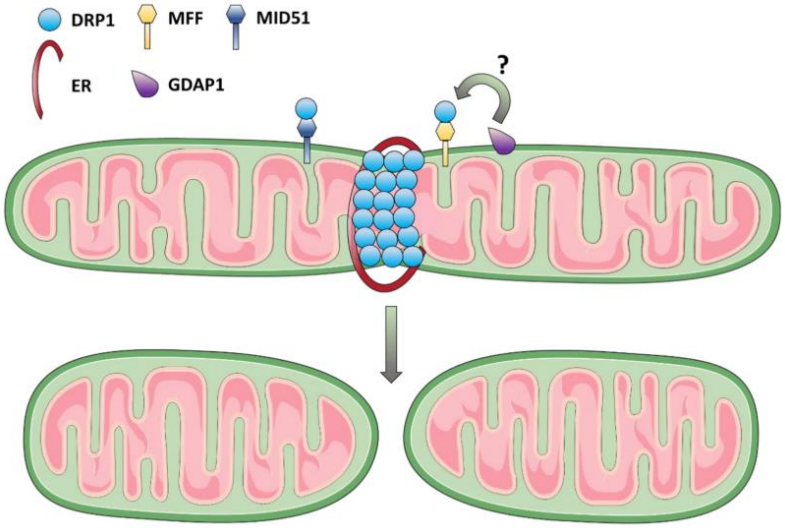

Figure 6. *Main proteins acting in mitochondrial fission and involved in ON pathogenesis. Image from (1).*

- **2.4 ON related to MAMs function**

The MAMs, where ER and mitochondria membranes are tightly bound, are important compartments with key roles in several pathways, such as mitochondrial morphology, Ca^{2+} homeostasis, lipid synthesis and trafficking, and autophagy (**Fig. 7**) (53).

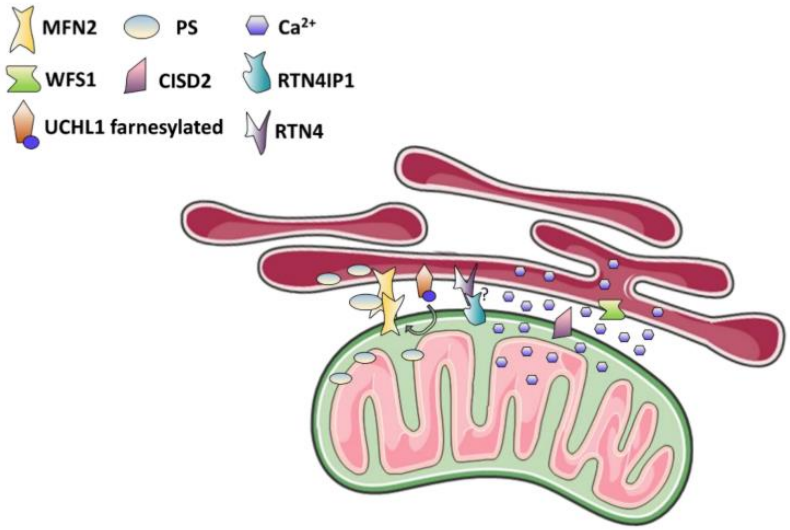

Figure 7. *Main proteins acting in MAMs function and involved in ON pathogenesis. Image from (1).*

Concerning mitochondrial dynamics, as already mentioned, MFN2 has a pivotal role, being anchored to both MAMs and OMM and physically tethering them (54). A recent study proposed this function as a possible pathogenic mechanism behind human disease caused by a non-mitochondrial gene, *UCHL1* (55). UCH-L1 is a very abundant deubiquitinating enzyme (DUB) specific of neurons, with cytoplasmic and ER-membrane localization, that targets MFN2 and thus regulates mitochondrial shape and ER contact sites (55). After first reports linking heterozygous variants to Parkinson's Disease (56,57), recent large cohort studies pointed to exclusion of the gene from risk factors for PD (58). Biallelic mutations in *UCHL1* were then associated with a complex phenotype resembling Behr syndrome: spastic paraplegia (SPG79, MIM#615491) with childhood-onset optic atrophy and peripheral neurodegeneration (59).

Another protein involved in mitochondria-ER tethering with still poorly understood activity is RTN4IP1, that interacts with RTN4/NOGO present on ER membrane and enriched in MAMs. Mutations in *RN4IP1* cause recessive ON, either isolated or syndromic with ataxia, mental retardation, and seizures (OPA10, MIM#616732), and even severe encephalopathy (60). Patients' fibroblasts show mitochondrial network fragmentation and respiratory complex I disassembly. Moreover, recent reports have highlighted cone-rod dystrophy as a typical symptom in addition to optic atrophy in *RN4IP1* patients (61,62) .

Finally, there is now evidence for a disorder traditionally treated as mitochondrial, the Wolfram syndrome, to primarily originate from MAMs alteration. The classic recessive form type 1 (WFS1, MIM# 222300) is linked to mutations in *WFS1*, and shows diabetes insipidus, diabetes

mellitus, optic atrophy, and deafness (63). Sometimes the full spectrum of symptoms is not present, but there are often more neurological symptoms, from cerebellar ataxia to psychiatric disorders, cataract or retinopathy (64). Besides, many of these phenotypes can occur isolated or in different combinations in a dominant fashion as Wolfram-like syndrome (WFSL, MIM# 614296) (65,66). Non-syndromic ON is therefore associated with both recessive and dominant mutations in *WFS1* (67). This gene encodes the ER-membrane glycoprotein Wolframin, involved in Ca^{2+} homeostasis and unfolded protein response (UPR). A protein sharing similar function and MAMs localization is CISD2, which however does not interact directly with Wolframin and is also bound to OMM. The recessive disease given by *CISD2* mutations is therefore similar, reported as Wolfram syndrome type 2 (WFS2, OMIM #604928), showing optic atrophy, sensorineural hearing loss and diabetes mellitus, but not insipidus (68).

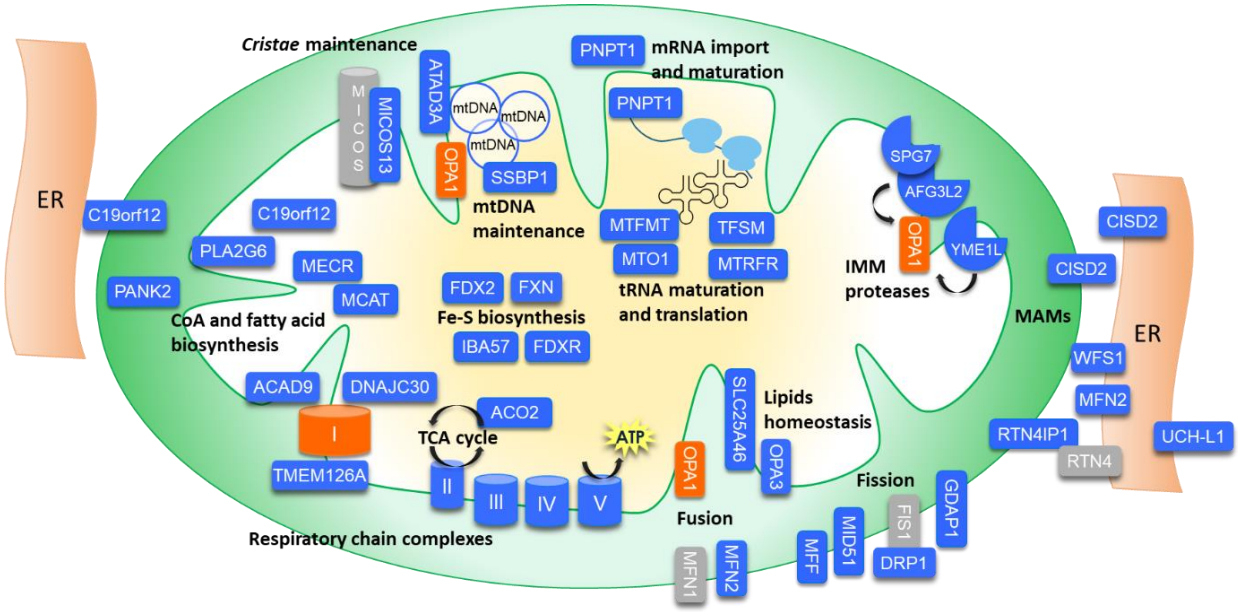

Figure 8. *Mitochondria and MAMs proteins with reported variants causing both isolated and syndromic ON (blue). The most prevalent ON-associated enzymes, OPA1 and OXPHOS complex I, are shown in orange, while key mitochondrial components still not related to human disease are shown in grey.*

- **2.5 ON related to mitochondrial bioenergetics**

Mitochondrial bioenergetics impairment is not only a secondary effect of mitochondrial dynamics alterations, but also a primary cause of ON, different from the classic LHON-like presentation. These proteins are summarized in **Fig. 8** with all other cited mitochondrial proteins related to ON phenotypes.

A gene with growing relevance in this context is *ACO2*, encoding the aconitase enzyme of the tricarboxylic acid (TCA) cycle that converts citrate into isocitrate. Biallelic variants were firstly associated with infantile cerebellar-retinal degeneration (ICRD, MIM#614559), a severe recessive syndrome with progressive cerebral and cerebellar degeneration, optic atrophy and retinal degeneration (29). Then, recessive forms where identified with variable severity, from syndromic optic atrophy with neuromuscular involvement or spastic paraplegia, to isolated ON (OPA9, MIM#616289) (69,70). The wide spectrum of *ACO2* disease further expanded after recent reports of several DOA pedigrees harbouring heterozygous mutations, making it one of the most common genetic causes for DOA, after *OPA1* (71,72).

Another enzyme part of the TCA cycle, as well as of the electron transport chain, is succinate dehydrogenase (complex II), composed of four subunits SDHA-D. Only the genes *SDHA*, *SDHB*, and *SDHD* are found to harbour recessive variants leading to severe complex II deficiency (MC2DN1, 4, 3, MIM#252011, 619224, 619167), similar in phenotype to Leigh syndrome and/or leukoencephalopathy, often including optic atrophy (73). For *SDHA* there are also reports of missense heterozygous mutations in DOA plus pedigrees with ataxia, intellectual disability, or cardiomyopathy (NDAXOA, MIM#619259) (74).

The core subunits and assembly factors of respiratory complex I are a recurrent target of biallelic variants that cause in severe Leigh syndrome/complex I deficiencies (MC1DN), often including OA as a minor symptom (75). The complex I genes reported in literature for MC1DN are summarized in **Table 1** (76,77). Only some of them show optic atrophy, but this aspect could be underrated in childhood syndromic cases, and further research in the future might identify milder forms with ON also for such genes.

TMEM126A is one of the complex I related genes with ON as a main phenotype, with its protein product being a recently characterized assembly factor for ND4 subunit (78,79). Mutations in *TMEM126A* cause recessive optic atrophy (OPA7, MIM#612989), isolated or with sensorineural hearing loss, mostly found in families of Maghrebian ancestry due to a founder event (80–82). Similarly, the protein ACAD9, that participates in fatty acid beta-oxidation and complex I assembly, is responsible for a recessive complex I deficiency (MC1DN20, MIM#611126). Mutations in *ACAD9* usually result in cardiomyopathy, sometimes with myopathy, leukoencephalopathy, lactic acidosis, or developmental delay and rarely optic atrophy (83,84), but a recent report describes a case with only ON plus peripheral neuropathy (85).

Table 1. *Genes with published variants causing OXPHOS complex I deficiency (MC1DN), indicating the type of CI subunit (core/ accessory/not part of CI) and if optic atrophy is reported in known cases (ON +/-).*

Gene	Phenotype	MIM#	CI subunit type	ON
NDUFS4	MC1DN1	252010	Core	+
NDUFS8	MC1DN2	618222	Core	-
NDUFS7	MC1DN3	618224	Core	-
NDUFV1	MC1DN4	618225	Core	+
NDUFS1	MC1DN5	618226	Core	+
NDUFS2	MC1DN6	618228	Core	+ (LHON)
NDUFV2	MC1DN7	618229	Core	+
NDUFS3	MC1DN8	618230	Accessory	+
NDUFS6	MC1DN9	618232	Accessory	-
NDUFAF2	MC1DN10	618233	Accessory	+
NDUFAF1	MC1DN11	618234	Accessory	-
NDUFA1	MC1DN12	301020	Accessory	- (+ mouse)
NDUFA2	MC1DN13	618235	Accessory	+
NDUFA11	MC1DN14	618236	Accessory	+
NDUFAF4	MC1DN15	618237	Accessory	+
NDUFAF5	MC1DN16	618238	Accessory	+
NDUFAF6	MC1DN17	618239	Accessory	-
NDUFAF3	MC1DN18	618240	Accessory	+
FOXRED1	MC1DN19	618241	Non CI, assembly	+
ACAD9	MC1DN20	611126	Non CI, assembly	+ (ON plus)
NUBPL	MC1DN21	618242	Non CI, assembly	+
NDUFA10	MC1DN22	618243	Accessory	-
NDUFA12	MC1DN23	618244	Accessory	+
NDUFB9	MC1DN24	618245	Accessory	-
NDUFB3	MC1DN25	618246	Accessory	-
NDUFA9	MC1DN26	618247	Accessory	-
NDUFA13	MC1DN28	618249	Accessory	+
TMEM126B	MC1DN29	618250	Non CI, assembly	-
NDUFB11	MC1DN30	301021	Accessory	+
TIMMDC1	MC1DN31	618251	Non CI, assembly	-
NDUFB8	MC1DN32	618252	Accessory	-
NDUFA6	MC1DN33	618253	Accessory	+
NDUFAF8	MC1DN34	618776	Accessory	+
NDUFB10	MC1DN35	619003	Accessory	-
NDUFC2	MC1DN36	619170	Accessory	+
NDUFA8	MC1DN37	619272	Accessory	-
DNAJC30	MC1DN38	619382	Non CI, turnover	+ (LHON)

- **2.6 ON related to other mitochondrial functions**

More key mitochondrial processes are relevant for human disease, and they recurrently show ON mostly in syndromic context.

Multiple enzymes involved in Fe-S cluster biosynthesis are mitochondrial, and almost all are linked to clinical phenotypes. The most relevant is undoubtedly frataxin, since a triplet repeat expansion in gene *FXN* cause the most common form of recessive spinocerebellar ataxia, Friedreich's ataxia (FRDA1, MIM#229300), which also includes optic atrophy (86). Besides, biallelic mutations in *FDXR* gene, encoding the adrenodoxin/ferredoxin reductase, lead to syndromic disease with ON as a primary feature, often paired with hearing impairment, retinopathy and movement disorders (ANOA, MIM#617717) (87,88). All genes involved in this pathway, and with optic atrophy reported, are listed in **Table 2**. A common manifestation is multiple mitochondrial dysfunctions syndrome (MMDS), a severe disorder resulting in weakness, respiratory failure, neurologic development delay, and lactic acidosis (89).

Table 2. *Genes involved in Fe-S cluster biosynthesis, with published complex phenotypes that also include optic atrophy as a symptom.*

Gene	Disease	Phenotype	MIM#
FXN	FRDA1	Friedreich ataxia	229300
FDX2	MEOAL	Mitochondrial myopathy, episodic, with optic atrophy and reversible leukoencephalopathy	251900
FDXR	ANOA	Auditory neuropathy and optic atrophy	617717
IBA57	MMDS3	Multiple mitochondrial dysfunctions syndrome 3	615330
BOLA3	MMDS2	Multiple mitochondrial dysfunctions syndrome 2 with hyperglycinemia	614299
GLRX5	SPAHGC	Spasticity, childhood-onset, with hyperglycinemia	616859
ISCA2	MMDS4	Multiple mitochondrial dysfunctions syndrome 4	616370
PMPCB	MMDS6	Multiple mitochondrial dysfunctions syndrome 6	617954

Mitochondria also host key enzymes for fatty acids biosynthesis, like the mitochondrial trans-2-enoyl-CoA reductase, MECR. Biallelic mutations in *MECR* gene are associated with childhood-onset dystonia, with basal ganglia abnormalities and, usually, optic atrophy (DYTOABG, MIM#617282) (90–92).

The OMM carrier SLC25A46 participates in membrane lipids homeostasis and regulation of *cristae* and network morphology (93). Biallelic mutations in *SLC25A46* cause a spectrum of phenotypes going from ON plus, usually combining optic atrophy with an axonal CMT disease (HMSN6B/CMT6B, MIM#616505), to most severe cases of infantile Leigh syndrome and

pontocerebellar hypoplasia (PCH1E, MIM#619303) (94). Recent studies (95) associate also the IMM protein OPA3 to lipid homeostasis, through which it regulates mitochondrial dynamics. The first mutations in *OPA3* were identified as responsible for recessive Costeff syndrome, or 3-methylglutaconic aciduria type III (MGCA3, MIM#258501), characterized by optic atrophy and extrapyramidal signs, spasticity and ataxia, essentially a Behr syndrome (96). Then, *OPA3* was recognized as cause of DOA, or DOA plus with often cataract, sensorineural hearing loss, and peripheral neuropathy (OPA3, MIM#165300) (2,97). Mitochondrial morphology is further regulated through *cristae* organization, maintained by the mitochondrial contact site and *cristae* organizing system (MICOS) complex. One of the subunits of MICOS complex, encoded by gene *MICOS13*, is linked to an infantile recessive multisystem disorder presenting as mitochondrial hepato-encephalopathy with mtDNA depletion (COXPD37, MIM#618329), also involving optic nerve degeneration (98). Finally, integrity of *cristae* and OMM-IMM contact sites are maintained through the mitochondrial AAA-ATPase ATAD3A, an IMM protein with multiple functions that also binds mtDNA nucleoids (99,100). Both heterozygous with dominant negative effect, and biallelic recessive alleles (often resulting from complex locus rearrangements) have been described for *ATAD3A* gene, leading to a severe syndrome with global developmental delay, hypotonia, optic atrophy, axonal neuropathy, and hypertrophic cardiomyopathy (HAYOS, MIM#617183) (101).

Moreover, all mitochondrial functions are dependent on efficient mRNA processing and translation in the organelle, performed by several fundamental enzymes that are often causative for diseases like syndromic ON forms. The import and subsequent maturation of RNAs into mitochondria is regulated by PNPT1, a polynucleotide nucleotidyltransferase located in the IMS. Biallelic mutations in *PNPT1* have been associated with variable oxidative phosphorylation deficiencies (COXPD13, MIM# 614932), that translate in a wide clinical spectrum where developmental delay, sensorineural hearing loss, optic atrophy, and movement disorders are common features (102,103). Part of this pathway is the mitochondrial elongation factor Ts, encoded by gene *TSFM,* which causes mitochondrial encephalomyopathy with hypertrophic cardiomyopathy, and in some cases peripheral neuropathy and optic atrophy (COXPD3, MIM#610505) (104). Another related protein, MTRFR (previous gene symbol *C12orf65*), is active during translation in rescuing stalled ribosomes. Mutations in *MTRFR* gene have been identified in both case of Leigh syndrome with optic atrophy and ophthalmoplegia

(COXPD7, MIM#613559) (105) and recessive spastic paraplegia with optic atrophy and neuropathy (SPG55, MIM#615035) (106).

The maturation of aminoacyl-tRNAs is also crucial for the translation process, and a key component of this pathway is the mitochondrial tRNA translation optimization protein (MTO1). Recessive syndromic manifestations linked to *MTO1* mutation usually show a combination of symptoms including hypertrophic cardiomyopathy, developmental delay, and in about half of cases optic atrophy (107,108). Then, biallelic mutations in *MTFMT* alter the function of this mitochondrial methionyl-tRNA formyltransferase, that modifies the first methionine needed for the start of translation. The clinical phenotype observed is usually a Leigh syndrome with variable manifestation, where the majority of cases shows ocular features including optic atrophy (COXPD15, MIM#15614947) (109,110).

Though usually associated with neuromuscular disorders, especially chronic progressive external ophthalmoplegia (CPEO), dysfunction of proteins involved in mtDNA maintenance is rarely associated with ON (111). The most striking exception is a recently described DOA plus form, presenting retinopathy and in some pedigrees also deafness, myopathy, and renal disease (OPA13, MIM#165510). The disease is caused by mostly heterozygous mutations (only one AR pedigree reported) in *SSBP1*, encoding the mitochondrial single-stranded DNA-binding protein that is essential for mtDNA replication, justifying the mtDNA copy number depletion detected in patients' tissues (112–114).

Finally, a mitochondrial involvement has been proposed the Bosch-Boonstra-Schaaf optic atrophy syndrome (BBSOAS, MIM#615722), presenting optic atrophy, intellectual disability, and developmental delay with dominant inheritance and variable severity. The causative gene *NR2F1* encodes a transcription factor (COUP-TF1) with many identified targets, including genes for mitochondrial enzymes, but the pathogenic mechanism is still unclear (115,116).

All cited ON-genes with respective phenotypes and mitochondrial function are summarized in **Table 3**, including genetic loci lacking identification of causative gene.

Table 3. *Genes with published variants causing isolated and syndromic ON, with protein product involved in mitochondrial function.*

Gene	OMIM	Function	OMIM Phenotype	MIM#	Inher.
OPA1 3q29 (OPA1)	*605290	IMM fusion	Optic atrophy 1 (DOA) Optic atrophy plus syndrome (DOA plus) Behr syndrome	165500 125250 210000	AD AD AR
YME1L 10p12 (OPA11)	*607472	OPA1 processing	Optic atrophy 11 (ROA)	617302	AR
AFG3L2 18p11 (OPA12)	*604581	OMA1 regulation	Optic atrophy 12 (DOA) Spastic ataxia 5, autosomal recessive Spinocerebellar ataxia 28	618977 614487 610246	AD AR AD
SPG7 16q24.3	*602783	OMA1 regulation	Spastic paraplegia 7, autosomal recessive (DOA)	607259	AD, AR
MFN2 1p36.22	*608507	OMM fusion; MAMs formation; PS transfer	Charcot-Marie-Tooth disease, axonal, type 2A2A Charcot-Marie-Tooth disease, axonal, type 2A2B Hereditary motor and sensory neuropathy VIA	609260 617087 601152	AD AR AD
DNM1L 12p11 (OPA5)	*603850	OMM fission	Optic atrophy 5 (DOA) Encephalopathy, lethal, due to defective mitochondrial peroxisomal fission	610708 614388	AD AD, AR
MFF 2q36.3	*614785	DRP1 adaptor	Encephalopathy due to defective mitochondrial and peroxisomal fission 2	617086	AR
MIEF1 22q13.1	*615497	DRP1 adaptor	Late-onset progressive optic neuropathy (DOA)	-	AD
GDAP1 8q21.11	*606598	DRP1 regulation	Charcot-Marie-Tooth disease, axonal, type 2K Charcot-Marie-Tooth disease, type 4A	607831 214400	AD, AR AR
UCHL1 4p13	*191342	Ubiquitin homeostasis	Spastic paraplegia 79, autosomal recessive	615491	AR
RTN4IP1 6q21 (OPA10)	*610502	CI assembly; RTN4 interactor	Optic atrophy 10 with or without ataxia, mental retardation, and seizures (ROA, ROA plus)	616732	AR
WFS1 4p16.1	*606201	Ca2+ homeostasis; UPR and ER stress response	Wolfram syndrome 1 Wolfram-like syndrome, autosomal dominant (DOA)	222300 614296	AR AD
CISD2 4q24	*611507	Ca2+ homeostasis; anti-oxidant activity	Wolfram syndrome 2	604928	AR
ACO2 22q13 (OPA9)	*100850	TCA cycle	Optic atrophy 9 (DOA, DOA plus) Infantile cerebellar-retinal degeneration	616289 614559	AR, AD AR
SDHA 5p15.33	*600857	TCA cycle/ OXPHOS	Mitochondrial complex II deficiency, nuclear type 1 Neurodegeneration with ataxia and late-onset optic atrophy	252011 619259	AR AD

SDHB 1p36.13	*185470	TCA cycle/OXPHOS	Mitochondrial complex II deficiency, nuclear type 4	619224	AR
SDHD 11q23.1	*602690	TCA cycle/OXPHOS	Mitochondrial complex II deficiency, nuclear type 3	619167	AR
TMEM126A 11q14 (OPA7)	*612988	CI assembly	Optic atrophy 7 (ROA)	612989	AR
MECR 1p35.3	*608205	Fatty acids biosynthesis	Dystonia, childhood-onset, with optic atrophy and basal ganglia abnormalities	617282	AR
SLC25A46 5q22.1	*610826	Mitochondria lipids homeostasis	Neuropathy, hereditary motor and sensory, type VIB Pontocerebellar hypoplasia, type 1E	616505 619303	AR AR
OPA3 19q13 (OPA3)	*606580	Mitochondria lipids homeostasis	3-methylglutaconic aciduria, type III Optic atrophy 3 with cataract (DOA plus)	258501 165300	AR AD
MICOS13 19p13.3	*616658	IMM cristae shape	Combined oxidative phosphorylation deficiency 37	618329	AR
ATAD3A 1p36.33	*612316	IMM *cristae* shape, mtDNA binding	Harel-Yoon syndrome PHRINL syndrome	617183 618810	AD, AR AR
PNPT1 2p16.1	*610316	Mitochondrial mRNA import	Combined oxidative phosphorylation deficiency 13	614932	AR
MTRFR 12q24.31	*613541	Mitochondrial translation	Combined oxidative phosphorylation deficiency 7 Spastic paraplegia 55, autosomal recessive	613559 615035	AR AR
TSFM 12q14.1	*604723	Mitochondrial translation	Combined oxidative phosphorylation deficiency 3	610505	AR
MTFMT 15q22.31	*611766	Mitochondrial methionyl-tRNA formylation	Combined oxidative phosphorylation deficiency 15 Mitochondrial complex I deficiency, nuclear type 27	614947 618248	AR AR
MTO1 6q13	*614667	Mitochondrial translation	Combined oxidative phosphorylation deficiency 10	614702	AR
SSBP1 7q34 (OPA13)	*600439	mtDNA replication	Optic atrophy 13 with retinal and foveal abnormalities (DOA/ROA plus)	165510	AD, AR
NR2F1 5q15	*132890	Transcriptional regulation	Bosch-Boonstra-Schaaf optic atrophy syndrome	615722	AD
Xp11.4-p11.21 (OPA2)	%311050	-	Optic atrophy 2, X-linked (ROA)	311050	XL
18q12.2-q12.3 (OPA4)	%605293	-	Optic atrophy 4 (DOA)	605293	AD
8q21-q22 (OPA6)	%258500	-	Optic atrophy 6 (ROA)	258500	AR
16q21-q22 (OPA8)	%616648	-	Optic atrophy 8 (DOA)	616648	AD

3. ON from different pathogenic mechanisms

Optic atrophy is a quite widespread feature in many other inherited syndromic disorders involving neurodegeneration, that may well impair mitochondrial function, but are however distinct from a classic mitochondrial disorder in the major clinical findings.

Neurodegeneration with brain iron accumulation (NBIA) generally characterizes different syndromic disorders, mainly leading to cognitive impairment and movement disorders (117). The forms also commonly showing optic atrophy are summarized in **Table 4**, with their causative gene. Interestingly, the proteins PANK2, PLA2G6 and C19orf12 are localized in mitochondria and participate in lipid homeostasis (118,119).

Table 4. *Genes with published variants causing neurodegeneration with brain iron accumulation (NBIA) also including optic atrophy as a symptom.*

Gene	Disease	Phenotype	MIM#	Localization
C19orf12	MPAN/NBIA4	Neurodegeneration with brain iron accumulation 4	614298	Mitochondria, MAMs
FA2H	FAHN/SPG35	Spastic paraplegia 35, autosomal recessive	612319	ER
PANK2	PKAN/NBIA1	Neurodegeneration with brain iron accumulation 1	234200	Mitochondria
PLA2G6	INAD/PLAN/NBIA2A	Neurodegeneration with brain iron accumulation 2A	256600	Cytosol, mitochondria
	aNAD/NBIA2B	Neurodegeneration with brain iron accumulation 2B	610217	
WDR45	BPAN/NBIA5	Neurodegeneration with brain iron accumulation 5	300894	Autophagosome

Hereditary spastic paraplegias (HSP) typically present lower-extremity weakness and spasticity, and optic atrophy is also found among the variable accompanying symptoms (120). The forms of HSP, with causative genes, where optic atrophy has been reported are listed in **Table 5** (121).

Table 5. *Genes with published variants causing hereditary spastic paraplegias (HSP) also including optic atrophy as a symptom.*

Gene	Disease	Phenotype	MIM#
PLP1	SPG2	Spastic paraplegia 2, X-linked	312920
KIF1A	NESCAVS	NESCAV syndrome	614255
DDHD2	SPG54	Spastic paraplegia 54, autosomal recessive	615033
KLC2	SPOAN	Spastic paraplegia, optic atrophy, and neuropathy	609541
NT5C2	SPG45	Spastic paraplegia 45, autosomal recessive	613162
TFG	SPG57	Spastic paraplegia 57, autosomal recessive	615658

PEHO syndrome refers to a group of rare childhood-onset disorders, originating from dysfunctions in multiple different pathways (**Table 6**), but sharing common clinical features as progressive encephalopathy with edema, seizures with hypsarrhythmia, intellectual disability, dysmorphism, and optic atrophy. A recent literature review identifies optic atrophy in 86% of PEHO cases and 52% of PEHO-like cases (122)..

Table 6. *Genes with published variants causing PEHO and PEHO-like syndromes also including optic atrophy as a symptom.*

Gene	Disease	Phenotype	MIM#	Syndrome
HESX1	Septooptic dysplasia	Septooptic dysplasia	182230	PEHO
ZNHIT3	PEHO	PEHO syndrome	260565	PEHO
SCN2A	DEE11	Developmental and epileptic encephalopathy 11	613721	PEHO
CASK	MICPCH	Mental retardation and microcephaly with pontine and cerebellar hypoplasia	300749	PEHO
PCLO	PCH3	Pontocerebellar hypoplasia, type 3	608027	PEHO and PEHO-like
PLAA	NDMSBA	Neurodevelopmental disorder with progressive microcephaly, spasticity, and brain anomalies	617527	PEHO and PEHO-like
CCDC88A	PEHOL	PEHO syndrome-like	617507	PEHO and PEHO-like

Unbalance in Ca^{2+} trafficking could also be rarely linked to phenotypes with optic atrophy. This is the case of *CACNA1F* mutations, typically causing a form of retinopathy, incomplete congenital stationary night blindness (CSNB2A, MIM#300071), that however is typically associated with optic disc pallor/optic atrophy, a previously underappreciated clinical feature in these cases (123,124). Another Ca^{2+} channel, *CACNA1A*, usually harbours heterozygous mutations leading to different diseases: episodic ataxia type 2 (EA2, OMIM#108500), familial hemiplegic migraine type 1 (FHM1, OMIM#141500), and spinocerebellar ataxia type 6 (SCA6, OMIM#183086). A single pedigree is reported with biallelic mutation in *CACNA1A* and severe phenotype of encephalopathy, progressive cerebral, cerebellar, and optic nerve atrophy with muscular hypotonia (125)Impairment of Very Long-Chain Fatty Acids (VLCFAs) synthesis and degradation can also bring syndromic diseases: recently described heterozygous mutations in *ELOVL1* cause dominant ichthyosis, spastic paraplegia, hypomyelination, deafness and optic atrophy (IKSHD, MIM#618527), and optic nerve is also affected in adrenoleukodystrophy from recessive mutations in *ABCD1* (ALD, MIM#300100) (121,126).

Besides, some metabolic disorders can present ON signs. For example, vitamin B2/riboflavin deficiency underlies Brown-Vialetto-Van Laere syndrome (BVVLS1/2, MIM#211530/614707), characterized by neuropathy, sensorineural deafness, and bulbar palsy. The disease is caused by mutations in genes *SLC52A3* and *SLC52A2*, encoding the membrane transporters for riboflavin, and optic atrophy is an additional common feature in the syndrome (127). Again, the presence of optic atrophy is also recurrent in deficiency of vitamin B7/biotin due to biotinidase deficiency (BTD deficiency, MIM#253260), a recessive disorder given by BTD gene mutations, that presents hypotonia, seizures, and rash, developing into a severe metabolic acidosis (128). Yet, more metabolic pathways can be linked to optic atrophy, like nucleotide synthesis in which phosphoribosyl pyrophosphate (PRPP) synthetase (PRPS1) is involved. Mutations in *PRPS1* cause in fact an X-linked recessive Charcot-Marie-Tooth disease with optic atrophy, hearing impairment, and peripheral neuropathy (CMTX5, MIM#311070) (129).

The list can grow much longer considering that ophthalmologic symptoms are common in many other metabolic syndromes, from mucopolysaccharidoses to 3-methylglutaconic aciduria, that however this study does not aim to explore (130,131).

4. Next-Generation Sequencing

Next-generation sequencing (NGS), or massively parallel sequencing (MPS), refers to high-throughput DNA sequencing technologies developed from the early 2000s. This approach managed to cut costs and turnaround times of molecular analysis to unprecedented lows, then becoming increasingly widespread during the last ten years. This technology proved to be particularly useful in medical genetics field, both through target genes sequencing and untargeted approaches like Whole Genome Sequencing (WGS) or RNA sequencing. When dealing with rare Mendelian diseases, the most effective analysis is a targeted sequencing of all coding genes (Whole Exome Sequencing, WES), to overcome the high genetic heterogeneity of these disorders (132,133).

Illumina's sequencing by synthesis is now the leading NGS technology and is established as standard in both research and clinical laboratories.

- **4.1. Technical principles of NGS**

NGS workflows for WES, compatible with Illumina sequencing, require some basic wet bench steps, namely library preparation, target enrichment, and sequencing on the chosen platform. Library preparation usually starts from extracted total genomic DNA (gDNA) and produces the short fragments that will be sequenced, with specific barcoding and adaptor oligonucleotides at both ends, that is the library. Fragmentation of gDNA is performed either mechanically through sonication or enzymatically, followed by enzymatic end repair and A-tailing. The fragments can now be ligated to adaptor sequences required for a further step of PCR amplification and insertion of index barcodes (**Fig. 9**). An alternative Illumina protocol from gDNA follows a tagmentation step, in which transposomes randomly cut DNA and directly ligate adaptors, generating fragments ready for indexing and amplification. The index barcodes are unique for each sample, so every read will be rightly assigned after the bulk sequencing of the pooled libraries.

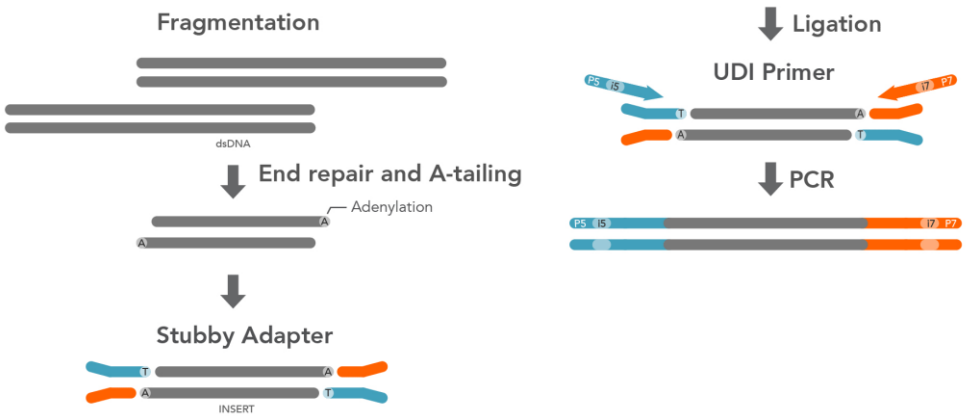

Figure 9. *Main steps of NGS library preparation for Illumina: gDNA fragmentation, end repair and A-tailing, adapter ligation, index oligos (UDI) insertion, and PCR amplification .*

The prepared sample libraries can be further processed to enrich the desired genomic regions, that in WES represent all exons of coding genes. Common commercial protocols perform the enrichment step through hybridization of the library fragments with biotinylated probes spanning the target sequences. Hybridized fragments can thus be captured with streptavidin-coupled beads, and further PCR amplified if necessary to increase yield (**Fig. 10**).

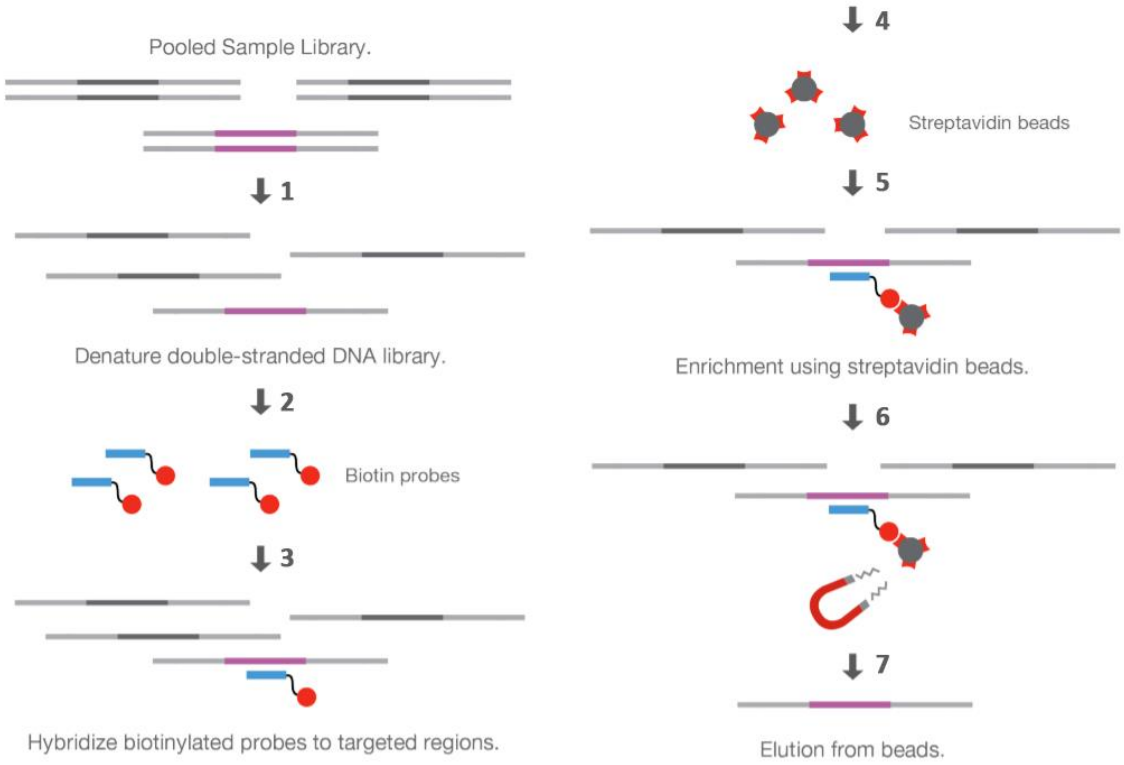

Figure 10. *Main steps of NGS targeted enrichment of pooled libraries: probe hybridization and target capture through magnetic beads, that will be followed by purification and PCR amplification of pool.*

The enriched pooled libraries are finally combined and diluted according to each Illumina sequencer specifications and to desired data output quality and yield. In the instrument, library fragments hybridize to oligonucleotides attached on the flow cell and are then clonally amplified through bridge-PCR. This step creates clusters of identical sequences, which will emit a fluorescent signal strong enough for detection on the CMOS sensor. During sequencing by synthesis reaction, the four fluorescently labelled terminator nucleotides (dNTPs) are added together and bind to complementary bases of the fragments. After excitation of the fluorophores and imaging of the flow cell, the blocker on the dNTPs is removed, and the following cycle starts. So, at each cycle the instrument takes a picture of all clusters, reading a single base per cluster (**Fig. 11**). The reversible terminator chemistry prevents sequence length errors in homopolymeric stretches. Moreover, accurate loading of the flow cell guarantees the optimal cluster density to be detected without signal saturation. If performing a paired end sequencing, which ensures more accurate read alignment, the whole process is repeated for the opposite end of each fragment, for a total of 150-300 cycles, depending on the chosen chemistry and instrument.

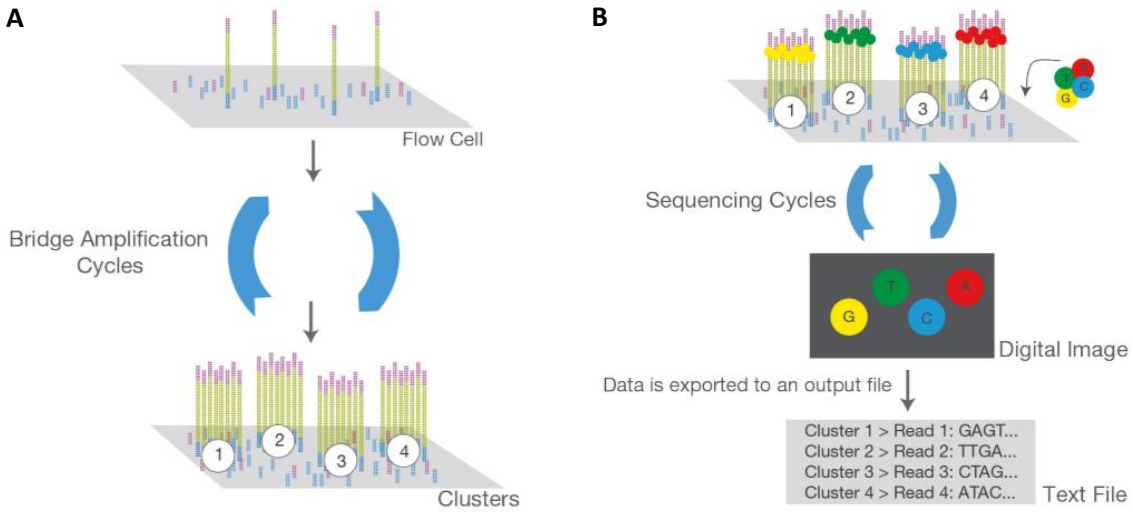

Figure 11. *Cluster generation through bridge-PCR on Illumina instrument flow cell (A) is followed by sequencing-by-synthesis (B) to produce raw data in BCL format.*

- **4.2. NGS bioinformatic pipeline fundamentals**

Illumina sequencers generate raw data that need several bioinformatic processing steps, a so called pipeline, to ultimately produce a Variant Call Format (VCF) file with called bases not matching the reference sequence (**Fig. 12**).

The raw output of sequencing by synthesis is stored in Binary Base Call (BCL) files. Following demultiplexing, each cluster sequence is assigned to a sample, based on index barcodes, thus creating individual FASTQ files. FASTQ is a text-based format storing both nucleotide sequence and its corresponding quality score, thus they are useful also for data quality control. The reads are then mapped to a reference genome assembly, in a Sequence Alignment/Map (SAM) file that is converted in a Binary Alignment/Map (BAM) file, easier to store and use (134). The alignment discards low mapping quality and duplicate reads, and variants to the reference present in multiple reads can be called using specific algorithms and stored in the VCF file (135). The default tool for this purpose is GATK HaplotypeCaller, that reassembles and realigns possible haplotypes with identified variants, choosing the best one based on posterior likelihoods and finally calling the most likely allele (136).

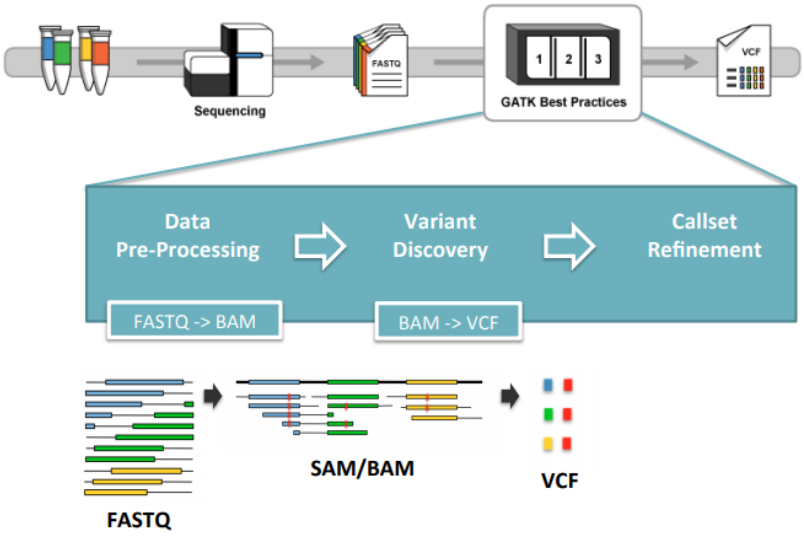

Figure 12. *Summary of bioinformatic analysis steps of NGS data from FASTQ file to VCF file.*

The VCF file requires more steps of annotation, in order to be filtered and analysed for possible pathogenic variants. Common annotations for WES variants include gene, severity of the mutation in the gene, nucleotide change on coding transcript, aminoacidic change in the protein, allele frequency in control population and in-house databases, and even disease phenotypes associated with pathogenic variants published for the gene.

- **4.3. Potential and pitfalls of WES**

In a clinical context, NGS has proven to be an invaluable technology: large cohorts as well as few urgent cases can be analysed in short time and with moderate costs, gaining genome-wide information to identify pathogenic variants in both known and novel genes.

The sensitivity in Single Nucleotide Variants (SNVs) and small insertion/deletions (indels) detection is higher than in Sanger sequencing, especially with deep coverage or application of specific protocols, and is now essential for mosaicism or somatic mutations identification. There are, however, some intrinsic limitations to NGS data for the detection of structural rearrangements or larger indels, as well as correctly mapping homologous, repetitive, or GC-rich regions. Besides, such limitations are more relevant in WES compared to Whole Genome Sequencing (WGS), mostly because of non-homogeneous coverage of exons, further complicating copy number variants (CNVs) discovery (137).

Nonetheless, WES has recently been the favourite choice for genetic studies of human disease since it is cheaper and easier to analyse than WGS. It requires, though, higher medium coverage than WGS, in order to adequately cover difficult regions. So, the American College of Medical Genetics and Genomics (ACMG) guidelines recommend a minimum mean coverage of 100X for WES, with 90–95% of target having at least 10X coverage (138). Typical exome targets now span about 35Mb, so around 1% of the genome, that usually cover 90–95% of exons of the ~20 000 known coding genes. But since ~85% of recognized pathogenic mutations are situated in coding regions, and variants in non-coding sequence are often of uncertain interpretation, WES is currently the best compromise between diagnostic yield and convenience (139).

5. Rare diseases genetics and molecular diagnostics

The rise of NGS technologies was a turning point for genetic studies and especially medical genetics, providing remarkable advancement in the understanding of inherited rare diseases. Indeed, new disease-gene discovery hit a historical high after widespread use of NGS, and especially of large gene panels or WES (**Fig. 13A**). A similar improvement in gene discovery is seen considering only mitochondrial diseases (**Fig. 13B**) (140) that are, combined together, a relevant group in rare diseases and frequently show optic atrophy phenotype.

- **5.1. Sequencing strategy for pathogenic variants discovery**

While WES allowed genetic basis of many Mendelian diseases to be elucidated, it is not always straightforward to pinpoint the pathogenic variants of interest. Since whole-genome studies reported an average for individual of ~3×10^6 SNPs (~5 000 private to one individual), ~700 000 indels (295 private), and ~200 large deletions (<1 private), even the few thousands variants identified by WES can be challenging to analyse (141).

Indeed, the majority of molecularly solved cases also through WES are attributable to pathogenic variants in well characterized disease-genes, for which interpretation can be easier. However, when dealing with very rare conditions, new or very rarely reported genes could harbour the actual genetic cause of disease, thus requiring extensive research for validation purpose (132).

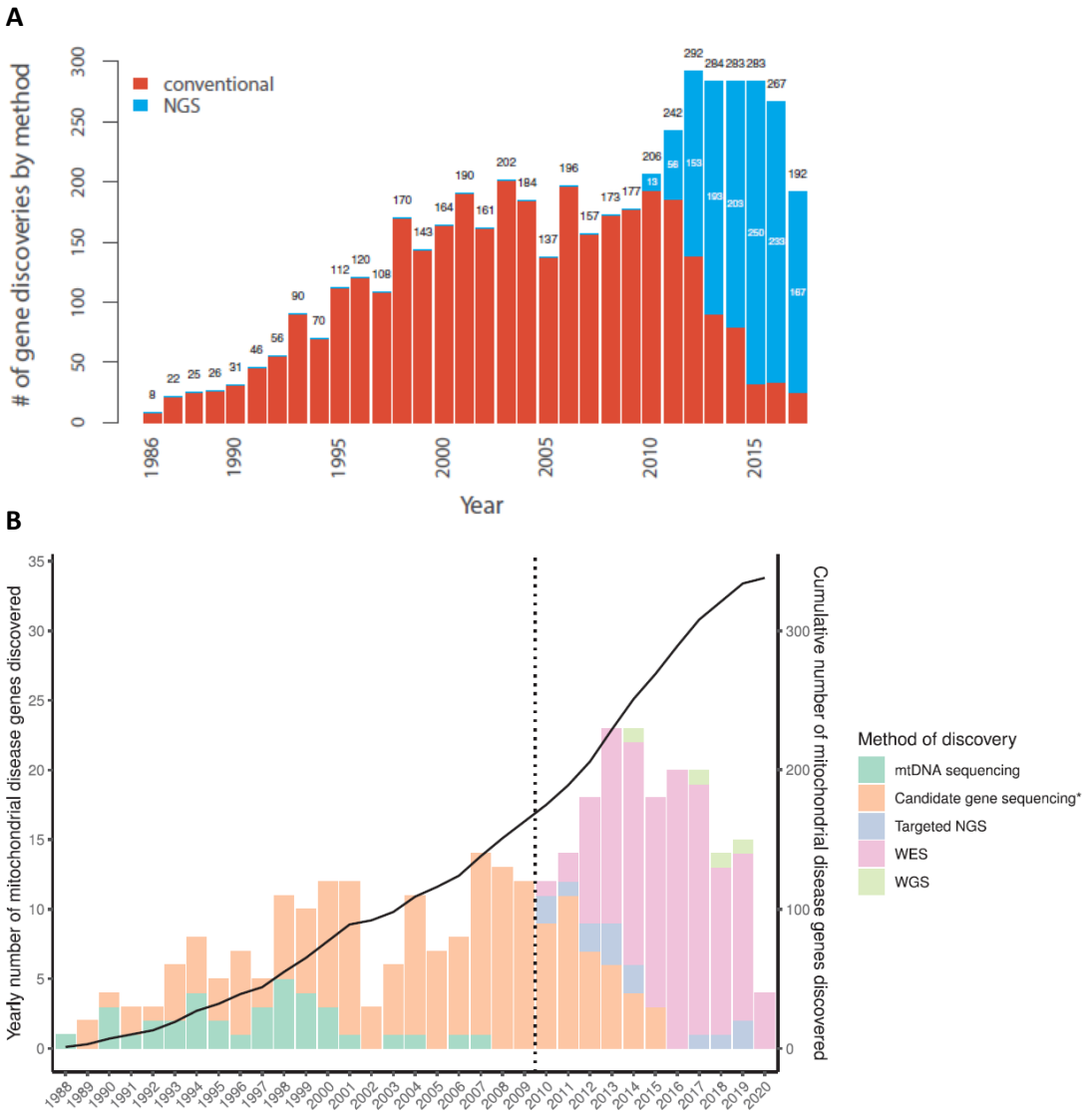

Figure 13. *(A) Annual number of disease-genes discovered through classic methods of linkage analysis and target sequencing or through NGS for Mendelian Diseases/Conditions (MCs) until year 2017, image from (133). (B) Annual gene discovery in mitochondrial diseases (140). Dashed line indicates NGS advent; candidate gene sequencing (*) includes linkage analysis, homozygosity mapping, and Sanger sequencing, also combined.*

Thus, the highest positive rate of WES is usually obtained with autosomal recessive (AR) or X-linked recessive (XLR) disorders, because analysis can focus on population-rare homozygous or compound heterozygous variants, relatively few per individual. For these cases, the sequencing of proband is usually sufficient, and further validation on available family members can be done on interesting variants. Instead, autosomal dominant (AD) disorders due to *de novo* mutations require sequencing of both proband and parents (trio), or, alternatively, a few affected

unrelated individuals in which the same causative gene is then identified. Inherited AD diseases also demand sequencing of a few related affected individuals, but pathogenic mutations are difficult to unravel, due to co-occurrence of multiple shared irrelevant variants between relatives. Moreover, AD variants can show incomplete penetrance of phenotype, further complicating their interpretation through segregation in the pedigree. Finally, somatic disorders can be mapped by sequencing in parallel affected and unaffected tissues, or looking for variants with low allelic fraction in known genes, but only with deep coverage available (**Fig. 14**) (139).

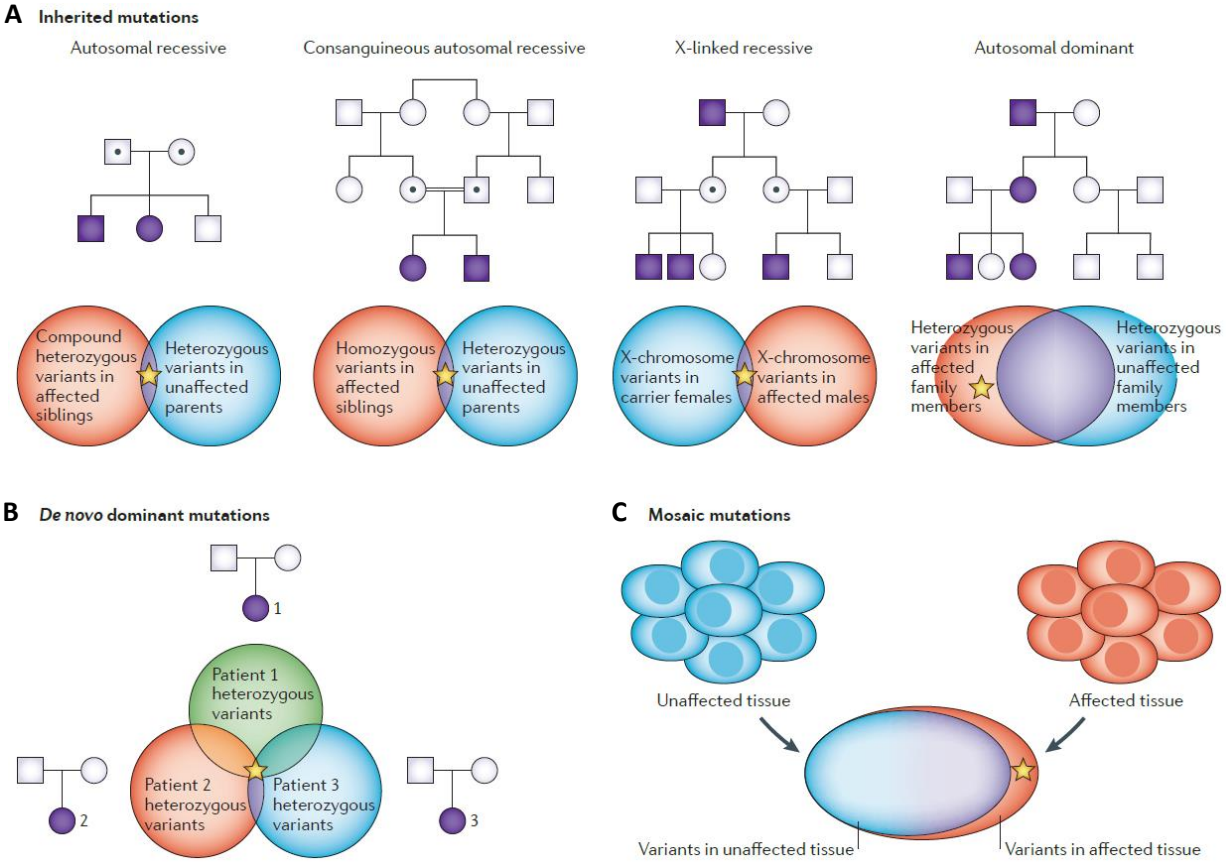

Figure 14. *(A) Inheritance patterns for Mendelian diseases with typical presentation in family tree and segregation analysis strategy for the identification of pathogenic variants. A causative variant can be identified by sequencing one or more members of a single family (A), more probands found to share a de novo variant (B) or different tissues of the proband to detect mosaicism (C). Image from (251).*

As a matter of fact, a considerable part of WES performed on rare Mendelian diseases concludes with one or more candidate variants in genes never reported as pathogenic. The first demonstration that a clinical phenotype is caused by mutations in a specific gene requires

strong evidence, so functional validation of the pathogenic mechanism and possibly more pedigrees with same mutated gene. In order to gather more of such families with rare genetic conditions, a valuable online tool, GeneMatcher (https://genematcher.org/), has been developed to connect clinicians and researchers studying the same genes, greatly improving the chances to identify and characterize novel disease-associated genes (142).

- **5.2. Genetic variants filtering and classification criteria**

The total annotated VCF of a sample can be manually or automatically filtered to select variants matching with inheritance mode and phenotypes observed in the pedigree.

A typical approach would be to discard common population polymorphisms (minor allele frequency, MAF >0.01 for AR, and >0.001 for AD cases) (143) found in large databases such as GnomAD (144), then keeping only variants predicted with a likely deleterious effect (e.g., non-synonymous SNVs, disruption of canonical splice-site/region, frameshift/in-frame indel). Additional filtering can be added to eliminate for example calls not reaching minimum desired coverage, or too far from splice-site junctions. The remaining variants can be further evaluated looking at scores from pathogenicity *in-silico* predictors (e.g., PolyPhen-2, SIFT, MutationTaster), or meta-predictors (e.g., CADD, REVEL) (145–149). However, prediction tools are numerous, but none is perfect, so it is advisable to use more than one tool, regularly updating them (150,151).

Predictors scores only inform about a variant's potential damage, more hints then are needed to confirm it as pathogenic. Here becomes important the thorough check of literature regarding the affected gene and allele: the phenotypes associated, pattern of inheritance, available functional studies, and similarity to known pathogenic mutations or gene-specific disease mechanisms. Online catalogues are available for research of inherited human disease and associated genes, like OMIM (152), and for storage of already found variants with inferred clinical significance, like ClinVar (153) and HGMD (154). Whenever possible, the variant segregation in the family following the clinical manifestation is one of the most robust indicators for pathogenicity.

The whole spectrum of criteria that can be adopted in sequence variant classification is reported in specific ACMG guidelines, including databases and prediction tools suggested to use (155). Criteria have different confidence levels, going from very strong to supportive, both towards a pathogenic and a benign classification of the variant. Precise combinations of the

fulfilled criteria lead to assignment of the variant to discrete categories: pathogenic, likely pathogenic, benign, likely benign. When criteria are not sufficiently satisfied or are contradictory, the classification is of variant of uncertain significance (VUS). Classification following the ACMG guidelines is possible through commercial software/pipelines or online tools, such as VarSome (156), but needs refinement and confirmation from the geneticist for the best accuracy.

Notably, WES can result in some incidental and secondary findings, that are variants with possible clinical meaning, but not directly linked to the investigated disease. Those variants are usually classified as pathogenic or likely pathogenic and found in medically actionable genes, mostly leading to muscular/cardiac diseases or cancer predisposition. The ACMG secondary findings guidelines list the genes for which notification of secondary findings is recommended, under patients' agreement (157).

- **5.3. Case phenotyping and phenotype-driven gene variant prioritization**

When dealing with rare diseases, a deep phenotyping of the proband and, upon availability, all family members is particularly valuable. Many genes can cause very similar symptoms, but the same gene may behave in AR or AD manner and also produce variable phenotypes, not always fitting known pathologies. With a complete list of symptoms and detailed pedigree, there are the best chances of unravelling the genetic origin of disease, even when variable penetrance and expressivity are involved.

The Human Phenotype Ontology (HPO) is a catalogue of standardized terms for pathogenic human phenotypes (158). Having a standard reference for every symptom of a patient makes classification of genetic variants more reliable, improving communication between diagnostic/research laboratory and clinicians.

Thanks to coded phenotypes, some automated approaches have been developed to prioritize, directly from a VCF file, the possible pathogenic variants causing the observed clinical features. These bioinformatic tools weigh several attributes of each variant to choose the best ones matching the given criteria, usually showing results in user-friendly html pages.

One of the first such tools developed, the Exomiser is always kept updated and implemented, and so far remains the most popular tool (159). The Exomiser workflow comprises variant annotation using Jannovar, removal of variants off the exomic target or with population frequency over the user-supplied threshold and ranking according to pathogenicity prediction.

Then, the genes with remaining variants are matched to the given HPO terms through phenotype-driven algorithms, like the most complete hiPHIVE (**Fig. 15**). This algorithm considers for each gene the human phenotypes described, as well as mutant mouse and zebrafish traits, further integrated by analysis of the protein-protein interaction network to highlight known pathogenic pathways. When no prioritized variant is found in genes functionally characterized in humans, animal models and interactome data could be particularly valuable for novel genes discovery (160).

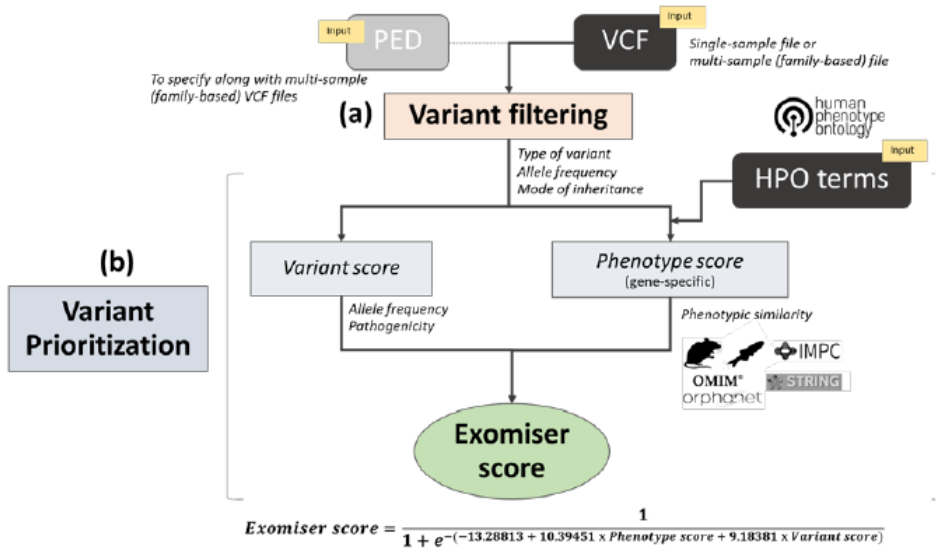

Figure 15. *The Exomiser main steps of filtering and prioritization algorithm. Image from (164).*

Another later described tool, MutationDistiller, for example does similar filtering from original VCF, with user-defined frequency in population and target regions to include. More criteria can be specified, like mode of inheritance, candidate genes or molecular pathways, tissue of expression and HPO terms, that will be integrated to MutationTaster pathogenicity prediction and phenotypes described in databases for each gene. Moreover, the tool prioritize variants already reported as pathogenic in ClinVar and highlight the genes present in ACMG secondary findings guidelines (161).

Recent advances in sequencing technology greatly increased the number of samples that can be processed in limited time, thus requiring fast and effective downstream analysis. The implementation of automated variant prioritization can produce faster, more standardized, results and can benefit both molecular diagnostic turnaround time and novel disease gene discovery (162–164).

Aim of thesis

Hereditary optic neuropathies, both as isolated disease and inside a syndromic clinical manifestation, are attributed to a variety of genetic causes. Most of HON cases can be linked to pathogenic variants in mtDNA, *OPA1*, or few other recurrent mitochondrial genes, but a significant percentage also involves variants in rarely reported genes. Besides, the majority of genetic HON shows wide phenotypic spectrum and variable severity, thus complicating their identification through clinical presentation alone. An untargeted, high-throughput approach is the most efficient option for molecular diagnostics of HON. Whole exome sequencing (WES) is now considered the most effective molecular analysis for detection of pathogenic variants in rare genes' coding region.

This work aims to identify through WES the genetic basis for HON in a cohort of 106 patients with both isolated and syndromic presentation. WES analysis will prioritize variants in known ON genes, but also in other mitochondrial or neural specific genes, which are more likely to be involved in ON pathogenesis. All variants of interest, classified through ACMG criteria, will be validated by Sanger sequencing in the proband and available family members, to also assess segregation with the clinical phenotype.

A first outcome of this study will be to estimate the diagnostic yield of WES analysis in a HON cohort, a data still lacking from literature.

Then, it aims to establish a pipeline for functional validation experiments of variants of uncertain significance, also applicable in the future. Thus, some of the prioritized variants will be characterized by yeast (*S. cerevisiae*) modelling, either by mutation of the hortolog gene or of the human gene expressed in yeast. This system is a fast and flexible solution for assessment of damaging potential and likely inheritance mode of candidate variants, but also for evaluation of mitochondrial function. The yeast validation is performed in collaboration with prof. Baruffini at University of Parma and is the only part of the study not developed inside our laboratory.

A second step of validation could be performed on primary fibroblast cell lines, a model closer to real target tissue of disease. Fibroblasts are well accepted for pathogenicity validation of novel genetic variants because they directly show molecular defects present in the patient.

Moreover, taking advantage of the untargeted approach, an objective of the study is to find novel genes with pathogenic variants leading to ON. Describing new genetic associations is particularly important for the improvement of future diagnostic rate in rare diseases like ON.

Notably, the validation protocol here followed is of capital importance also when novel disease-genes are involved.

Apart from research purpose, the diagnosis of rare diseases to a molecular level is a first advance for a better clinical management of the patients and may lead also to specific therapeutic approaches. Only a few pharmaceutical treatments are currently effective in HON cases, like idebenone for optic atrophy caused by respiratory CI dysfunction or vitamin supplementation for syndromic optic atrophy found in metabolic disorders.

More research on genetic causes and pathogenic mechanisms linked to HON is therefore fundamental for future improvement in therapeutic strategies, even considering the fast developing field of gene therapy and editing.

Materials and Methods

All techniques here presented are performed in the Laboratory of Neurogenetics at IRCCS Institute of Neurological Sciences of Bologna and funded as part of the Ministry of Health Project "Italian Project on Hereditary Optic Neuropathies (IPHON): from genetic basis to therapy" (GR-2016-02361449), led by Dr. Leonardo Caporali.

The work of DNA sequencing and secondary analysis of genetic data, as well as validation studies on target RNA and proteins were performed by thesis author.

1. Cohort description

Patients with clinical hallmarks of HON were included in the WES study as part of the "Italian Project on Hereditary Optic Neuropathies (IPHON): from genetic basis to therapy". Most patients were recruited after clinical evaluation in the Neurophtalmology Clinic at IRCCS Institute of Neurological Sciences of Bologna, led by Dr. Chiara La Morgia and Prof. Valerio Carelli. The same clinicians also confirmed inclusion in the study of patients examined in other Institutes, after checking available clinical documentation.

The total cohort (*n*=106) was further divided in 74 isolated ON (ON_*, Appendix Table 2), showing only optic atrophy or minor additional symptoms (e.g., nystagmus, sensorineural hearing impairment), and in 32 syndromic ON (sON_*, Appendix Table 3), where optic atrophy was found in a broader pathological context of neurodegeneration.

Patients with clinical presentation and familiar history compatible with DOA were usually firstly screened for *OPA1* mutations by target Sanger sequencing of coding exons (165) and often also by MLPA assay (SALSA MLPA Probemix P229 OPA1, MRC Holland) following manufacturer's instructions. Similarly, the common mtDNA LHON mutations (m.3460G>A, m.11778G>A, m.14484T>C) were screened through Sanger sequencing for cases presenting suspected or proven sub-acute vision loss. Only in cases compatible with a mitochondrial disease from mtDNA mutation, given inheritance pattern and clinical manifestation, whole mitochondrial genome sequencing was performed with an amplicon-based NGS protocol, as described in (8). The WES cohort thus includes both patients with no previous genetic testing, and negative for OPA1 and/or mtDNA sequencing. It also includes a subset of cases negative for ON targeted gene panel (*ACO2*, *AFG3L2*, *C12orf65*, *C19orf12*, *CISD2*, *DNM1L*, *IBA57*, *MFN2*, *NEFH*, *NR2F1*,

OPA1, *OPA3*, *PRPS1*, *RTN4IP1*, *SDHA*, *SLC25A46*, *SPG7*, *TMEM126A*, *WFS1*, *YME1L1*), previously performed following Nextera Rapid Capture protocol (Illumina).

2. Sample collection

Samples (*n*=106) were collected for analysis at the Neurogenetics Laboratory of IRCCS Institute of Neurological Sciences of Bologna, under written informed consent and with approval of the Independent Ethical Committee "Area Vasta Emilia Centro CE-AVEC" (CE 211/2018/SPER/ AUSLBO).

For in-house samples, total genomic DNA was extracted from buffy coat of peripheral blood using Maxwell 16 System (Promega) and checked for 260/230 and 260/280 optimal absorbance ratio on a NanoDrop 2000 Spectrophotometer (Thermo Scientific). For patients (*n*=12) recruited in the project from other Institutes, DNA samples were requested with similar quality parameters.

The DNA of probands' family members, available for sampling and potentially informative for variant segregation, was collected as well. Other than Sanger sequencing with validation purpose, some family members underwent WES to solve AD pedigrees (*n*=12), or to perform trio analysis in suspected *de novo* cases (*n*=2).

3. Targeted sequencing

In all NGS protocols, DNA was quantified with a Qubit 4 Fluorometer (Invitrogen), using the dsDNA BR Assay Kit for input gDNA and the 1X dsDNA HS Assay Kit for individual and pooled libraries.

As reported on Table 8 for each sample, the WES libraries were prepared by either Illumina, IDT, or Twist workflows, thus enriched with different probes design.

For the Illumina workflow, libraries were prepared using Nextera DNA Exome/TruSeq Rapid Exome Library Prep Kit (Illumina), following manufacturer's instructions. Briefly, 50 ng of gDNA is fragmented, and adapter sequences are added in a single step of tagmentation. After magnetic beads clean-up, the tagmented DNA is PCR amplified, introducing index sequences to the fragments. Following an additional clean-up, 500 ng of each library are combined in a 9-plex pool for the enrichment step. The pool is then hybridized to Coding Exome Oligos (Illumina) and captured with streptavidin conjugated magnetic beads, followed by washing steps.

Hybridization and capture are repeated for a second time, and after the washes the pool is PCR amplified and purified with magnetic beads.

WES prepared with IDT workflow used as input 750 ng of gDNA, mechanically sheared with a M220 Focused-ultrasonicator (Covaris) to a medium size of 250 bp. The protocol of NEBNext Ultra II DNA Library Prep Kit (New England Biolabs) then performs end repair, 5'-phosphorylation and dA-tailing in a single reaction, followed by ligation of universal NEBNext adaptors. Since the adaptors are hairpins with an uracil base, there is a USER enzyme step for uracil excision. A clean-up with magnetic beads is then performed, the library is PCR amplified introducing the UDI index sequences, and another clean-up follows. Finally, 12-plex pool with 500 ng of each sample library is made for xGen hybridization capture protocol (Integrated DNA Technologies). The pool is hybridized for 16 h to xGen Exome Research Panel probes v1 or v2 (Integrated DNA Technologies) and captured using streptavidin conjugated magnetic beads, part of XGen Hybridization and Wash Kit (Integrated DNA Technologies). After the single capture, the pool is washed, amplified by PCR, and purified with magnetic beads.

The Twist workflow starts from 50 ng of gDNA mechanically fragmented to a medium size of 200 bp, as input for Twist Library Preparation Kit for Mechanical Fragmentation (Twist Bioscience). The first step consists in end repair and dA-tailing in a single mix, then ligation of Twist universal adapters. The fragments are purified with magnetic beads and UDI indexes are added via PCR amplification. After a last clean-up with beads, 187.5 ng of each library are pooled in 8-plex for the 16 h hybridization with Comprehensive Exome probes (Twist Bioscience). Following steps of Twist Target Enrichment Protocol (Twist Bioscience) include capture of targets with streptavidin magnetic beads, serial washes, PCR amplification and final bead clean-up.

Pooled final libraries were checked for sizing on a Fragment Analyzer 5200 (Agilent) with HS NGS Fragment Kit (1-6000bp), quantified on Qubit 4, and diluted to 4 nM concentration. Sequencing was performed on a NextSeq 500 System (Illumina) with High Output flow cell and 2x151 paired-end reads setting.

4. Bioinformatic analysis of NGS data

NextSeq raw data in BCL files were demultiplexed with bcl2fastq v2.20 (https://emea.support.illumina.com/sequencing/sequencing_software/bcl2fastq-conversion-

software.html), generating FASTQ files, checked for optimal metrics using FastQC v0.11.9 (https://www.bioinformatics.babraham.ac.uk/projects/fastqc/).

Further steps follow the GATK Best Practises workflow for germline variant discovery (166). Reads were aligned to reference genome GRCh37/hg19 with Burrows-Wheeler Aligner v0.7.17 (http://bio-bwa.sourceforge.net/) in BWA-MEM algorithm (167), and obtained mapped SAM files were converted to binary format BAM through SAMtools v1.13 (http://www.htslib.org/) (168).

Duplicate reads were identified and removed using MarkDuplicates tool in Picard v2.26.0 (http://broadinstitute.github.io/picard/) to avoid sequencing errors propagation and allele overrepresentation. Besides, different tools from the Genome Analysis Toolkit v3.8 (GATK, https://gatk.broadinstitute.org/hc/en-us) (169) were used to perform the following pipeline steps: local realignment around indels (RealignerTargetCreator, IndelRealigner), base quality recalibration (BaseRecalibrator), target region coverage metrics calculation (DepthofCoverage). Finally, the last steps also use GATK tools for the generation of a total, updated, genomic VCF v4.1 (gVCF): SNV and indel variants calling in gVCF output (HaplotypeCaller -ERC GVCF), joint genotyping to obtain the multi-sample gVCF (GenotypeGVCFs), Variant Quality Score Recalibration (VQSR) for identification of low quality, probably inaccurate, calls (VariantRecalibrator, ApplyRecalibration).

A SQL database was built from all variants in the combined gVCF through GEMINI framework v0.20.1 (https://gemini.readthedocs.io/en/latest/), enabling a flexible annotation strategy and rapid dataset query for samples of interest (170). GEMINI database was integrated with annotations from several sources, like GnomAD (144), OMIM (152), ClinVar (153), MitoCarta3.0 (171), and CADD (148). For manual analysis of each sample, variants were selected with MAF <0.01 in GnomAD database and with deleterious effect on gene transcript (nonsynonymous, nonsense, frameshift, and splice-affecting).

For trio analysis, *de novo* variants were detected using Platypus variant caller (https://github.com/andyrimmer/Platypus/), an optimised calling tool (172), and then annotated with ANNOVAR (https://annovar.openbioinformatics.org/en/latest/) (173).

For cases with acknowledged or suspected consanguinity, runs of homozygosity (ROH) were mapped with H3M2 tool, with subsequent filtering of deleterious variants found within those regions (174).

5. Manual WES data analysis and classification

Further filtering and curation of variants was performed, based on frequency in GnomAD, prioritizing alleles that are ultra-rare or never found, and never observed in homozygosity/hemizygosity. Moreover, variants called in >5% of our in-house samples were also discarded as recurrent sequencing errors or overrepresented common alleles. Good quality of calls and correct mapping of small structural variants in candidate genes were confirmed checking manually the BAM file, with the Integrative Genomics Viewer (IGV, https://software.broadinstitute.org/software/igv/) (175,176). Variants selected according to inheritance pattern, pathogenicity prediction, and gene function or associated disease, were validated by Sanger sequencing and segregated in available family members.

Final variant classification was assessed on VarSome (https://varsome.com/), with ACMG criteria manually refined: PS2 was added for *de novo* identified variants, PM3 if another pathogenic variant was present in *trans*, and PP1 for variants cosegregating with disease in multiple affected family members (155,156). Variant nomenclature follows HGVS recommendations (177).

The candidate genes for novel phenotypes were also shared on GeneMatcher (https://genematcher.org/) (142) to find consistent pedigrees, awaiting functional validation with *in vitro* models (fibroblast cell lines, yeast).

Cases with pathogenic/likely pathogenic variants, or predicted damaging rare VUS, matching the phenotypes reported in literature were considered “Solved”, after further case review with the clinicians. Cases with predicted damaging variants in disease genes, but not perfectly matching clinical manifestation or inheritance pattern described in literature, were labelled as “VUS”. Cases with predicted damaging variants in genes of uncertain significance (GUS), whose involvement in human disease is yet to be confirmed, were labelled as “GUS”.

6. Automated prioritization tools

For automated variant prioritization single-sample VCF files were extracted from multi-sample gVCF using GATK SelectVariants tool. If more than one sample per dominant pedigree was sequenced, the VCF file were intersected with isec command of BCFtools v1.11

(https://github.com/samtools/bcftools), in order to produce a single file with shared variants, compatible with inheritance (168).

Further filtering on VCF files included removal with BCFtools (-isec) of variants called in >5% of our in-house samples, likely recurrent sequencing errors or overrepresented common alleles, and with VCFtools v0.1.16 (https://vcftools.github.io/index.html) (135) of all calls on mtDNA-chrM (--not-chr option), since mtDNA is not adequately covered by WES probes used.

All WES cases unsolved from manual analysis were reanalysed through The Exomiser tool. Moreover, unsolved AD pedigrees providing a single intersected VCF file were reanalysed combing ranking from The Exomiser and MutationDistiller tools, to increase novel genes discovery possibilities.

- **6.1. The Exomiser**

Automated variant prioritization on single-sample and intersected VCFs was performed using The Exomiser v12.1.0 (https://github.com/exomiser/Exomiser) (164). In the YAML analysis file for Exomiser, HPO terms were given for each sample, and appropriate inheritance mode selected (all modes except “Mitochondrial” for sporadic cases). Default parameters were given for all filtering sources and criteria, but with addition of CADD in the “pathogenicitySources”, and 100 prioritized genes were shown as output.

- **6.2. MutationDistiller**

Filtered intersected VCF files for AD samples of the same family were given as input for MutationDistiller, setting “Filter polymorphism” to 0 homozygotes and 5 heterozygotes as maximum reported alleles in population databases. Phenotype in HPO terms was then added, mode of inheritance set to “dominant (strict)”, and variant selection to “all DMs”, to finally show the first 100 prioritized genes. Ranking from this tool was annotated on TSV files generated as Exomiser output.

7. Sanger sequencing

Sanger validation of variants identified by WES was performed on probands and all sampled individuals in the pedigree. The gene regions with target variants were PCR amplified using GoTaq DNA Polymerase (Promega) or Platinum II Taq Hot-Start DNA Polymerase (Invitrogen)

following standard protocols, and product was checked on a 1% agarose gel. The PCR product was then purified with MagSi-NGSPREP Plus beads (Magtivio) and used for sequence reaction with BigDye Terminator v1.1 or v3.1 (Applied Biosystems). Products were purified with MagSi-DT Removal beads (Magtivio) and run on a 3500 Dx Genetic Analyzer (Applied Biosystems), the obtained chromatogram was analysed on Sequencher software v4.10 (Gene Codes).

8. Targeted *OPA1* and *UCHL1* cDNA sequencing

Total RNA of the proband and a healthy control was extracted from buffy coat of peripheral blood (for *OPA1* experiment) or from fibroblast cell line pellet (for *UCHL1* experiment), using PureLink RNA Mini Kit (Invitrogen). The RNA was treated with DNase I (Sigma-Aldrich) with standard protocol, then extraction yield and purity were checked on NanoDrop 2000 Spectrophotometer (Thermo Scientific). Synthesis of cDNA was performed with 1 µg of RNA as input for SuperScript VILO cDNA Synthesis Kit (Invitrogen), strictly following manufacturer instructions.

Specific PCR primers were designed to amplify *OPA1* transcript region including exons 9 to 15 and *UCHL1* from exon 2 to 3' UTR (Table 7). Amplification products were run on 4% MetaPhor Agarose gel (Lonza Bioscience), and single bands purified using QIAquick PCR Purification Kit (Qiagen). Purified products were then sequenced according to Sanger sequencing protocol already described.

Table 7. *Primer designed for target sequencing of aberrant spliced forms in cDNA of OPA1 and UCHL1.*

Gene	Primer position	Primer sequence	WT product size
OPA1	Ex.9	TCTGGGGAGATGATGACACG	578
	Ex.15-16	TCAGAGCTGTTCCCTTTTCCT	
UCHL1	Ex.1-2	GAGATGCTGAACAAAGTGCTGT	917
	3' UTR	CCAAAGTAGCCATTTAAAGCGTTAG	

9. Cell cultures

Primary fibroblast cell lines were established from skin biopsies, after having obtained informed and written consent from all patients and controls for the study and for all procedures, after approval of the Independent Ethical Committee "Area Vasta Emilia Centro CE-AVEC" (CE 211/2018/SPER/AUSLBO).

The cell cultures were grown in Dulbecco's Modified Eagle's Medium (DMEM, Gibco) containing 4,5 g/L D-glucose and 0,11 g/L sodium pyruvate, with addition of 10% fetal bovine serum (FBS, Gibco), 2mM L-glutamine (Gibco), and 100 U/ml Penicillin-Streptomycin antibiotic (Gibco). Cell culture incubator was maintained at 37 °C and 5% CO^2, cells were harvested at 75% confluence and pellet stored at -80 °C prior to RNA or protein extraction.

10. Protein levels analysis

- **10.1. Protein extraction and quantification**

Total proteins of fibroblast cell lines were obtained after lysis in RIPA buffer (50 mM TrisHCl pH 7.6, 150 mM NaCl, 0,1% SDS, 1% NaDOC, 5 mM EDTA) containing 25X cOmplete EDTA-free Protease Inhibitor Cocktail (Roche). Briefly, cell pellet was resuspended in buffer and incubated 15 min on ice, then two rapid freeze-thaw cycles were performed, and was treated with Benzonase Nuclease (Millipore) 15 min at RT to remove nucleic acids. The supernatant with total protein lysate was recovered after centrifugation at 18 000 g for 10 min (4 °C).

Protein quantification was performed with standard Bradford assay (0,01% Coomassie Brilliant Blue G-250, 4,7% EtOH, 8,5% orthophosphoric acid), calibrated on a standard curve from dilutions of 10 mg/ml Bovine Serum Albumin (BSA). Absorbance at 595 nm was detected using EnSpire Multimode Plate Reader (PerkinElmer).

For protein extraction from skeletal muscle the same protocol was adopted, except for the first mechanical homogenization step in modified RIPA buffer (50 mM TrisHCl pH 7.6, 150 mM NaCl, 1% SDS, 1% NaDOC, 5 mM EDTA) and quantification with Bradford assay read on V-550 Spectrophotometer (Jasco).

- **10.2. SDS-PAGE and Western Blotting**

Protein lysates (20-30 µg input) were loaded, with NuPAGE LDS sample buffer 4x (Life Technologies) and NuPAGE Sample Reduction Agent 10x (Life Technologies), on pre-cast NuPAGE 4-12% Bis-Tris Glycine gels (Life Technologies) for separation under denaturing conditions in the XcellSure Lock (Life Technologies) apparatus.

Proteins were then transferred on 0.45 µm nitrocellulose membranes (Bio-Rad) using the Mini-PROTEAN Tetra system (Bio-Rad). After blocking with 5% non-fat milk, membranes were blotted with primary antibodies for target proteins. Antibodies used are listed as follows, with

target and working concentration: Actin 1:5000 (code ab1801), Citrate synthetase 1:5000 (code ab129095), NDUFA9 1:1000 (code ab14713), OXPHOS cocktail 1:500 (code ab110411), TFAM 1:1000 (code ab47517), UCH-L1/PGP9.5 1:2000 (code ab72911), and UQCRC2 1:1000 (code ab14745) from Abcam; DRP1 1:1000 (code H00010059-M01), and MFN2 1:1000 (code H00009927-M01) from Abnova; OPA1 1:1000 (code 612607), and Tim23 1:2000 (code 611222) from BD Biosciences; Tom20 1:10000 (code 42406) from Cell Signaling Technology; SDHA 1:10000 (code 459200) from Invitrogen; GAPDH 1:10000 (code MAB374) from Sigma-Aldrich; COX4 1:1000 (code GTX114330) from GeneTex; MFN1 1:1000 (code 13798-1-AP) from Proteintech.

Fluorescent secondary anti-rabbit or anti-mouse antibodies (code 926-32210 and 926-68071, LI-COR) were used for immunodetection using an Odyssey Fc Imaging System (LI-COR). Data from densitometry were normalized to the control cells and are shown as mean+SD of 3 independent experiments, biological replicates for cell line proteins and technical replicates for muscle proteins.

- **10.3. BN-PAGE of respiratory complexes**

For complexes analysis, mitoplasts were isolated from 106 cells/ml using 50 µg/ml digitonin and then suspended in a buffer containing 750x10-3 mol/L aminocaproic acid, 50x10-3 mol/L bis–tris, pH 7.0, and solubilized with 2.5 g of dodecyl-maltoside (DDM) for 1 g of protein. The suspension was incubated on ice for 10 min, centrifuged at 13000g and the protein content of supernatant determined. BN sample buffer (5 % Serva G Blue in 750x10-3 mol/L aminocaproic acid, 50x10-3 mol/L Bis–Tris and 0.5x10-3 mol/L EDTA) was added to mitoplast aliquots and samples were loaded on pre-cast NativePAGE Novex® Bis-Tris Gel 4-16 % gels (Life Technologies). After electrophoresis, BN-PAGE gels were used for western blotting of the other complexes. Antibodies used are listed as follows, with target and working concentration: NDUFA9 1:1000 (code ab14713), ATP5A 1:1000 (code ab14748), UQCRC2 1:1000 (code ab14745) from Abcam; SDHA 1:10000 (code 459200) from Invitrogen.

11. Statistical analysis

Data from densitometry of Western Blot analysed proteins were elaborated on Prism v9.0.0 (GraphPad) and appropriate test and significance range reported for each experiment.

Results

1. WES metrics and diagnostic rate

- **1.1 Coverage metrics**

The total ON cohort recruited for WES study amounts to 106 cases, sequenced with a mean depth of 126x ±44x and over 96% of target covered with at least 20x depth.

Different WES workflows used yielded a variable target mean coverage (**Fig. 16A**), lowest for Illumina workflow (86x ±19x) and highest for IDT with v2 probes (168x ±21x). Good coverage of target regions was achieved (**Fig. 16B**), with a mean percentage of bases covered at least at 20x going from mean 91% (Illumina) to 99% (IDT v1 and v2). All samples satisfied metrics thresholds of minimum mean coverage (~60x) and target over 10x sequencing depth (~90%).

Individual samples metrics are reported in Appendix Table 1.

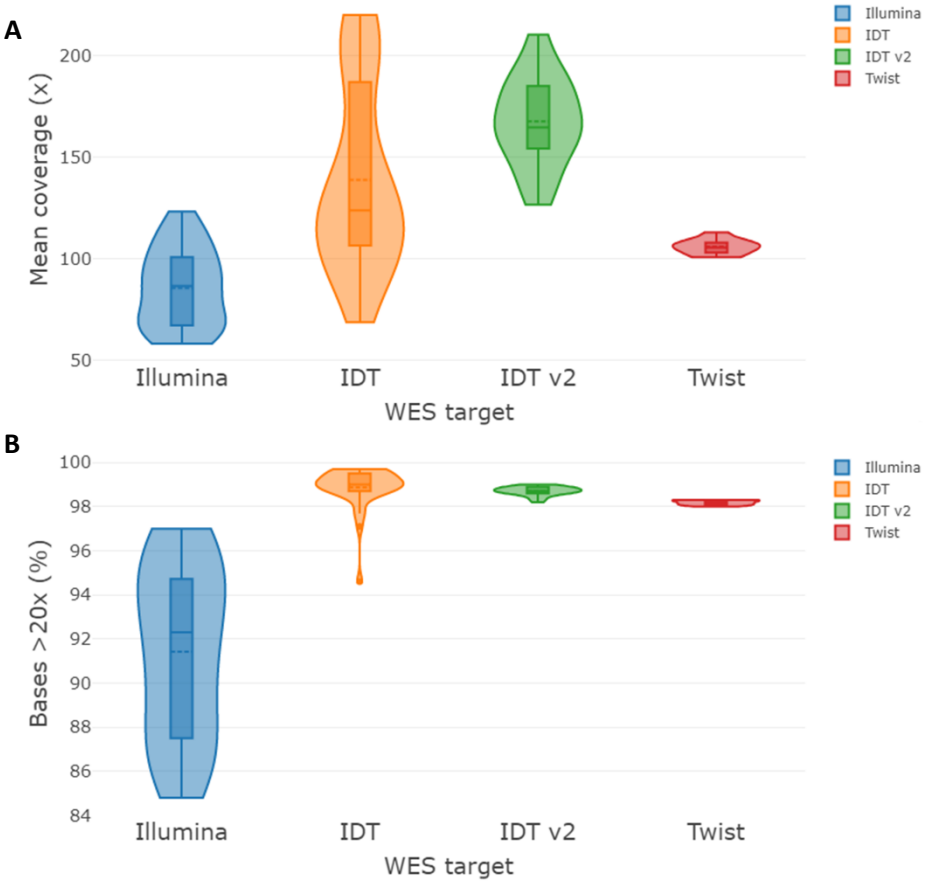

Figure 16. *Violin plot depicting mean coverage (A) and percentage of bases covered over 20x (B) for all WES samples divided by probes target (Illumina n=35, IDT n=35, IDT v2 n=27, Twist n=9).*

- **1.2 Diagnostic rate**

After analysis of WES data, cases are classified as “Solved”, when pathogenic, likely pathogenic variants, or VUS with pathogenic evidence are identified in genes compatible with observed phenotype. When pathogenicity of a variant has not yet been well established, or when inheritance mode or clinical phenotype do no not match with reported cases, the sample is labelled “VUS”. If novel candidate disease genes are found, that need functional evidence to be confirmed as pathogenic, the case is part of “GUS” (gene of uncertain significance) category.

According to this classification, we obtained a 27% of solved cases across the whole cohort, with 9% of VUS cases and an additional 5% of GUS cases (Figure 17).

Isolated ON (ON_*) patients were prevalent in the total cohort, with 74 patients sequenced, the remaining 32 being syndromic ON patients (sON_*). Solved cases rate is slightly higher in syndromic ON patients (31%) compared to isolated ON (26%), but the difference is more pronounced for VUS cases, accounting for 19% and 5% of cohorts, respectively, and GUS cases, with 13% and 1% (**Fig.17**). A positive result was so obtained for 32% of ON cohort and 63% of sON cohort, considering both genes identified with good confidence and the ones requiring confirmation.

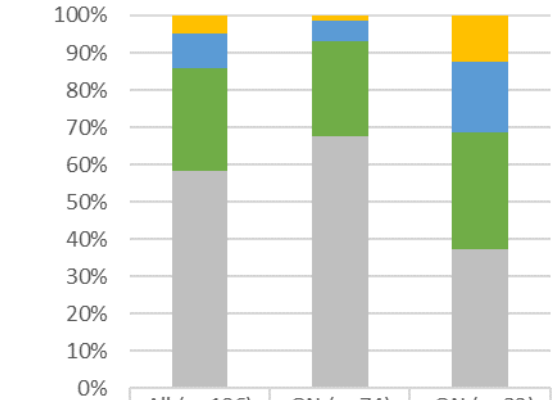

	All (n=106)	ON (n=74)	sON (n=32)
GUS	5	1	4
VUS	10	4	6
Solved	29	19	10
Unsolved	62	50	12

Figure 17. *Number of samples in whole, ON, and sON cohorts categorized as unsolved, solved, VUS, or GUS.*

In order to assess WES diagnostic rate on a more uniform cohort, a subset of ON and sON samples only negative to previous *OPA1* screening was considered, including 47 ON and 15 sON cases. WES analysis solved 19% of ON cases, compared to a 13% that would have been solved

through classic target gene panel analysis (targeted genes in Materials and Methods). Moreover, while a single case categorized as VUS would be found by gene panel, WES identified 2 more VUS and 1 GUS cases, so that a total of 28% of ON had some positive results pending further confirmation (**Fig. 18**). For sON the solved rate through WES was 33%, improving the 20% solvable only analysing the HON gene panel. Only through WES 5 more sON cases classified as VUS were found, reaching 67% as rate of samples with a positive result (**Fig. 18**). Taken together, the cumulative solved rate in *OPA1*-negative subset of ON and sON (n=62) is 23%, compatible with the 27% of total cohort considering the lack of *OPA1* cases.

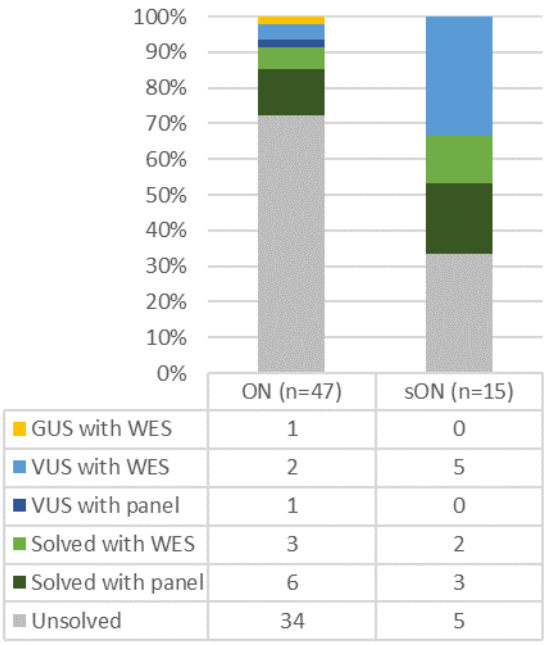

	ON (n=47)	sON (n=15)
GUS with WES	1	0
VUS with WES	2	5
VUS with panel	1	0
Solved with WES	3	2
Solved with panel	6	3
Unsolved	34	5

Figure 18. *Number of samples in ON, and sON cohorts, subsampled for OPA1-only negative cases. The unsolved, solved, VUS and GUS cases are reported, dividing the ones positive for genes in HON target gene panel (Solved/VUS with panel) and the positive cases only detectable through a WES analysis (Solved /VUS/GUS with WES).*

- **1.3. Identified genes inheritance**

The pattern of inheritance for identified genes (AD, AR, and XLR) showed a variable distribution between the ON and sON cohorts of solved and VUS samples (**Fig. 19**). So, in solved ON we found the same numbers of dominant and recessive cases (10 vs 10 including 1 X-linked), and only 4 dominant VUS cases. In sON cohort, solved dominant cases were far less numerous than recessive (1 vs 9, including 1 X-linked), however equally represented in VUS category (3 AD and 3 AR/XLR). For GUS category, the single ON case has hypothesized AD inheritance, while 4 sON are proposed with AR/XLR inheritance. One of the candidate samples in sON is labelled as "AD?", because a single candidate variant was prioritized, but it should act with incomplete penetrance accordingly to segregation in the pedigree.

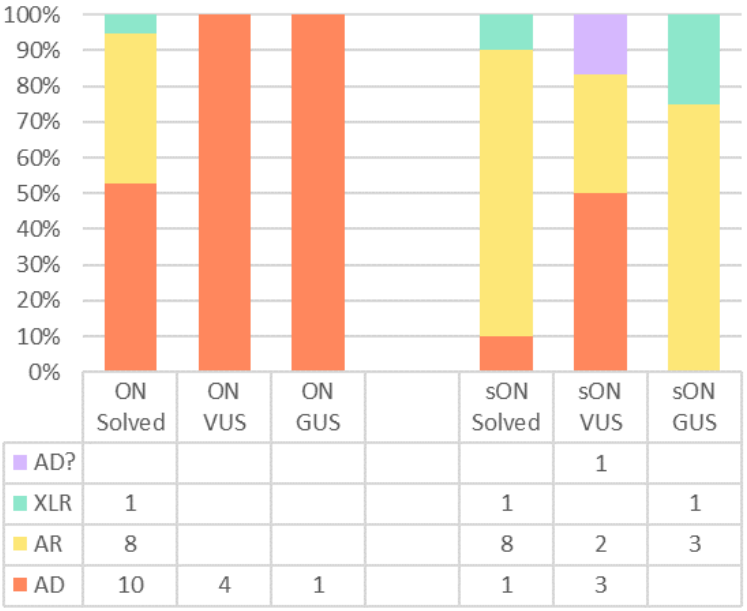

Figure 19. *Inheritance pattern identified for solved, VUS, and GUS samples in ON and sON cohorts.*

- **1.4. Gene function in positive results cases**

The solved, VUS, and GUS cases were then categorized as mitochondrial (mito) or non-mitochondrial (non-mito), considering function and localization of proteins produced by the identified genes (**Fig. 20**). So, the mitochondrial group includes genes encoding a known mitochondrial protein and accounts for 95% and 80% of cases in solved ON and sON. In VUS ON the "mitochondrial" percentage decrease to a 50%, and even to 17% in VUS sON cases. Finally, all GUS cases in both ON and sON cohorts are considered "non-mitochondrial", based on current knowledge on these proteins' function.

The genes related to mitochondrial function found in cases with positive results are known to harbour pathogenic variants causing optic atrophy, often among other symptoms: *ACO2*, *AFG3L2*, *C19orf12*, *DNAJC30*, *FDXR*, *MECR*, *MTFMT*, *NDUFAF2*, *NDUFB11*, *NDUFV2*, *OPA1*, *PDSS1*, *SDHA*, *SSBP1*, and *WFS1*. The non-mitochondrial genes identified are linked to some major intracellular pathways: cellular components turnover systems of lysosomes-autophagy *(LYST*, *SNF8*, *WDR45*) and ubiquitin-proteasome (*UCHL1*), axonal transport (*KIF1A*), neural cells development (*GFAP*, *EPHB2*), vitamin metabolism (*SLC52A2*, *BTD*), cilia structure (*USH2A*), calcium influx in neurons (*CACNA1A*, *CACNA1F*), and nuclear pore shuttling (*NUTF2*).

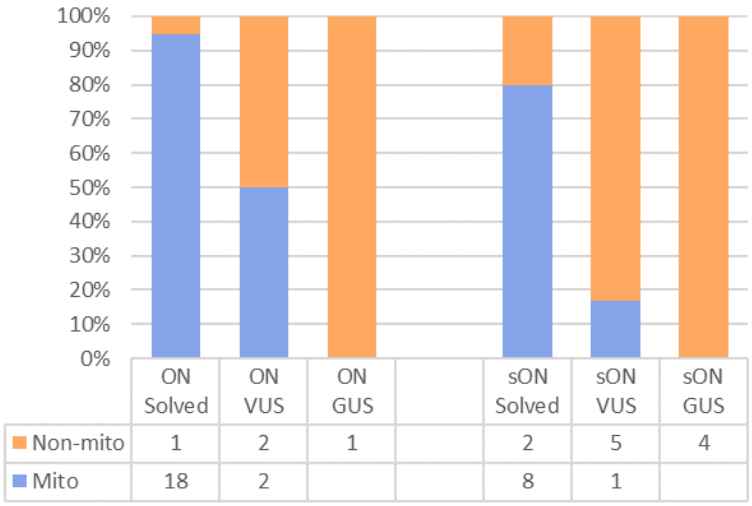

Figure 20. *Mitochondrial (mito) or non-mitochondrial (non-mito) cases in solved, VUS, and GUS groups for ON and sON cohorts.*

2. WES results in Optic Neuropathies

In the ON cohort 19 of the 74 cases are considered solved, for a diagnostic yield of 26%. The majority of recruited ON patients had already been tested negative for OPA1 mutations, however *OPA1* remains the most prevalent gene, together with the autosomal dominant *ACO2*, both accounting for 21% of solved ON (**Fig. 21**). Then, autosomal recessive *DNAJC30* and *WFS1*, are both identified in 16% of samples, and single cases were solved finding AD variants in *SDHA* and *SSBP1*, as well as AR variants in *MECR* and *NDUFV2* genes, and XLR variant in *CACNA1F*.

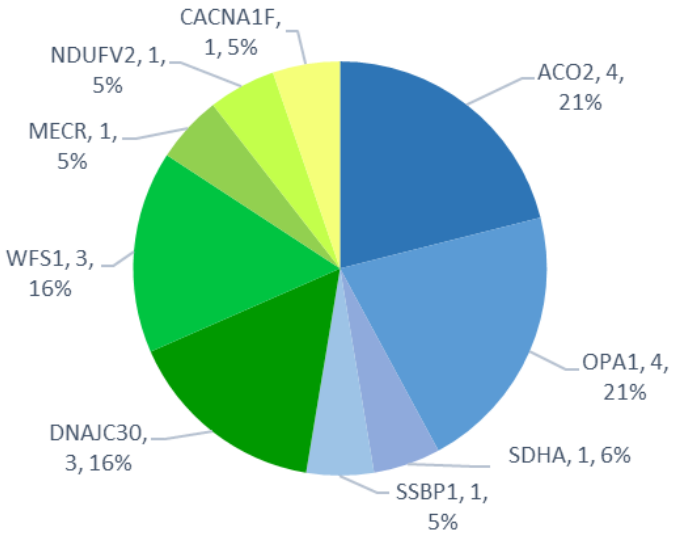

Figure 21. *Pie chart with number of cases and overall percentage of genes identified in solved ON cohort.*

Details for all solved cases, including age of onset and sampling, complete HPO terms phenotyping, and compatible inheritance at presentation for ON are listed in Appendix Table 1, describing the whole cohort.

- **2.1. Autosomal Dominant solved ON cases**

The 10 autosomal dominant solved cases (14% of ON cohort) are summarized in **Table 8**.
Of these, 4 patients presenting with isolated optic atrophy are positive for *ACO2* pathogenic or likely pathogenic variants, in line with recent evidence that *ACO2* is a common genetic cause of DOA (**Fig. 22**).

Table 8. *Gene and annotated variants identified in solved AD samples of ON cohort. HPO terms are shown except for HP:0000648-Optic atrophy, common to whole cohort.*

Sample	Sex	Age of onset	HPO Term Identifier	Gene	Transcript variant	Aminoacidic change	Variant class.	ACMG Criteria
ON_1	F	13 y	HP:0000646 HP:0001135 HP:0000821 HP:0007906	*ACO2*	c.2011C>T	p.Arg671Trp	LP	(PS1), PM2, PP2, PP3
ON_2	M	6 y	HP:0001952	*ACO2*	c.1761+1G>A	Splice site	P	PVS1, PM2, PP3
ON_3	M	7y	-	*ACO2*	c.1438A>G	p.Asn480Asp	LP	PM2, (PP1), PP2, PP3
ON_4	M	10y	-	*ACO2*	c.494T>C	p.Phe165Ser	LP	PM2, (PP1), PP2, PP3
ON_5	M	NA	-	*OPA1*	c.2713C>T	p.Arg905Ter	P	PVS1, PM2, PP3
ON_6	F	NA	-	*OPA1*	c.893_936dup	p.Ile313 ValfsTer10	P	PVS1, PM2, PP3
ON_7	M	Childhood	-	*OPA1*	c.1212+5G>A	Splice region	LP	(PS3), PM2, (PP4)
ON_8	M	9 y	-	*OPA1*	c.1212+6T>G	Splice region	LP	PM2, (PM6), (PP1), (PP4)
ON_9	M	14y	HP:0011347	*SDHA*	c.1351C>T	p.Arg451Cys	P	(PS1, PS3), PM2, PP3
ON_10	F	16 y	HP:0000822	*SSBP1*	c.151A>G	p.Lys51Glu	VUS (P)	PM1, PM2, (PP1), BP4

The case ON_1 presented as an only case, with optic atrophy and dystrophic retinal signs, and was diagnosed with change c.2011C>T, leading to missense mutation p.Arg671Trp. This allele is reported in a single individual in GnomAD database (max MAF: 6.162E-5), but is located in a mutational hotspot of the gene, where the same mutation and an alternative aminoacidic change (p.Arg671Gln), were found in other DOA families (72). Preliminary results on yeast modelling of this variant show reduced ACO2 protein levels and its enzymatic activity, severely

impairing mitochondrial function (A. De Giorgi, E. Baruffini, pers. comm.). In the sample ON_2 we found a null allele due to a change c.1761+1G>A in the 5' splice site of intron 14 (dbscSNV ADA score 0.9999). An haploinsufficiency pathogenic mechanism for *ACO2* is also supported by other splice-affecting variants reported in other pedigrees (72). The variant was inherited from the mother, that shows a subclinical optic nerve defect at OCT examination. Patients ON_1 and ON_2 are included in the large set of DOA cases recently published (72). In the samples ON_3 and ON_4, two novel missense variants were identified, respectively c.1438A>G (p.Asn480Asp) and c.494T>C (p.Phe165Ser), absent from GnomAD control population and predicted to be highly damaging. For ON_3, the variant segregates in the mildly affected father, while for ON_4 the mother of proband carries the same p.Phe165Ser variant and has a subclinical ON phenotype with macular drusen.

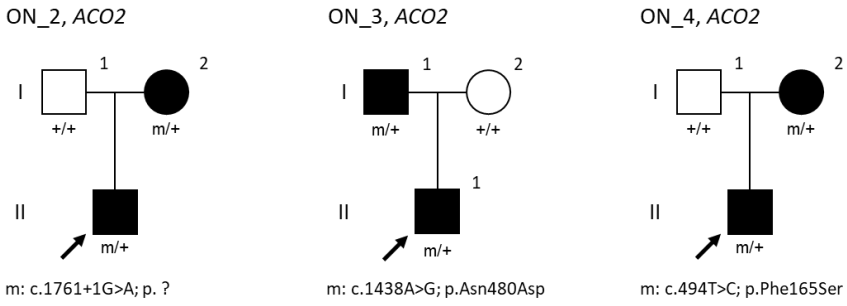

Figure 22. *Family trees for available ACO2 solved cases (ON_2 to ON_4)*

In other 4 cases (ON_5, 6, 7, 8) with typical DOA phenotype of pure optic atrophy, were identified *OPA1* variants classified as pathogenic or likely pathogenic with adjusted ACMG criteria. All variants are predicted to result in null alleles and are never reported in control population in GnomAD.

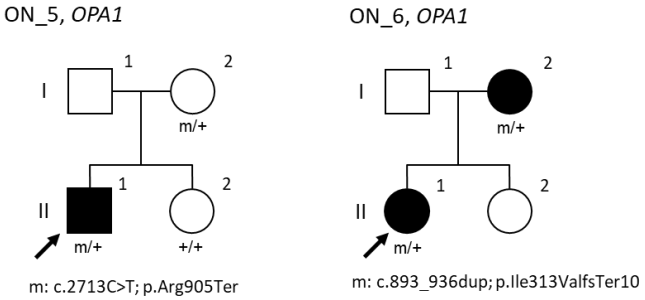

Figure 23. *Family trees for OPA1 solved cases (ON_5 and ON_6).*

Case ON_5 does not have a familiar history of disease (**Fig. 23**), and was found with change c.2713C>T that translates into a premature stop codon (p.Arg905Ter), already described in literature (18). The variant is inherited by the mother, reported as unaffected but not properly assessed through OCT exam. In case ON_6 a novel duplication of 43 bases was found (c.893_936dup), with a frameshift effect leading to premature translation termination (p.Ile313ValfsTer10). Also in this case, the variant is shared with the mother which however showed the expected DOA phenotype (**Fig. 23**). The ON_7 and ON_8 cases share both a familiar history compatible with AD transmission (**Fig. 24**) and identified variants in the 5' splice region of intron 12, where multiple splice-affecting mutations are described. For ON_7 case, the change c.1212+5G>A is already present in OPA1 LOVD database (DB-ID: OPA1_000353) as unpublished VUS and predicted to disrupt splice site (dbscSNV ADA score 0.9997). Furthermore, different nucleotide substitutions in the same position are classified as Pathogenic in ClinVar (c.1212+5G>T, VCV000214908.2) and in literature (c.1212+5G>C) (178). In ON_8 was involved the adjacent nucleotide (c.1212+6T>G), in a site never reported in literature or databases, but predicted to highly affect splicing (dbscSNV ADA score 0.9837). Moreover, variant segregation in the pedigree, supports the pathogenic role as it occurred *de novo* in the affected mother of the proband.

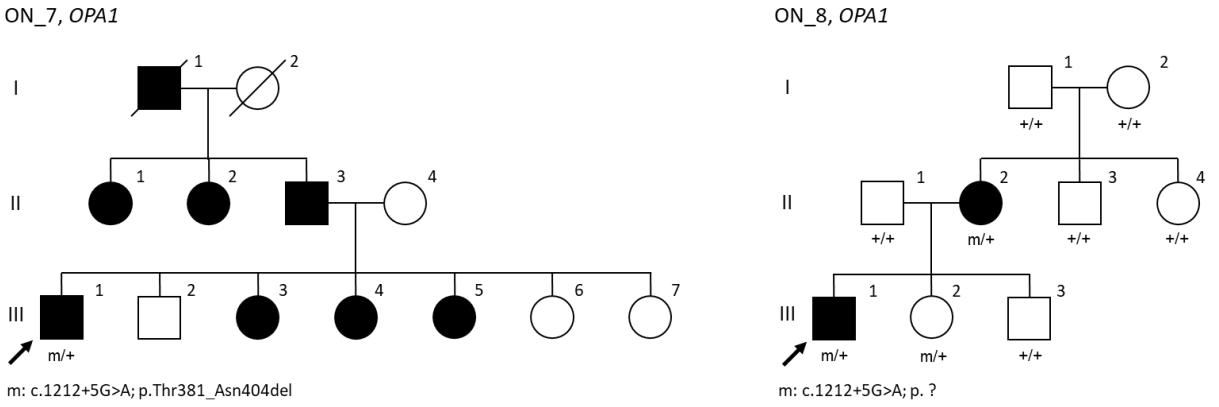

Figure 24. *Family trees for OPA1 solved cases (ON_7 and ON_8).*

For ON_7, since no affected family member was available for DNA sampling and variant segregation, a validation of impaired splicing of intron 12 was achieved through mRNA extraction from patient's blood PBMC and cDNA synthesis. A target *OPA1* transcript amplification then produced two bands, compared to a single band in a healthy control, and Sanger sequencing of the gel excised bands was performed. Sequencing results confirmed the predicted skipping of exon 12, as shown in **Fig. 25**.

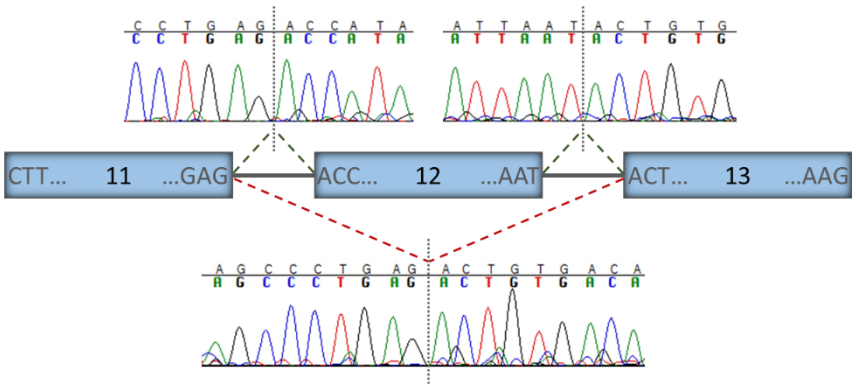

Figure 25. *Schematic representation of OPA1 cDNA splicing alteration in ON_7 due to variant c.1212+5G>C, showing wild-type (top) and mutant (bottom) amplification products chromatograms. The sequence derived from mutant allele shows an aberrant junction between exon 11 and 13, with skipping of exon 12.*

A sporadic case presenting optic atrophy and abnormal ocular abduction, ON_9, was found to harbour the change c.1351C>T in *SDHA*, encoding a subunit of respiratory complex II, causing a pathogenic missense mutation (p.Arg451Cys) already described in two unrelated AD pedigrees (179,180). While a few families have been reported with recessive forms of complex II deficiency due to *SDHA* mutations, leading to Leigh syndrome-like phenotypes, the AD cases usually show a combination of optic atrophy, myopathy/cardiomyopathy, ataxia, and developmental delay (73). With isolated optic atrophy, the case here described has a milder presentation than families described having the same p.Arg451Cys change, moreover it shows an incomplete penetrance since the proband's mother is unaffected carrier of the variant (**Fig. 26**).

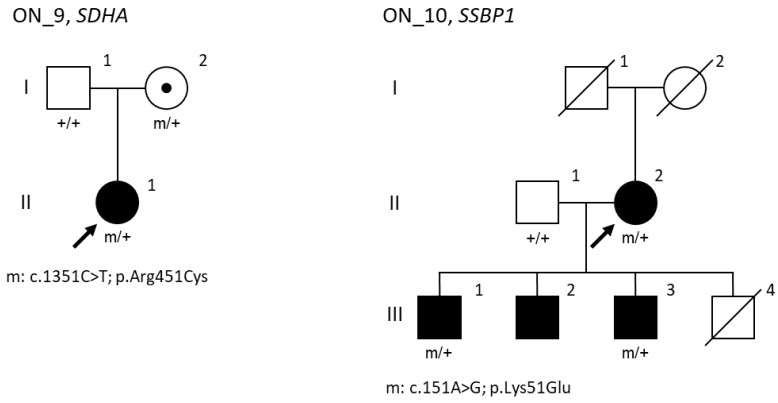

Figure 26. *Family trees for SDHA (ON_9) and SSBP1 (ON_10) solved cases.*

A last isolated dominant ON case was solved, ON_10, with the identification of a novel variant in *SSBP1* gene segregating with phenotype in the affected mother and brother (**Fig. 26**). Moreover, the missense change c.151A>G (p.Lys51Glu) is not present in GnomAD database but is classified as VUS with some pathogenic evidence by not having a strong *in silico* prediction of

pathogenicity. Recent works described mutation of mitochondrial single-stranded DNA-binding protein as causative of DOA/DOA plus phenotype mechanistically determined by mtDNA depletion and subsequent respiration defect (112–114), so this case is compatible with known *SSBP1* disease.

- **2.2. Autosomal and X-linked Recessive solved ON cases**

The 9 solved ON cases with recessive inheritance (12% of ON cohort) are listed in **Table 9**. Samples ON_11, ON_12, and ON_13 all presented without a family history of disease (**Fig. 27**), showing subacute-onset optic atrophy, coupled in ON_11 and ON_12 with exercise-induced lactic acidemia. The symptoms were suggestive of mitochondrial disease and especially LHON, but mtDNA tested negative for pathogenic mutations.

Table 9. *Gene and annotated variants identified in solved AR/XLR samples of ON cohort. HPO terms are shown except for HP:0000648-Optic atrophy, common to whole cohort.*

Sample	Sex	Age of onset	HPO Term Identifier	Gene	Transcript variant	Aminoacidic change	Variant class.	ACMG Criteria
ON_11	M	17 y	HP:0004901	*DNAJC30*	c.152A>G Homozygous	p.Tyr51Cys	P	PS3, PP5, PM1, PP3
ON_12	M	16 y	HP:0004901 HP:0000739	*DNAJC30*	c.152A>G Homozygous	p.Tyr51Cys	P	PS3, PP5, PM1, PP3
ON_13	M	15 y	-	*DNAJC30*	c.152A>G Homozygous	p.Tyr51Cys	P	PS3, PP5, PM1, PP3
ON_14	F	26 y	HP:0000407	*MECR*	c.772C>T Homozygous	p.Arg258Trp	P	PP5, PM2, (PP1), PP2, PP3
ON_15	M	16 y	-	*NDUFV2*	c.163T>G	p.Phe55Val	VUS (P)	PM2, (PM3), PP3
					c.674G>A	p.Cys225Tyr	VUS (P)	PM2, (PM3), PP3
ON_16	F	33 y	-	*WFS1*	c.2194C>T	p.Arg732Cys	LP	PM1, PM2, (PM3), PP2, PP3, PP5
					c.1656_ 1680dup	p.Ile561 ArgfsTer53	P	PVS1, PM2, (PM3), PP3
ON_17	M	7 y	-	*WFS1*	c.2213C>A	p.Ala738Asp	LP	PM2, (PM3), PP2, PP3
			-		c.1514_ 1528del	p.Cys505_ Val509del	LP	PM1, PM2, (PM3), PM4, PP3
ON_18	F	43 y	HP:0000020 HP:0002076	*WFS1*	c.1597C>T Homozygous	p.Pro533Ser	LP	PM1, PM2, PM5, PP2, PP3
ON_19	M	4 y	HP:0007642 HP:0000556	*CACNA1F*	c.2038C>T Hemizygous	p.Arg680Ter	P	PVS1, PP5, PM2, (PP1), PP3

WES then identified in the three patients a homozygous variant in *DNAJC30* gene, c.152A>G (p.Tyr51Cys), that is relatively common in Eastern Europe as result of a founder effect (GnomAD max MAF: 4.765E-3). Recent work described DNAJC30 as the most relevant AR cause of LHON phenotype, well characterizing p.Tyr51Cys pathogenic mechanism due to a reduced turnover of complex I N-module subunits, and our cases are included in the published families (10).

The samples ON_16, ON_17, and ON_18 (**Fig. 27**) showed clinical manifestation of isolated optic atrophy and were found to carry pathogenic or likely pathogenic variants in *WFS1* gene. Wolframin protein is located in MAMs, at interface between mitochondria and endoplasmic reticulum, and its dysfunction due to pathogenic mutations can cause recessive Wolfram syndrome as well as isolated DOA/ROA. In ON_16 we identified two variants in compound heterozygous state: one novel duplication with frameshift effect (c.1656_1680dup, p.Ile561ArgfsTer53) and one missense mutation in a mutational hotspot (c.2194C>T, p.Arg732Cys). The change p.Arg732Cys is present 15 times in GnomAD (max MAF: 6.092E-5) without homozygotes, and is also published as recessive allele in other two cases of Wolfram syndrome (181). Similarly, in ON_17 one novel in-frame deletion (c.1514_1528del, p.Cys505_Val509del), never observed in population, and one ultra-rare missense variant (c.2213C>A, p.Ala738Asp), with only 14 alleles in GnomAD (max MAF: 1.115E-4), were found in compound heterozygosity. The third case, ON_18, harbours instead the change c.1597C>T in a homozygous state, leading to missense change p.Pro533Ser. This variant is rare in population with 211 alleles in GnomAD (max MAF: 1.464E-3) and no homozygotes, and is already reported as pathogenic in recessive Wolfram syndrome cases (182,183).

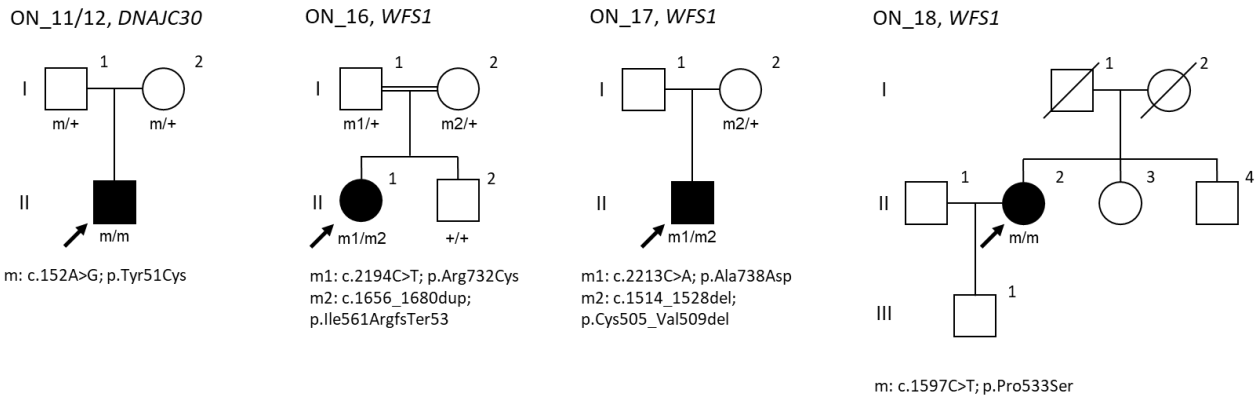

Figure 27. *Family trees for available DNAJC30 (ON_11 and ON_12) and WFS1 (ON_16, ON_17, and ON_18) solved cases.*

The recessive case ON_14 was one of two affected sisters showing an early-onset optic atrophy and a mild sensorineural hearing impairment (**Fig. 28A**). Through WES we identified a homozygous variant in *MECR* gene (c.772C>T, p.Arg258Trp), then confirmed also in the affected sister. This variant is present in GnomAD database with 18 alleles (max MAF:1.385E-4) and is the most frequently reported in the few syndromic infantile cases with DYTOABG described in literature, always in compound heterozygous state (90,91,184).

Since MECR protein is involved in mitochondrial fatty acids biosynthesis, its dysfunction can be observed through defect in mitochondrial proteins lipoylation and subsequent respiration impairment. For the assessment of pathogenic mechanism and possible therapeutic strategy, a yeast strain was established expressing in a multi-copy plasmid the human *MECR* gene, also with variant R258W, to compensate for low conservation of yeast hortolog *ETR1*. Mutant R258W yeast has reduced growth phenotype on oxidizable carbon sources (**Fig. 28B**) and a defect in mitochondrial respiration.

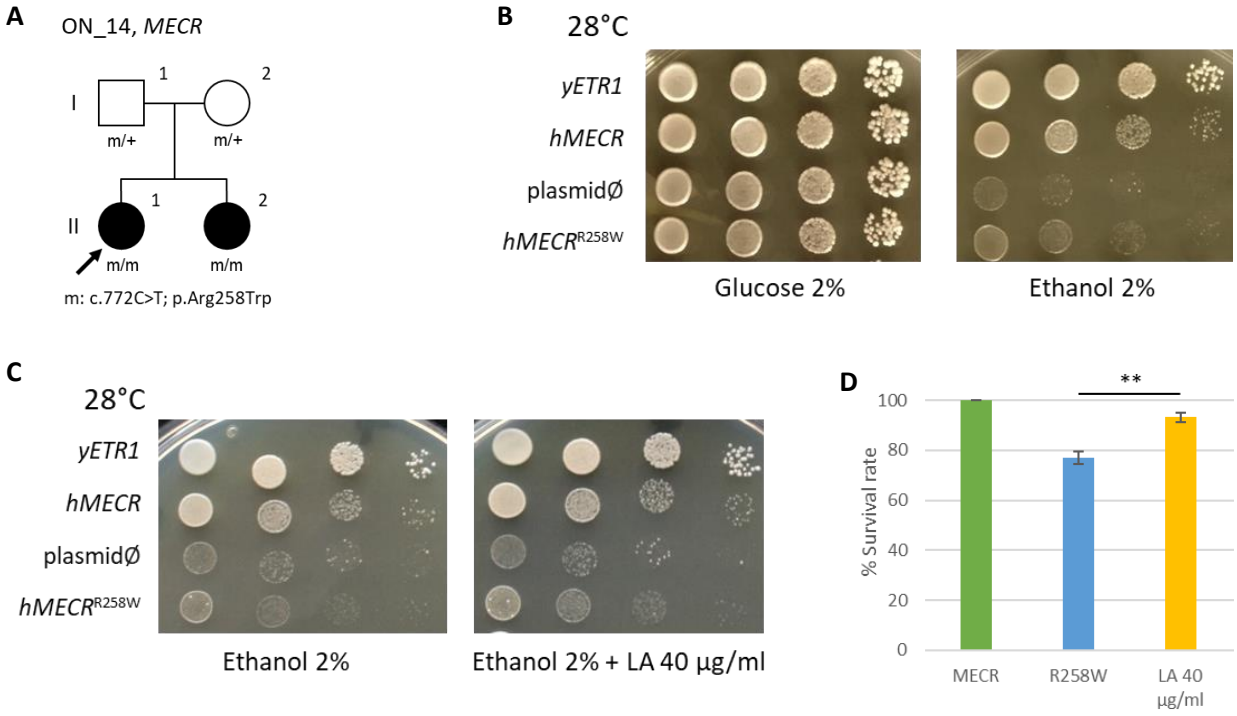

Figure 28. *(A) Family tree of ON_14 . (B) Growth of yeast strains wild-type (yETR1), complemented with human MECR gene (hMECR), expressing empty vector (plasmidØ), and mutant for R258W variant (hMECRR258W), with Glucose as fermentable carbon source, or Ethanol as oxidizable carbon source inducing obligate oxidative phosphorylation, at 28 °C. (C) Growth phenotype of the same yeast strains on Ethanol medium with addition of 40 µg/ml lipoic acid (LA), at 28 °C. (D) Survival rate of hMECR and hMECRR258W exposed to H2O2 1mM for 2h, with addition of 40 µg/ml lipoic acid. **P < 0.01, t-test*

The R258W enzyme is associated with relevant protein instability, moreover the lack of lipoic acid biosynthesis is reflected in no detectable lipoylation of TCA cycle enzymes pyruvate dehydrogenase and α-ketoglutarate dehydrogenase (data not shown). As a possible treatment for MECR mutants, lipoic acid was then supplemented to culture medium at 40 μg/ml: a modest growth rescue on non-fermentable substrate was observed, as well as protection against oxidative stress cause by H_2O_2 to which R258W mutant strain is particularly sensitive (**Fig. 28C, D**).

Another sporadic case, ON_15 (**Fig. 29**), presenting with subacute-onset optic atrophy clinically resembling LHON, was solved with identification of two compound heterozygous variants in complex I subunit *NDUFV2*, predicted as VUS with pathogenic evidence. The change c.674G>A (p.Cys225Tyr) is novel and affects a conserves aminoacidic residue with damaging prediction, while the change c.163T>G (p.Phe55Val) is an ultra-rare allele in population, with 3 carriers reported in GnomAD (max MAF:1.39E-4), that also is largely predicted as damaging. While optic atrophy is a common feature after complex I impairment, the literature reports only severe cases carrying loss-of-function and missense variants in *NDUFV2*, showing Leigh syndrome-like phenotype, with or without cardiomyopathy, or leukoencephalopathy (46).

Finally, ON_19 is the only ON case harbouring an X-linked variant. The patient presented with optic atrophy, night blindness and retinal dystrophy, and a family history compatible with XLR inheritance with affected maternal grandfather but healthy parents (**Fig. 29**). We found in *CACNA1F* gene a hemizygous stop-gain variant, c.2038C>T (p.Arg680Ter) that is absent from GnomAD database and is reported in literature for different pedigrees with congenital stationary night blindness (185,186). This gene encodes a voltage-sensitive calcium channel specific of the retina, and combined presence of stationary night blindness and optic atrophy appears to be a common feature of *CACNA1F* cases (124).

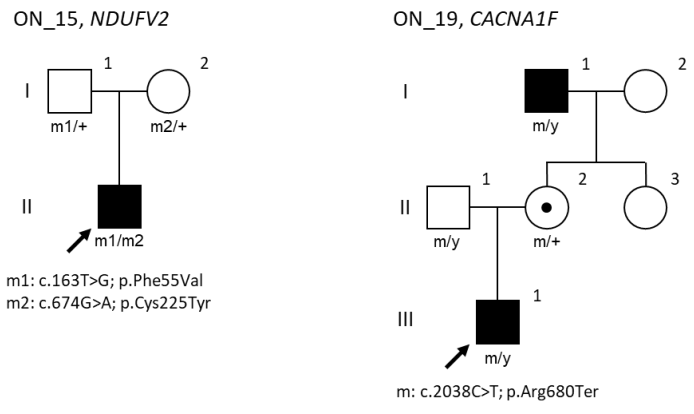

Figure 29. *Family tree for NDUFV2 (ON_15) and CACNA1F (ON_19) solved cases.*

- **2.2. VUS and GUS cases in ON cohort**

As shown in **Table 10**, all ON samples categorized as VUS (*n*=4, 5% of ON cohort) or GUS (*n*=1, 1% of ON cohort) harbour variants compatible with AD inheritance.

The sporadic case ON_20 presented with isolated optic atrophy and, noticeably, two different candidate pathogenic variants were identified in WES data. The first one is a novel variant (c.1515A>G, p.Lys505=) in *OPA1* gene, that does not alter the aminoacidic residue but is classified as VUS considering that is absent from population. Since c.1515A>G is located at -2 position in exon 15 3' junction, probably impacting this canonical splice donor site (ADA score 0.9996), the variant could also be classified as likely pathogenic with further evidence of splicing impairment. The second variant in *WFS1* gene (c.2302A>C, p.Lys768Gln) is classified as VUS of likely pathogenic effect and this gene is also compatible with DOA-like phenotype. This variant is not published nor reported in GnomAD, where, however, there is 1 allele (max MAF: 9.066E-6) for a different aminoacidic change in the same residue (p.Lys768Arg). Since no family member of ON_20 is available for segregation of the variants, the case is best left in the VUS category, pending experimental evidence of splicing alteration in *OPA1* transcript or functional validation of *WFS1* missense variant.

Table 10. *Gene and annotated variants identified in VUS and GUS samples of ON cohort. HPO terms are shown except for HP:0000648-Optic atrophy, common to whole cohort.*

Sample	Sex	Age of onset	HPO Term Identifier	Cat.	Gene	Transcript variant	Aminoacidic change	Variant class.	ACMG Criteria
ON_20	F	NA	-	VUS	*OPA1*	c.1515A>G	p.Lys505=	VUS	PM2
		NA	-		*WFS1*	c.2302A>C	p.Lys768Gln	VUS (LP)	PM2, PP2, PP3
ON_21	F	Birth	HP:0000556 HP:0006934	VUS	*SDHA*	c.1877C>A	p.Thr626Asn	VUS (P)	PM2, (PM6), PP3
ON_22	M	12 y	-	VUS	*UCHL1*	c.586-2A>C	Splice site	P	PVS1, PM2, (PP1), PP3
ON_23	F	23? y	-	VUS	*UCHL1*	c.284T>G	p.Leu95Arg	VUS (LP)	PM2, PP2, PP3
ON_24	F	Childhood	HP:0000501	GUS	*NUTF2*	c.365C>T	p.Ala122Val	VUS	PM2

In another sporadic case, ON_21, with clinical manifestation of optic atrophy, retinal dystrophy, and nystagmus, was identified a novel missense variant in *SDHA* gene (c.1877C>A, p.Thr626Asn). The variant occurred *de novo* in the proband, in absent from GnomAD database and is predicted to be damaging, thus gaining a likely pathogenic classification. Since only two

missense dominant variants (p.Arg451Cys and p.Arg662Cys) in *SDHA* are reported in literature (74,180), pathogenic mechanism should be validated for this novel proposed dominant variant, hence the VUS label for case ON_21.

Case ON_22 is the proband of a family showing AD transmission of isolated optic atrophy. After extensive segregation studies on all family members of identified deleterious variants, only one variant in *UCHL1* resulted to segregate with phenotype also in the two affected siblings and subclinical affected mother (**Fig. 30**). The c.586-2A>C change, never reported in GnomAD database, is predicted to disrupt a canonical splice acceptor site at 5' of exon 9 (dbscSNV ADA score 0.9999), acting as a null allele and so classified as pathogenic. Another novel variant in *UCHL1* was found in sample ON_23, with c.284T>G substitution resulting in a missense change p.Leu95Arg. The variant is classified as VUS with minor pathogenic evidence since absent from control population and affecting a well conserved aminoacid with predicted deleterious effect. Moreover, it segregates with optic atrophy in the mother, but the affected sister is not available for sampling and further segregation. The *UCHL1* gene encodes a deubiquitinating enzyme (DUB) with numerous targets identified, especially abundant in neurons and in some cancers (187). Mutations in *UCHL1* are so far associated with a severe Behr syndrome-like phenotype with AR inheritance (188–190), thus functional studies are ongoing to validate AD inheritance pattern here observed and are presented in Results paragraph 5.

Finally, case ON_24 (**Fig. 30**) presented a sporadic optic atrophy and glaucoma, and a novel VUS (c.365C>T) was detected in *NUTF2* gene, leading to a missense change (p.Ala122Val) with moderate pathogenicity prediction due to conservative substitution. This gene is located inside the OPA8 locus (16q21-q22) established by linkage analysis (191) and so considered here a gene of uncertain significance (GUS). Experimental validation is however required to demonstrate the causative role for *NUTF2* in DOA, also considering the gene product is a nuclear transport factor and can act on many targets and pathways involved in mitochondrial function.

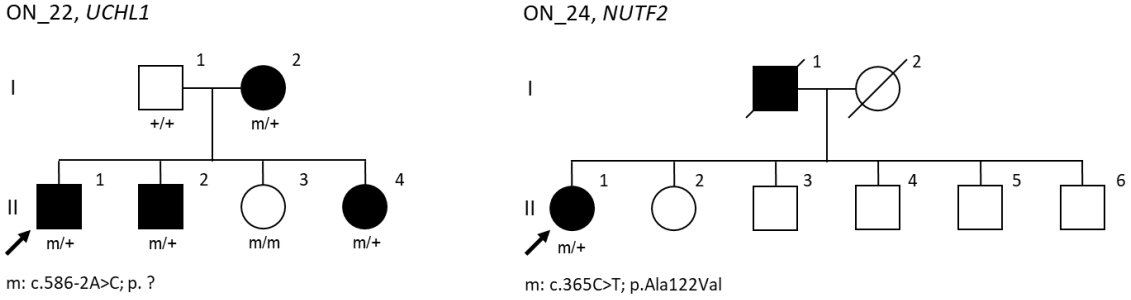

Figure 30. *Family tree available for UCHL1 (ON_22) and NUTF2 (ON_24) VUS and GUS cases.*

3. WES results in syndromic Optic Neuropathies

In the sON cohort 10 cases are labelled as solved, with total diagnostic yield of 31%. A different causative gene was identified in each of the samples, namely AFG3L2 for AD cases, and C19orf12, FDXR, LYST, MTFMT, NDUFAF2, PDSS1, SLC52A2, WFS1, and NDUFB11 for AR/XLR cases. Details for all sON cases, including age of onset and sampling, complete HPO terms phenotyping, and compatible inheritance at presentation are listed in Appendix Table 2, describing the whole cohort.

- **3.1. Autosomal Dominant solved sON cases**

A single AD case can be classified as solved in sON cohort (3% of sON cohort), reported in **Table 11** with variant annotation and classification.

Table 11. *Gene and annotated variants identified in solved AD samples of sON cohort. HPO terms are shown except for HP:0000648-Optic atrophy, common to whole cohort.*

Sample	Sex	Age of onset	HPO Term Identifier	Gene	Transcript variant	Aminoacidic change	Variant class.	ACMG Criteria
sON_1	M	Childhood	HP:0001249 HP:0002650 HP:0001760 HP:0002174 HP:0002345 HP:0002451 HP:0007256	*AFG3L2*	c.1064C>T	p.Thr355Met	P	(PS1), (PS2), PS3, PM1, PM2, (PM6) PP2, PP3

The patient sON_1 presented as a sporadic case (**Fig. 31**) with childhood-onset movement disorders, including tremor, limb dystonia and pyramidal signs, with addition of intellectual disability and optic atrophy. WES allowed the identification of a missense variant (c.1064C>T, p.Thr355Met) in the *AFG3L2* gene, which was subsequently sequenced in the parents revealing a *de novo* mutational event.

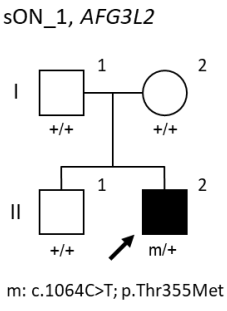

Fig. 31. *Family tree for AFG3L2 (sON_1) solved case.*

The same variant, also absent from control population, was recently described in literature (37) with dominant effect and overlapping phenotype of optic atrophy plus dystonia and cognitive impairment, a typical presentation for DOA plus associated with *AFG3L2* mutation (OPA12, MIM#618977).

- **3.2. Autosomal and X-linked Recessive solved sON cases**

For recessive sON, 9 cases (28% on sON) are considered solved and are listed in Table 10 with respective annotated variants.

Table 12. *Gene and annotated variants identified in solved AR/XLR samples of sON cohort. HPO terms are shown except for HP:0000648-Optic atrophy, common to whole cohort.*

Sample	Sex	Age of onset	HPO Term Identifier	Gene	Transcript variant	Aminoacidic change	Variant class.	ACMG Criteria
sON_2	F	NA	HP:0001251 HP:0001256 HP:0001300 HP:0002180 HP:0012675	*C19orf12*	c.172G>A Homozygous	p.Gly58Ser	P	(PS1), PM1, PM2, PP2, PP3
sON_3	M	Childhood	HP:0002131 HP:0000708 HP:0000407 HP:0011712 HP:0003477 HP:0000639 HP:0007687 HP:0001290 HP:0002460 HP:0001284 HP:0002066 HP:0001761	*FDXR*	c.1A>G c.1102G>A	p.Met1? p.Asp368Asn	P P	PVS1, PM2, (PM3), PP3 PS3, PM2, (PM3), PP2, PP3
sON_4	F	25 y	HP:0001251 HP:0003477 HP:0002360 HP:0001388 HP:0000407 HP:0001171 HP:0003202 HP:0001324 HP:0007256 HP:0001336 HP:0001310	*LYST*	c.3296C>A Homozygous	p.Ser1099Ter	P	PVS1, PM2, PP3
sON_5	M	Childhood	HP:0004901 HP:0002075 HP:0002403 HP:0030891 HP:0003390 HP:0002076 HP:0100507	*MTFMT*	c.518C>T Homozygous	p.Thr173Ile	LP	PM2, (PP1), PP2, PP3

sON_6	F	Childhood	HP:0008587 HP:0003390 HP:0003128 HP:0002514 HP:0002624 HP:0100502	*NDUFAF2*	c.95A>G c.148del	p.Tyr32Cys p.Arg50 GlufsTer3	LP P	PM2, (PM3), (PP1), PP3 PVS1, PM2, (PM3), PP3
sON_7	M	9 y	HP:0000407 HP:0001256 HP:0001324	*PDSS1*	c.735G>T Homozygous	p.Gln245His	LP	PM2, PP1, PP3, PP4
sON_8	F	4 y	HP:0008587 HP:0003477 HP:0003390 HP:0007002 HP:0001649 HP:0100507 HP:0003710	*SLC52A2*	c.1244G>C c.1255G>A	p.Gly415Ala p.Gly419Ser	LP LP	PM1, PM2, (PM3), PP2, PP3 PM1, PM2, (PM3), PP2, PP3, PP5
sON_9	M	26 y	HP:0002120 HP:0001272 HP:0007366 HP:0000819 HP:0000407	*WFS1*	c.2029G>A c.2206G>A	p.Ala677Thr p.Gly736Ser	LP LP	PM2, (PM3), PP2, PP3 PM2, (PM3), PM5, PP5, PP2, PP3
sON_10	M	Birth	HP:0001889 HP:0100507 HP:0005264	*NDUFB11*	c.276_278del Hemizygous	p.Phe93del	P	(PS2), PM1, PM2, (PM6), PP3, PP5

The case sON_2 presented with iron accumulation in brain at MRI, ataxia, mild intellectual disability, and parkinsonian features, that are consistent with identified homozygous variant in *C19orf12* (c.172G>A, p.Gly58Ser). Protein C19orf12 is located in mitochondrial and ER membrane, as well as in MAMs, where it participates in lipid homeostasis and Ca^{2+} handling. Pathogenic variants in this gene are associated with a distinctive form of neurodegeneration with brain iron accumulation (NBIA4), also known as mitochondrial membrane protein-associated neurodegeneration (MPAN). The variant detected in sON_2 case is ultra-rare in GnomAD database with 1 allele (max MAF: 8.859E-6) and already published as pathogenic in one Italian NBIA4 case, with functional validation in cell line models showing impaired protein localization, response to oxidative stress, and Ca^{2+} homeostasis (192,193).

The complex clinical manifestation of sporadic case sON_3 (**Fig. 32**) included ataxia, peripheral axonal neuropathy, sensorineural hearing impairment, hypotonia, areflexia, nystagmus, and optic atrophy. The sample was found compound heterozygous for two deleterious variants in FDXR gene, encoding the mitochondrial ferredoxin reductase involved in biosynthesis of iron–sulfur (Fe-S) clusters, needed as cofactors in respiration complexes. A wide clinical spectrum is described for *FDXR* disease, and our case's phenotype matches the most common symptoms of optic atrophy, hearing impairment, and movement disorder (88). In sON_3 we found a change

c.1A>G (p.Met1?) leading to a null allele due to start loss, absent from population and reported in literature as pathogenic (194). The second allele c.1231G>A (p.Asp368Asn) is present in 2 individuals in GnomAD database (max MAF: 3.266E-5) and results in a damaging missense change also classified as pathogenic and found in literature (195).

For sample sON_4, without a family history of disease (**Fig. 32**), mainly neuromuscular involvement was described, with ataxia, peripheral axonal neuropathy, muscle weakness and atrophy, myoclonus, then hearing impairment, sleep disturbance and mild optic atrophy. A homozygous novel variant in *LYST* gene was discovered (c.3296C>A) leading to a stop-gain (p.Ser1099Ter), never reported in GnomAD database and classified as pathogenic. The Lysosomal-trafficking regulator (LYST) protein regulates intracellular vesicles biogenesis, such as lysosomes, and is involved in exocytosis. Typically, *LYST* mutations cause the lysosomial Chediak Higashi syndrome (196) with severe infantile-onset, but late-onset heterogeneous milder phenotypes characterized by neurodegeneration are reported (197,198).

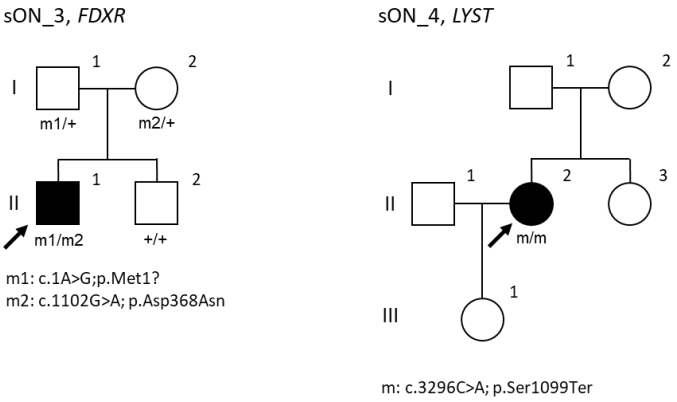

Fig. 32. *Family tree for FDXR (sON_3) and LYST (sON_4) cases.*

The case sON_5 presented with exercise-induced lactic acidemia, white matter hyperdensities, dysdiadochokinesis, sensory axonal neuropathy, migraine, and optic atrophy. The pedigree of sON_8 (II-2) was compatible with AR inheritance disease, as it is one of 4 siblings of which the other male (II-1) has a Leigh-like encephalomyopathy with optic atrophy phenotype, one female (II-3) has minor symptoms (hypogonadism, hearing loss) and another female is unaffected (II-4) (**Fig. 33A**). A missense likely pathogenic variant in homozygous state in *MTFMT* (c.518C>T, p.Thr173Ile) was identified, corresponding to an ultra-rare allele reported 2 times in GnomAD (max MAF: 1.771E-5) with strong pathogenicity prediction. This variant segregated in the 3 affected siblings and observed clinical features are consistent with the ones found in *MTFMT*-associated Leigh syndrome of variable severity and progression (110).

Further validation of *MTFMT* variant T173I was done in yeast, using a specific strain built to express a plasmid containing the human gene, instead of using targeted mutagenesis of the yeast hortolog *FMT1* which is not highly conserved. Yeast model with introduced T173I shows impaired growth on non-fermentable carbon sources due to respiration impairment (**Fig. 33B**) and has lower levels of MTFMT protein (~60% of wild-type, P < 0.01, data not shown). Since MTFMT deficiency impacts mitochondrial protein synthesis through the lack of formylated methionyl-tRNA, translation assays were performed. A significant reduction (P < 0.01) of mitochondrial protein synthesis was confirmed, with a small decrease (~20%) in complex IV subunits levels and consequent biochemical activity impairment (~60% of wild-type, P < 0.01, data not shown).

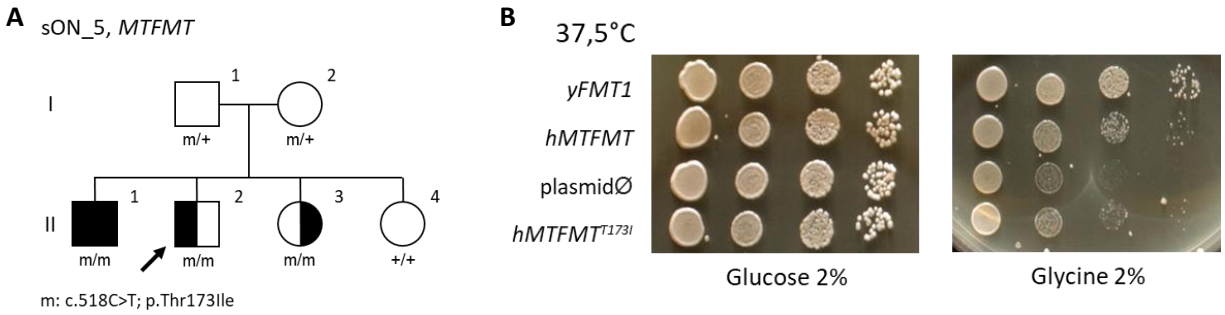

Fig. 33. *(A) Pedigree of sON_5. (B) Growth of yeast strains wild-type (yFMT1), complemented with human MTFMT gene (hMTFMT), expressing empty vector (plasmidØ), and mutant for T173I variant (hMTFMTT173I), with Glucose as fermentable carbon source, or Glycine as oxidizable carbon source inducing obligate oxidative phosphorylation, at 37.5 °C.*

In sON_6 patient, the clinical presentation included cerebral calcifications, lactic acidosis, mild hearing impairment, venous anomalies, and optic atrophy, with available pedigree pointing to an AR disease (**Fig. 34**). Two compound heterozygous variants were detected in *NDUFAF2* gene, encoding an assembly factor of respiratory complex I: a missense change classified a VUS with pathogenic evidence (c.95A>G, p.Tyr32Cys), ultra-rare in population (2 GnomAD alleles, max MAF: 1.759E-5), and a novel deletion with frameshift effect (c.148del, p.Arg50GlufsTer3), thus classifies ad pathogenic. Moreover, the changes segregated with phenotype in one affected brother of the proband. The cases previously described in literature also commonly presented with optic atrophy, but included a severe early-onset complex I deficiency (199).

Case sON_7 is born from consanguineous parents, presenting in childhood with sensorineural hearing impairment, mild intellectual disability, and muscle weakness, followed by progressive

optic atrophy. In gene *PDSS1*, a novel likely pathogenic variant (c.735G>T) was identified, leading to damaging missense change (p.Gln245His) of a highly conserved residue, located in a region of homozygosity of 12 Mb. The same phenotype and homozygous variant were present in one affected sister of the proband (**Fig. 34**), and they are now part of a published case report (200). PDSS1 (All trans-polyprenyl-diphosphate synthase) protein is a key component for synthesis of ubiquinone (CoQ10) side chain and its mutation is therefore associated with CoQ10 deficiency. Only two AR pedigrees have been reported in literature with *PDSS1* pathogenic variants: the first one with early-onset deafness, optic atrophy, peripheral neuropathy and mental retardation (201), consistent with presentation of our sON_8 case, and a second one with severe developmental delay and lethal nephrotic syndrome (202).

Patient sON_8 showed hearing impairment and optic atrophy, together with peripheral, sensory, and motor axonal neuropathy, and without a family history of disease (**Fig. 34**). Two compound heterozygous likely pathogenic variants were found in gene *SLC52A2*, compatible with Brown-Vialetto-Van Laere syndrome (BVVLS) that has overlapping clinical features to our case. The first missense variant (c.1244G>C, p.Gly415Ala) is ultra-rare in control population with 3 alleles (max MAF: 2.649E-5), moreover, it is reported in ClinVar as likely pathogenic (VCV000959515.3) and in an undefined neurological disease patient in literature (203). A second missense variant (c.1255G>A, p.Gly419Ser) is absent from GnomAD database, classified as pathogenic in ClinVar (VCV000040232.1) and already discovered in a case of BVVLS in compound heterozygosity (204). As a riboflavin transporter deficiency, riboflavin supplementation is an effective treatment to this clinical manifestation and was started also in sON_9 case after molecular diagnosis.

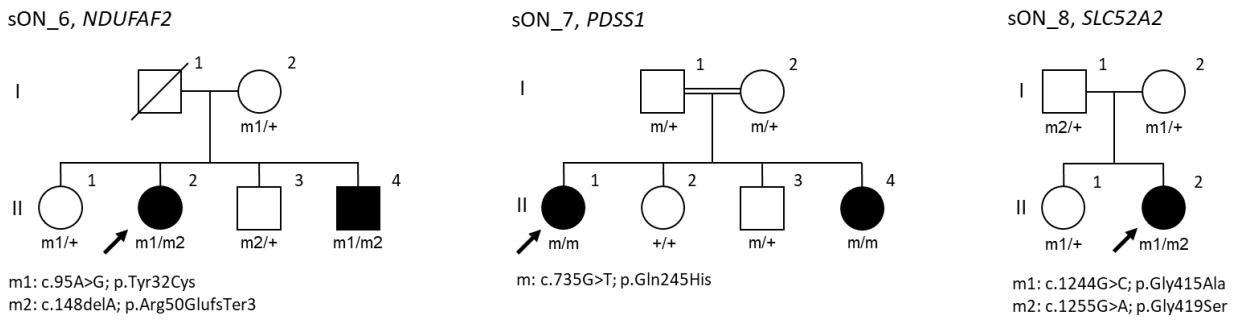

Fig. 34. *Family trees for NDUFAF2 (sON_6), FDXR (sON_7), and SLC52A2 (ON_8) solved cases.*

The clinical situation of sON_9 included optic atrophy, sensorineural hearing impairment, diabetes mellitus, cerebral, cerebellar and brainstem atrophy (**Fig. 35**). The presentation is

compatible with Wolfram syndrome and explained by compound heterozygous variants found in *WFS1* gene. The variant c.2029G>A, classified as likely pathogenic and leading to missense deleterious p.Ala677Thr change, is found in 22 alleles in GnomAD database (max MAF: 1.634E-4) and classified as VUS in ClinVar (VCV000198834.3) in association with deafness. The second variant c.2206G>A is classified as pathogenic, is even rarer in population with 8 alleles in GnomAD (max MAF: 5.556E-5) and consequent change p.Gly736Ser is published in two Wolfram syndrome pedigrees (205,206). Besides, also two other missense changes, with a different aminoacidic residue (p.Gly736Ala and p.Gly736Asp), are reported in literature in Wolfram syndrome (207,208). The two variants p.Ala677Thr and p.Gly736Ser segregate separately in proband's daughters, that respectively show only deafness (II-2) and optic atrophy (II-1) symptoms, pointing to a possible semidominant behaviour.

Lastly, the case sON_10 presented with sporadic optic atrophy, megaloblastic anemia, folate deficiency and abnormal gallbladder. A pathogenic in-frame hemizygous deletion (c.276_278del) was detected in X-linked *NDUFB11* gene, causing a single aminoacid loss in the protein (p.Phe93del), that occurred *de novo* in the proband (**Fig. 35**). NDUFB11 protein is an accessory subunit of mitochondrial respiratory CI and its dysfunction is reported to cause different clinical phenotypes: a severe infantile syndrome Linear Skin Defects with Multiple Congenital Anomalies (LSDMCA3, MIM#300952) (209), a congenital lactic acidosis with hypertrophic cardiomyopathy and CI deficiency (210), or a pure/syndromic X-linked sideroblastic anemia. This phenotype is recurrently caused by p.Phe93del also present in sON_10, often with *de novo* origin, and usually coupled with optic atrophy (211,212).

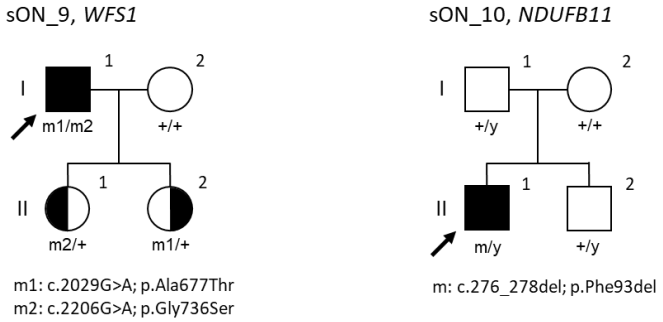

Fig. 35. *Family trees for WFS1 (sON_9) and NDUFB11 (sON_10) solved cases.*

- **3.2. VUS and GUS cases in sON cohort**

A total of 6 cases are considered VUS in the sON cohort (19% of sON cohort), with 3 identified with AD inheritance and 2 with AR inheritance, plus an "AD?" case that needs further genetic study. Samples classified as VUS are listed in Table 12 with respective annotated variants.

Table 13. *Gene and annotated variants identified in VUS samples of sON cohort. HPO terms are shown except for HP:0000648-Optic atrophy, common to whole cohort.*

Sample	Sex	Age of onset	HPO Term Identifier	Inher.	Gene	Transcript variant	Aminoacidic change	Variant class.	ACMG Criteria
sON_11	F	NA	HP:0001256 HP:0001272 HP:0000508	AD	*CACNA1A*	c.5381T>C	p.Phe1794Ser	LP	PM1, PM2, PP2, PP3
sON_12	M	60 y	HP:0004944 HP:0000726 HP:0001300 HP:0002134 HP:0030891 HP:0002120 HP:0000011 HP:0002360	AD	*GFAP*	c.1068G>C	p.Lys356Asn	LP	PM1, PM2, (PP1), PP2, PP3
sON_13	F	Birth	HP:0001258 HP:0000924	AD	*KIF1A*	c.3749+7G>A	Splice region	VUS (LP)	PM2, PP1, BP4
sON_14	M	3 y	HP:0001332 HP:0002174 HP:0002134 HP:0001249 HP:0000407 HP:0031931 HP:0000639	AD?	*SDHA*	c.1127T>C	p.Leu376Pro	VUS (LP)	PM2, PP3
sON_15	M	17 y	HP:0001251 HP:0001324 HP:0007351	AR	*BTD*	c.956C>A c.98_104 delinsTCC	p.Ser319Tyr p.Cys33 PhefsTer36	VUS (P) P	PM1, PM2, PP3 PVS1, PP5, PM2
sON_16	M	2y	HP:0000486 HP:0000639 HP:0000407 HP:0003690 HP:0003124 HP:0025379 HP:0004901 HP:0006827 HP:0100561	AR	*USH2A*	c.5858C>G c.9614G>A	p.Ala1953Gly p.Arg3205His	VUS (LP) VUS (LP)	PM2, PP2, PP3 PM2, PP2

In sON_11, clinical manifestations of optic atrophy, mild intellectual disability, cerebellar atrophy, and ptosis were attributed to a novel likely pathogenic missense variant in calcium channel gene *CACNA1A* (c.5381T>C, p.Phe1794Ser). The variant is not present in GnomAD database, has concordant pathogenicity predictions as damaging, and patient shows common features to *CACNA1A* phenotypes like spinocerebellar ataxia. This case, however, falls in the

VUS category since optic atrophy is only rarely present in *CACNA1A* patients, reported in rare biallelic condition (125), and there is no available family member to confirm segregation of the variant with phenotype, thus requiring functional validation for the pathogenic effect of the variant. The case sON_12 presented with adult-onset dementia, parkinsonism, abnormality of basal ganglia and white matter, cerebral cortical atrophy, sleep disturbance and optic atrophy. Moreover, familiar history pointed to an AD disease, with mother affected by dementia and a sister with an overlapping phenotype (**Fig. 36**). A novel missense variant in *GFAP* gene was discovered (c.1068G>C, p.Lys356Asn), classified as likely pathogenic being absent in GnomAD database and predicted to have a deleterious effect. Variants in this gene, encoding the glial fibrillary acidic protein that is an astrocyte-specific intermediate filament, usually cause Alexander disease (ALXDRD, MIM#203450), a neurological progressive syndrome that varies from neonatal lethal forms to mild heterogeneous adult forms (213). The variant could not be responsible for the whole clinical spectrum observed, especially optic atrophy, so VUS classification is best applied for sON_12.

Another case compatible with AD inheritance is sON_13 (**Fig. 36**), presenting with congenital optic atrophy, spastic paraplegia, and abnormality of the skeletal system. A c.3749+7G>A variant in *KIF1A* gene was identified, with possible impact on splice donor region of intron 35, also segregating in the affected brother of proband. The variant is ultra-rare in GnomAD database with 1 allele (max MAF: 1.131E-5) and classified as VUS with minor pathogenic evidence. *KIF1A* encodes a kinesin involved in anterograde axonal transport of synaptic vesicle precursors and is also a genetic cause of AD neurodegeneration and spasticity with or without cerebellar atrophy or cortical visual impairment (NESCAVS, MIM#614255), a form of PEHO so including optic atrophy (214,215). Our patients' phenotype could be part of a NESCAV syndrome presentation, but validation of the real effect on mRNA of a splice region variant is mandatory.

The sON_14 (**Fig. 36**) case showed clinical features of dystonia, postural tremor, abnormality of the basal ganglia, intellectual disability, sensorineural hearing impairment, nystagmus, and optic atrophy. A single novel missense variant in *SDHA* gene was detected (c.1127T>C, p.Leu376Pro), predicted as damaging and classified as VUS with minor pathogenic evidence. Similarly to ON_20 case, also here functional validation must be performed to confirm its pathogenic role, especially because proband's mother is unaffected carrier of the variant. For

this case, data from fibroblast lines and muscle biopsy experiments are presented in Results paragraph 4.

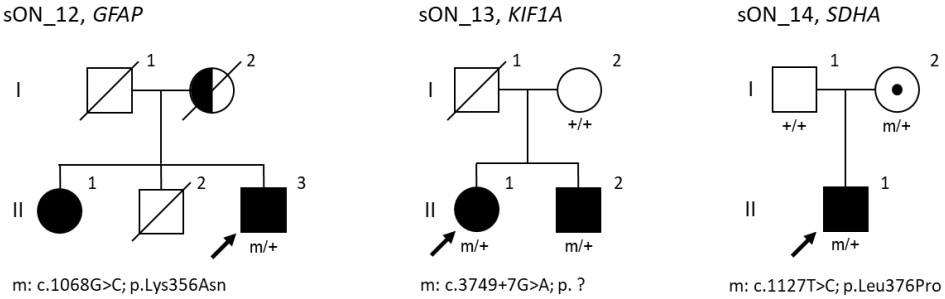

Fig. 36. *Family trees for GFAP (sON_12), KIF1A (sON_13), and SDHA (sON_14) VUS cases.*

The sporadic patient sON_15 (**Fig. 37**), presenting with ataxia, muscle weakness, upper limb postural tremor, and optic atrophy, was found to carry two heterozygous variants in *BTD* gene. One variant is a common, well established pathogenic frameshift (c.98_104delinsTCC, p.Cys33PhefsTer36) (216), while the second one (c.956C>A, p.Ser319Tyr) is a novel likely pathogenic missense, absent from both GnomAD and *BTD* pathogenic mutations database (https://arup.utah.edu/database/BTD/BTD_welcome.php) (128). The VUS status of sON_17 is justified by lack of variants segregation studies, to confirm the two alleles are present *in trans*, and of functional validation of novel variant. Known phenotype for AR biotinidase deficiency (BTD, MIM#253260) caused by *BTD* mutation is a good match to our case, and this diagnosis can have direct impact on patient management since the symptoms are known to recover at least partially after biotin supplementation (217).

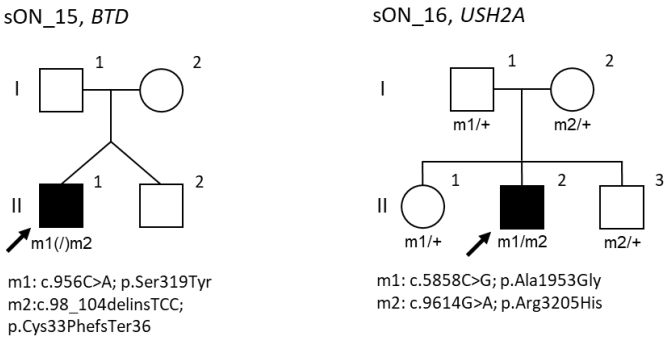

Fig. 37. *Family trees for BTD (sON_15) and USH2A (sON_16) VUS cases.*

Finally, for sporadic case sON_16 (**Fig. 37**), whose clinical features include optic atrophy, hearing impairment, exercise-induced lactic acidemia, spinal cord atrophy and limb muscle weakness, two compound heterozygous missense variants were identified in *USH2A* gene. The protein Usherin encoded by this gene is a component of cilia found in inner ear sensory cells

and in retinal photoreceptors, and its dysfunction causes Usher syndrome type 2A (USH2A, MIM#276901) with hearing impairment and retinitis pigmentosa. The first variant (c.5858C>G) results in change p.Ala1953Gly and possibly affects splice acceptor site of exon 30, it is however not rare on GnomAD, where 233 alleles but no homozygotes are recorded (max MAF: 1.944E-3). ClinVar classify it with conflicting interpretations of pathogenicity (VCV000048546.15), because of its frequency in population that can explain the findings in multiple cases of Usher syndrome (218,219) where other causative variants in the gene are present. The second variant (c.9614G>A, p.Arg3205His) is classified as VUS with minor pathogenic evidence, because observed in 26 GnomAD alleles (max MAF: 1.96E-4) but never in homozygosity and without strong pathogenicity prediction. This variant in not published in Usher syndrome cases and ClinVar labels it with conflicting interpretations of pathogenicity (VCV000432352.5). The contrasting reports and patient's phenotype not completely overlapping with Usher syndrome put this sample in VUS category, pending further clinical and experimental findings.

Table 14. *Gene and annotated variants identified in GUS samples of sON cohort. HPO terms are shown except for HP:0000648-Optic atrophy, common to whole cohort.*

Sample	Sex	Age of onset	HPO Term Identifier	Inher.	Gene	Transcript variant	Aminoacidic change	Variant class.	ACMG Criteria
sON_17	M	Birth	HP:0006934 HP:0000708 HP:0012433 HP:0000563 HP:0007754 HP:0033725	AR	*EPHB2*	c.1279G>A c.2387C>T	p.Val427Met p.Pro796Leu	VUS P LP	PM2, (PM3), PP3 PM1, PM2, (PM3), PP3
sON_18	M	6 y	HP:0001249 HP:0000708 HP:0000609 HP:0025163 HP:0002079	AR	*SNF8*	c.304G>A c.673_683 delinsTGGA	p.Val102Ile p.Asp225 TrpfsTer99	VUS P	(PM3), BS1 PVS1, PM2, PP3
sON_19	M	4 y	HP:0011342 HP:0001272 HP:0003458 HP:0001260 HP:0012043 HP:0020036 HP:0001348	AR	*SNF8*	c.304G>A c.423-1G>C	p.Val102Ile Splice site	VUS P	(PM3), BS1 PVS1, PM2, PP3
sON_20	M	17 y	HP:0011342 HP:0001249 HP:0002079 HP:0000639 HP:0002066 HP:0030217	XLR	*WDR45*	c.166A>G Hemizygous	p.Met56Val	VUS (LP)	PM2, PP3

The sON cohort presents 4 cases labelled as GUS (12% of sON cohort) as well, all with AR/XLR putative inheritance. Samples classified as GUS are listed in **Table 14** with respective annotated variants.

Two samples, sON_18 and sON_19 (**Fig. 38A**), share a comparable phenotype of optic atrophy, mild intellectual disability, and brain MRI findings, respectively more prominent on corpus callosum and cerebellum. For sON_18, moreover, an equally affected brother suggested an AR inheritance of disease, while sON_19 was sporadic. Both were found to carry compound heterozygous variants in *SNF8* gene, sharing one missense change (c.304G>A, p.Val102Ile) ultra-rare in population with 46 GnomAD alleles (max MAF: 3.096E-4), most common in Europe (Fig. xxB). This aminoacidic residue is quite conserved (**Fig. 38B**) and can be classified as VUS since found in trans with pathogenic variants, with loss-of function effect in both patients. Indeed, in sON_19 the second allele harbours a deletion-insertion (c.673_683delinsTGGA) leading to frameshift and premature termination (p.Asp225TrpfsTer99) and in sON_20 a change in a canonical splice acceptor site 5' of exon 6 (c.423-1G>C) predicted to affect splicing (dbscSNV ADA score 0.9999).

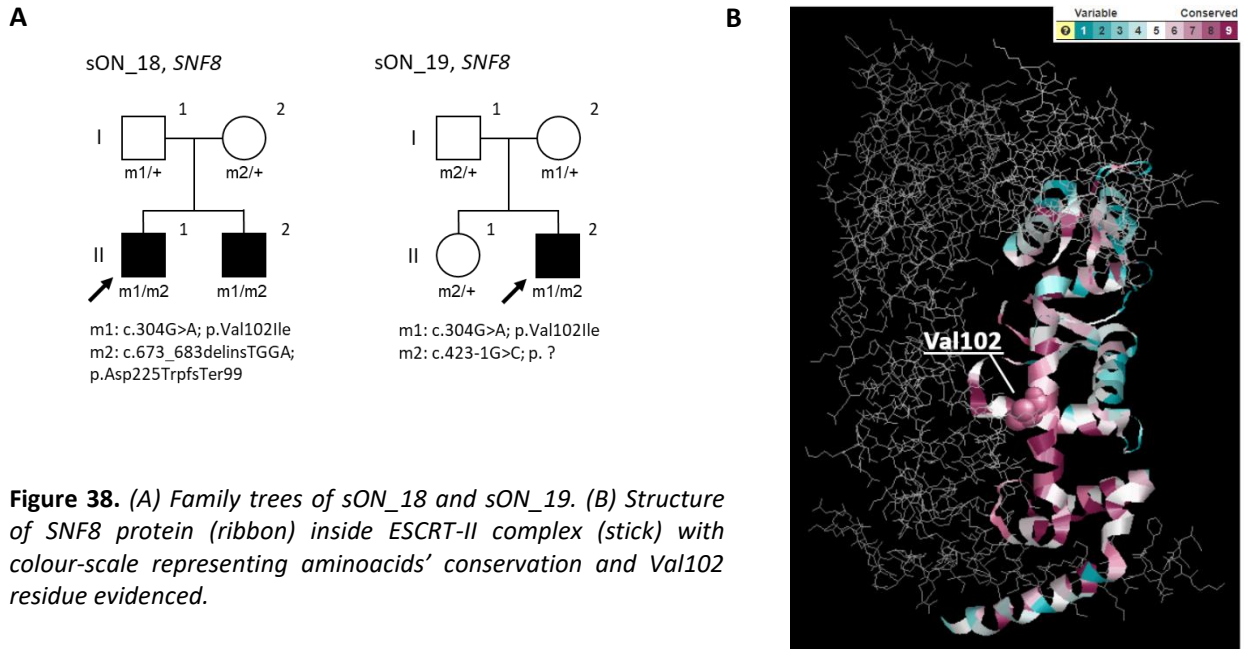

Figure 38. *(A) Family trees of sON_18 and sON_19. (B) Structure of SNF8 protein (ribbon) inside ESCRT-II complex (stick) with colour-scale representing aminoacids' conservation and Val102 residue evidenced.*

The variants in *SNF8* were discovered following automated gene prioritization with the Exomiser tool, used for reanalysis of unsolved cases in the cohort. SNF8 protein is part of ESCRT-II complex involved in membrane remodelling for endosome formation and no pathogenic variant has ever been documented (220). Three more cases with candidate

deleterious variants were obtained through GeneMatcher, showing more severe early-onset leukoencephalopathy phenotypes, thus pointing to a wide spectrum of neurodegeneration for *SNF8* disease. Ongoing studies are evaluating the pathological alterations of autophagy and mitochondrial function in patient's fibroblast lines.

Sample sON_17 presented as a sporadic case (**Fig. 39**), characterized by behavioural abnormality, keratoconus, macular dystrophy, thin corpus callosum, congenital nystagmus, and optic atrophy. Two compound heterozygous missense variants were discovered in *EPHB2* gene: c.1279G>A with change p.Val427Met is reported with 1 allele in GnomAD (max MAF: 8.975E-6) and classified as VUS with pathogenic evidence, and c.2387C>T with change p.Pro796Leu is present wit 3 alleles in GnomAD (max MAF: 4.619E-5) and classified as likely pathogenic. Protein EPHB2 is the tyrosine kinase receptor of ephrin ligand and is mainly involved in axonal guidance, but mutation of *EPHB2* is yet only associated with a recessive defect in platelet aggregation (221). We then received information about cases with matching phenotype and mutations through GeneMatcher, so functional studies on patient's fibroblast are programmed to elucidate the novel pathogenic mechanism linked to this gene.

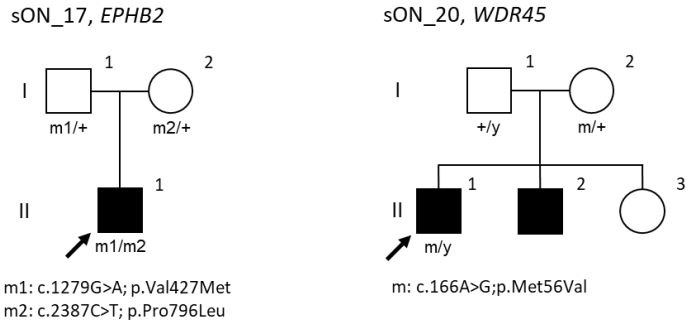

Figure 39. *Family trees for EPHB2 (sON_17) and WDR45 (sON_20) GUS cases.*

A last sample in the GUS category is sON_20, with familiar history suggesting AR/XLR inheritance (**Fig. 39**) and clinical presentation of mild developmental delay and intellectual disability, hypoplasia of the corpus callosum, gait ataxia, limb apraxia, nystagmus, and optic atrophy. In the gene *WDR45* we detected a novel missense variant (c.166A>G p.Met56Val) predicted to be damaging, classified as a VUS with minor pathogenic evidence. This gene encodes a key element of autophagy machinery, involved in the assembly of autophagosome. Mutations in *WDR45* are known to cause different pathological entities, of which the first and most reported is beta-propeller protein associated neurodegeneration (BPAN/NBIA5, MIM#300894) (222). Patients usually present an X-linked dominant form of neurodegeneration with brain iron accumulation, most severe in the few male cases identified, since most *WDR45*

variants are probably embryonic lethal in males (223). Thus, inclusion of sON_21 in GUS samples is due to X-linked recessive inheritance, only rarely found for this this gene's variants, but still not possible to confirm through segregation of the variant in the affected brother and unaffected sister. Besides, the milder clinical phenotype primarily characterized by optic atrophy is still undescribed and demands for functional evidence of pathogenic mechanism.

4. *In vitro* validation for *SDHA* variants in ON_10 and sON_15

Two patients were found to harbour heterozygous variants in *SDHA* gene: ON_10 with c.1351C>T (p.Arg451Cys) and sON_15 with c.1127T>C (p.Leu376Pro). The variant p.Arg451Cys is known from two families reported in literature (179,180), but in ON_10 the clinical presentation is milder, with isolated optic atrophy, and shows incomplete penetrance, with the proband's mother being an asymptomatic carrier (**Fig. 26**). The variant p.Leu376Pro is a novel VUS with pathogenic potential, thus requiring further *in vitro* studies to validate its pathogenic role, besides that also in this pedigree the mother is an asymptomatic carrier (**Fig. 36**). In both ON_10 and sON_15 WES was also performed on unaffected mothers to ascertain that no other variants in coding genes could account for phenotypic variability observed.
Another VUS in *SDHA* is here described (c.1877C>A, p.Thr626Asn), occurring *de novo* in ON_22, but results of functional validation are still lacking because recently identified.

- **4.1. *SDHA* variants yeast modelling**

Firstly, the variants effect on energy metabolism was evaluated through modelling in yeast (*S. cerevisiae*), courtesy of Prof. Baruffini. Yeast Sdh1 is the homolog of human SDHA, and the aminoacidic residues of interest are here conserved. So, strains were produced with introduction of equivalent point mutations, L367P for human L376P and R444C for human R451C, and growth impairment on oxidizable carbon sources was assessed (**Fig. 41**).
As shown in **Fig. 41**, The R444C yeast line showed a strong effect on growth, confirming the behaviour from published yeast validation studies (224). The L367P mutant was not severely impacted in phenotype, unless grown in non-permissive conditions (37 °C). Such thermosensitive phenotypes are most commonly observed in milder, recessive variants.

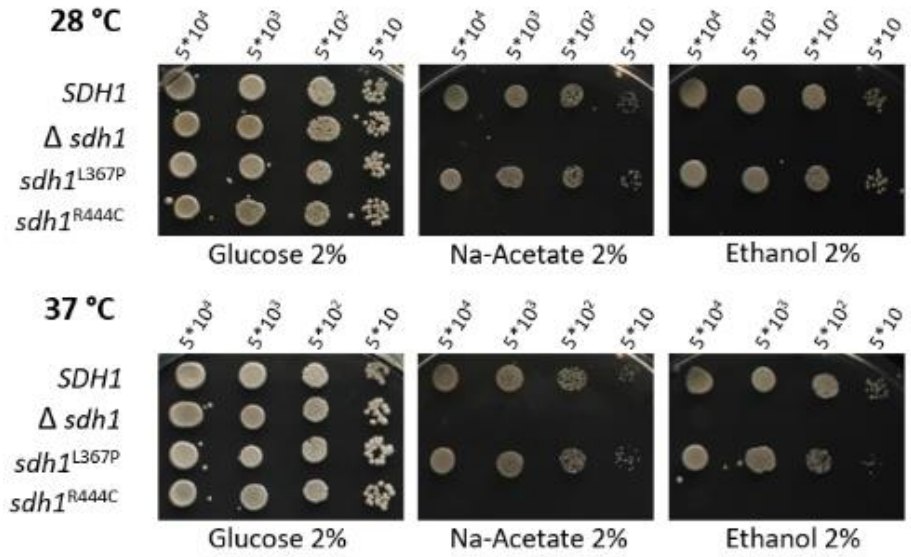

Figure 40. *Growth of yeast strains wild-type (SDH1), knock-out for SDH1 (Δ sdh1), mutant for equivalent of human L376P (sdh^{L367P}), and mutant for equivalent of human R451C (sdh1^{R444C}) with Glucose as fermentable carbon source, or Na-Acetate and Ethanol as oxidizable carbon source inducing obligate oxidative phosphorylation, at 28 °C or 37 °C.*

Respiration measurements and CII activity were significantly reduced for R444C strain, and for L367P at 37 °C (results summarized in **Table 15**). Studies of inheritance, introducing the single variants in diploid strains, demonstrated a dominant negative effect for R444C variant having the same impaired growth that haploid strain, while L367P acted as a recessive allele (data not shown).

Table 15. *Summary of phenotype severity in the performed assays, from low impact (+) to high impact (+++) on the assayed function.*

Line	T (°C)	Oxidative growth	Enzymatic activity	Respiration rate	Protein stability	Inheritance
***sdh1*^{L367P}**	37	+	++	++	++	Recessive
***sdh1*^{R444C}**	28	+++	+++	++	+	Dominant

- **4.2. Protein levels and activity on skeletal muscle**

Since skeletal muscle biopsies were available for ON_10 (L376P II) and his unaffected carrier mother (L376P I), biochemical activity of respiratory complexes was assayed. Only the proband showed a markedly reduced activity, below of control confidence interval values, for complex I, II and IV (**Table 16**), while the mother resulted normal.

We then performed Western blot on protein extracted from the same skeletal muscle samples, targeting subunits of the respiratory complexes (**Fig. 41A, B**).

Table 16. *Respiratory complexes activity on skeletal muscle biopsy of ON_10 (L376P II) and mother (L376P I), values marked with * are outside control range.*

	CI	CII	CIII	CIV	CS
Ctrls mean ± SD (*n*=27)	39.0 ± 27.5	42.6 ± 36.8	284.7 ± 229.5	68.5 ± 48.2	81.0 ± 55.0
Ctrls range (*n*=27)	11.4 - 66.5	5.8 - 79.4	55.3 - 514.2	20.4 - 116.7	26.0 - 136.0
L376P I	17.0	60.6	282.9	155.8	47.0
L376P II	**5.8***	**4.8***	127.4	**19.0***	89.6

The protein levels of CI subunit NDUFB8 were significantly higher in both L376P I and L376P II ($P < 0.001$ and 0.01, respectively), to double control values. A minor but significant increase in levels was seen also for CIII subunit UQCRC2 in both samples, compared to controls ($P < 0.05$). The proband L376P II, finally, showed a marked decrease in CII subunits SDHA and SDHB, to about half the values of controls ($P < 0.001$ and 0.01) and L376P I ($P < 0.01$ and 0.05).

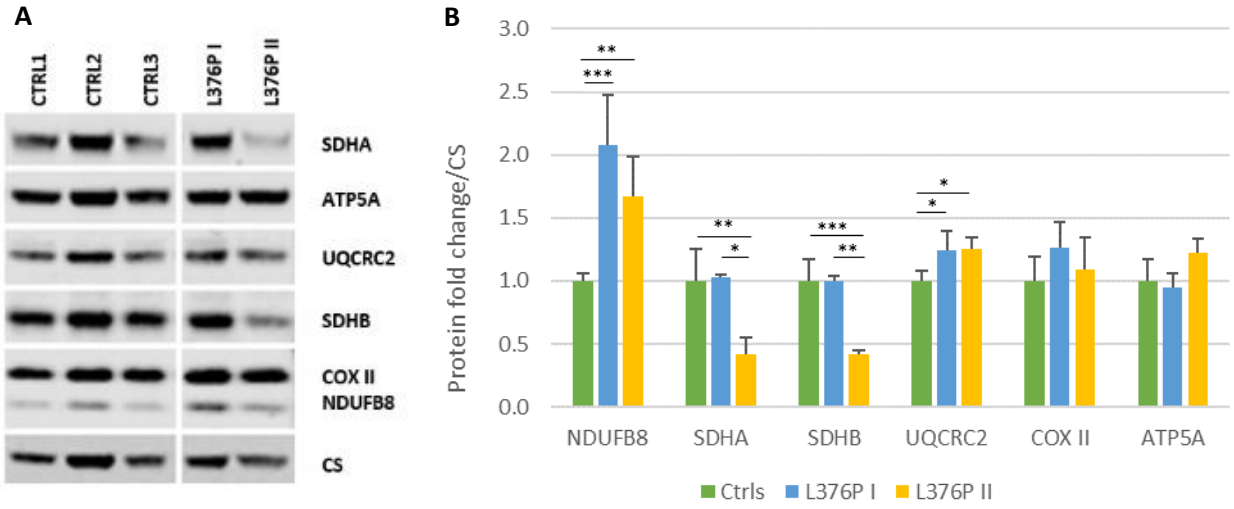

Figure 41. *(A) Western blot from muscle biopsies of controls and SHDA patients, OXPHOS subunits expression (CI-NDUFB8, CII-SDHA/SDHB, CIII-UQCRC2, CIV-COXII and CV-ATP5A); CS was used as a loading control. One representative experiment out of 3 is shown. (B) Densitometric analysis of the OXPHOS complex subunits (mean ± SD, n=3). *P < 0.05; **P < 0.01; ***P < 0.001, 1-way ANOVA test.*

- **4.3. Protein levels on fibroblast cell lines**

Finally, fibroblast cell lines were obtained for both *SDHA* pedigrees' probands and unaffected mothers (L376P I, II and R451C I, II), to better characterize pathologic phenotype. While R451C I and II lines were similar to controls in all OXPHOS complexes subunit levels, in L376P II was confirmed the decrease of both SDHA and SDHB subunits ($P < 0.01$ and 0.05, respectively) and, as in skeletal muscle, this defect was not detectable in L376P I (**Fig. 42A, B**). Our findings on R451C I and II are consistent with literature, showing that this variant affects enzymatic activity of SDHA but not its expression.

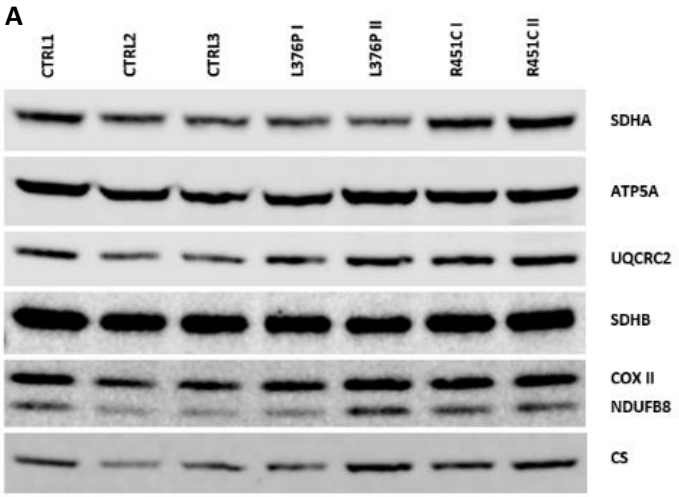

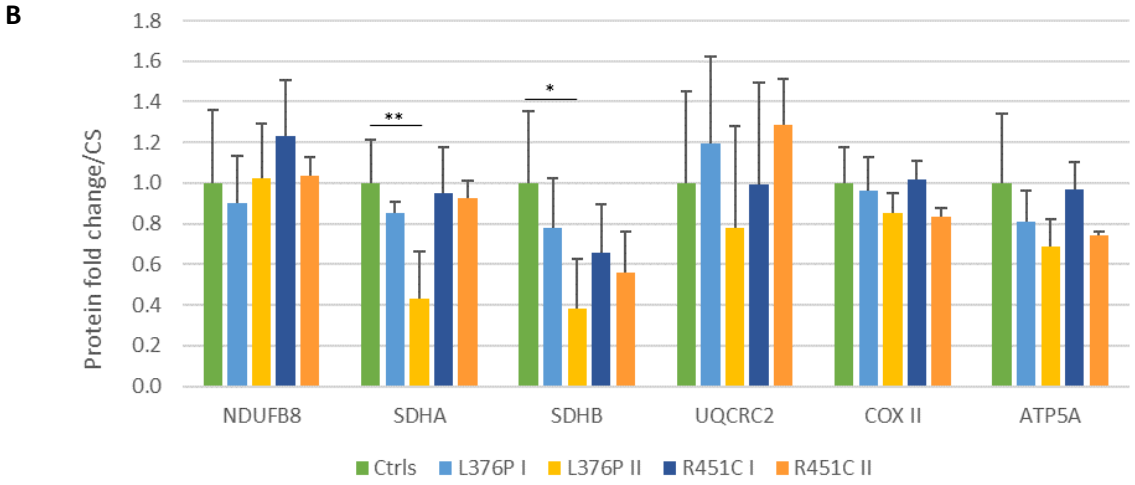

Figure 42. *(A) Western blot from control and SDHA fibroblast, OXPHOS subunits expression (CI-NDUFB8, CII-SDHA/SDHB, CIII-UQCRC2, CIV-COXII and CV-ATP5A); CS was used as a loading control. One representative experiment out of 3 is shown. (B) Densitometric analysis of the OXPHOS complex subunits (mean ± SD, n=3). *P < 0.05; **P < 0.01, 1-way ANOVA test*

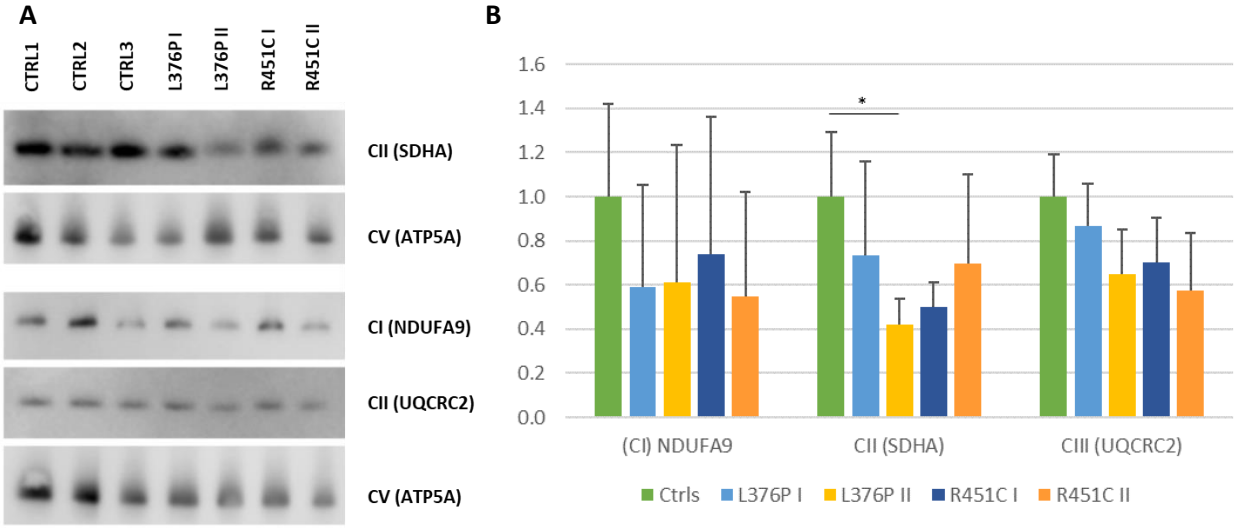

Figure 43. *(A) BN-PAGE from fibroblast lines of controls and SHDA patients, mitochondrial OXPHOS isolated assembled complexes (CI-NDUFA9, CII-SDHA, CIII-UQCRC2). ATP5A was used as loading control. Two representative experiments for different complexes out of 3 in total are shown. (B) Densitometric analysis of the OXPHOS complex subunits (mean ± SD, n=3). *P < 0.05; **P < 0.01; ***P < 0.001, 1-way ANOVA test.*

The reduction in subunit SDHB in parallel to SDHA, prompted us to also check the assembly of whole OXPHOS complexes in fibroblasts through BN-PAGE. In native state, the amount of assembled CII was significantly reduced ($P < 0.05$) in L376P II, while a tendency in CII reduction was present in unaffected carrier R451C I (**Fig. 43A, B**).

5. *In vitro* validation for *UCHL1* variant in ON_23

We discovered two pedigrees, ON_22 and ON_23, with VUS in *UCHL1* gene that should act as dominant variants and thus add a new inheritance pattern for *UCHL1*-linked disease, with milder phenotype than AR cases. Since UCHL1 protein is primarily found in neurons, modelling its impairment in yeast was not ideal. We then conducted studies on the only mutant fibroblast cell line available, derived from the mildly affected mother (I-2 in **Fig. 30**) of proband ON_22 carrying c.586-2A>C variant.

- **4.1. *UCHL1* transcript analysis**

Firstly, total RNA was extracted from patient's cells, and cDNA synthesized then PCR amplified to identify the exact aberrant transcript arising from the variant. Sequencing confirmed that c.586-2A>C alters splicing of last exon, creating an alternative new splice acceptor site in the canonical 3' UTR region of the gene (**Fig. 44**).

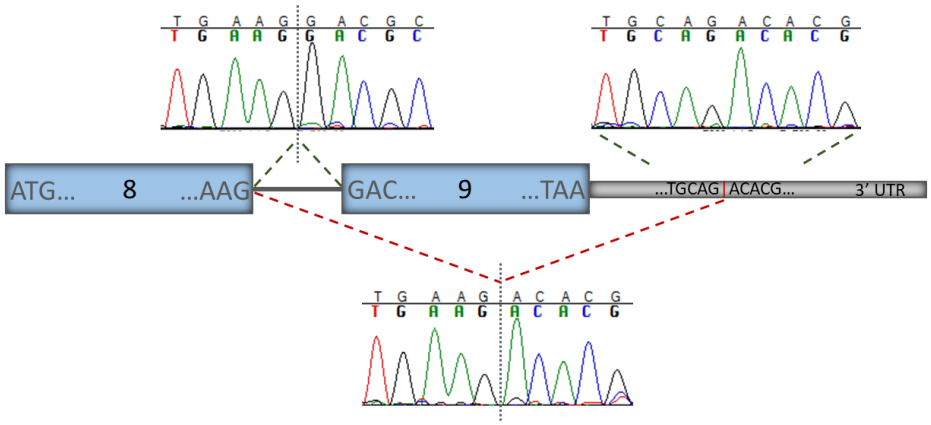

Figure 44. *Schematic representation of UCHL1 cDNA splicing alteration in ON_22 due to variant c.586-2A>C, showing wild-type (top) and mutant (bottom) amplification products chromatograms. The sequence of mutant allele shows skipping of last exon (9) with a new junction forming in the 3' UTR of the gene.*

This alternative transcript is predicted to skip the 28 aminoacids of exon 9 and continue the open reading frame (ORF) with additional 46 residues until a stop condon (**Fig. 45**).

```
>ORF sequence | 223 aa
MQLKPMEINPEMLNKVLSRLGVAGQWRFVDVLGLEEESLGSVPAPACALLLLFPLTAQHE  60
NFRKKQIEELKGQEVSPKVYFMKQTIGNSCGTIGLIHAVANNQDKLGFEDGSVLKQFLSE  120
TEKMSPEDRAKCFEKNEAIQAAHDAVAQEGQCRVDDKVNFHFILFNNVDGHLYELDGRMP  180
FPVNHGASSEDTLLKDAAKVCREFTEREQGEVRFSAVALCKAA  223

>ORF sequence | 241 aa
MQLKPMEINPEMLNKVLSRLGVAGQWRFVDVLGLEEESLGSVPAPACALLLLFPLTAQHE  60
NFRKKQIEELKGQEVSPKVYFMKQTIGNSCGTIGLIHAVANNQDKLGFEDGSVLKQFLSE  120
TEKMSPEDRAKCFEKNEAIQAAHDAVAQEGQCRVDDKVNFHFILFNNVDGHLYELDGRMP  180
FPVNHGASSEDTLLKTRLPLSHTQALKHKQSAQLSTGPLWCELQMVKHSPQCMSCIRYLTL  241
```

Figure 45. *Protein sequence from wild-type ORF and predicted mutant protein sequence derived from splice defect.*

- **4.1. Protein levels and activity on fibroblast lines**

As a consequence of splice defect, we also detected through Western Blot a significantly reduced quantity of UCH-L1 protein in patient fibroblasts, compared to healthy controls chosen with wide variability in age and sex (**Fig. 46A, B**). Moreover, no additional band was detected using monoclonal anti-UCH-L1 antibody, pointing to instability of mutant translation product.

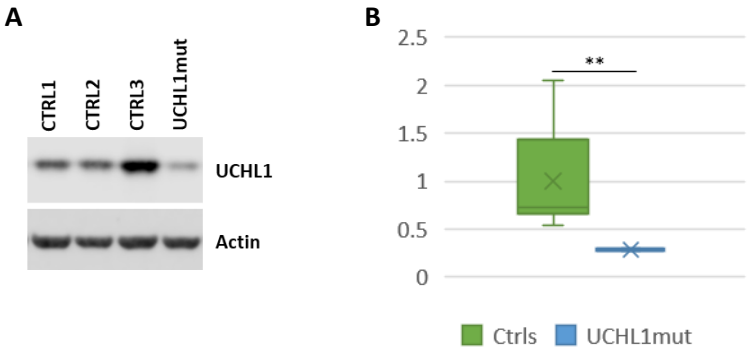

Figure 46. *(A) Western blot from control and UCHL1 fibroblast, UCH-L1 expression; Actin was used as a loading control. One representative experiment out of 3 is shown. (B) Densitometric analysis of UCH-L1 (mean ± SD, n=3). **P < 0.01, unpaired t-test.*

Since *in vitro* experiments on UCHL1-silenced cell lines show an impairment in mitochondrial morphology through downregulation of MFN2, we then analysed protein levels of the principal components of mitochondrial dynamics machinery. However, no differences were evident between UCHL1 mutant and controls for MFN1, MFN2, OPA1 and DRP1 proteins (**Fig. 47A, B**).

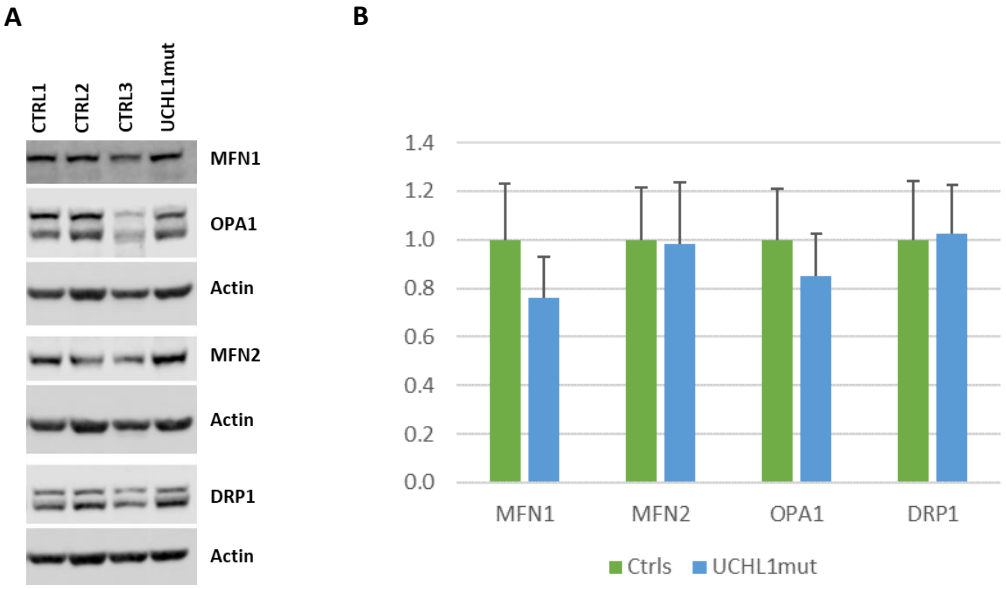

Figure 47. *(A) Western blot from control and UCHL1 fibroblast, mitochondrial dynamics proteins (MFN1, MFN2, OPA1, DRP1) expression; Actin was used as a loading control. One representative experiment out of 3 is shown. (B) Densitometric analysis of mitochondrial dynamics proteins (mean ± SD, n=3).*

Clinical phenotype of UCHL1-associated disease, as well as optic atrophy present in our patients, is however compatible with a mitochondrial disorder, so more mitochondrial protein levels were assessed to elucidate the pathogenic mechanism. Mitochondrial mass markers (CS, TOM20, TIM23, TFAM) resulted within controls variability (**Fig. 48A, B**).

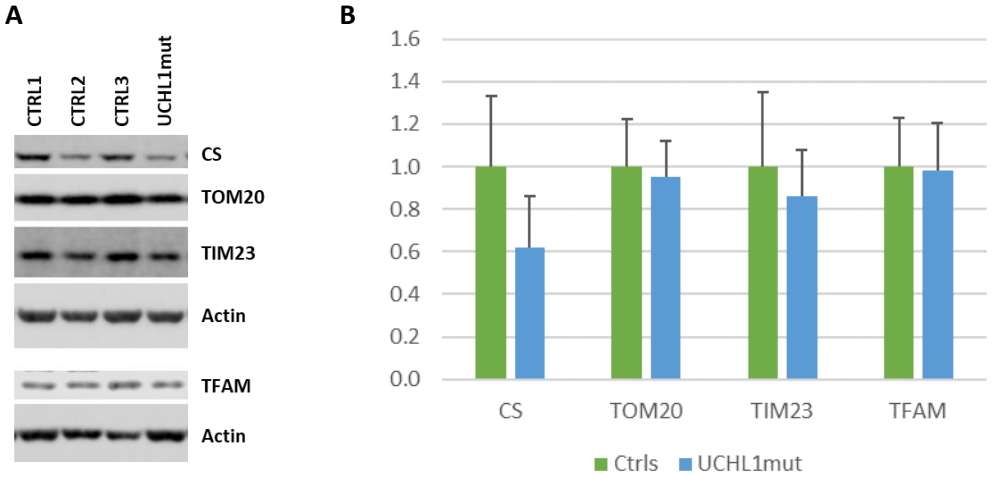

Figure 48. *(A) Western blot from control and UCHL1 fibroblast, mitochondrial mass proteins (CS, TOM20, TIM23, TFAM) expression; Actin was used as a loading control. One representative experiment out of 3 is shown. (B) Densitometric analysis of mitochondrial mass marker proteins (mean ± SD, n=3).*

Finally, subunits of OXPHOS complexes were analysed and a tendency towards lower protein levels detected in CI, CII, and CIV subunits, statistically significant for CI (NDUFA9) and CIV (COXII, COXIV) (**Fig. 49A, B**).

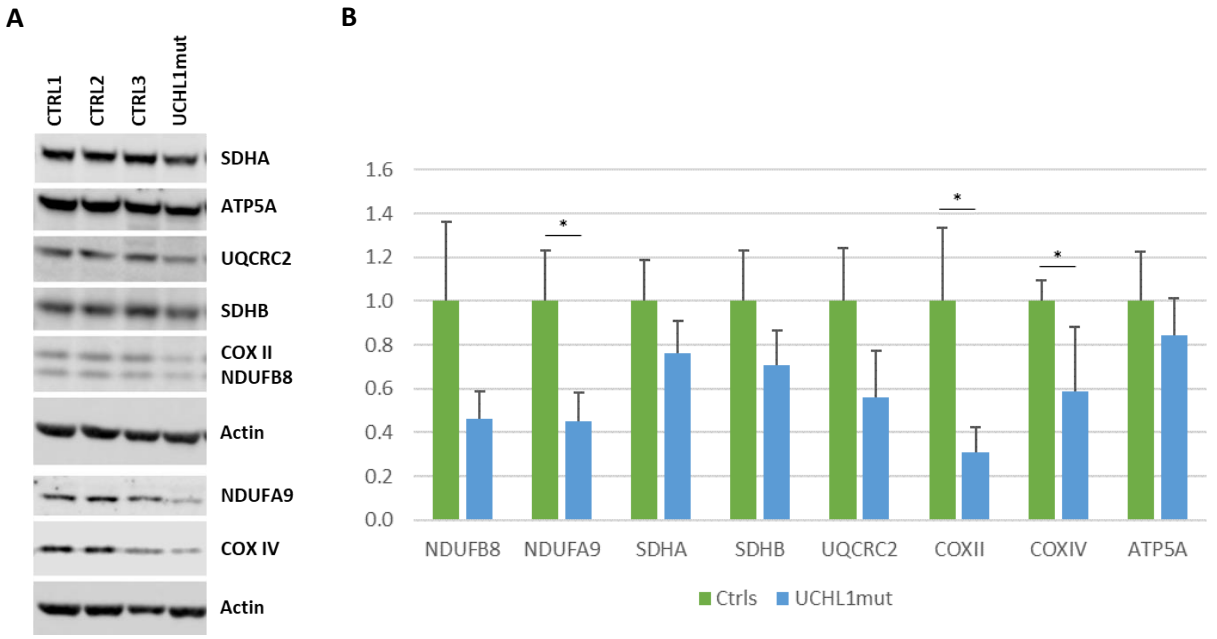

Figure 49. *(A) Western blot from control and UCHL1 fibroblast, OXPHOS subunits expression (CI-NDUFB8, CII-SDHA/SDHB, CIII-UQCRC2, CIV-COXII and CV-ATP5A); Actin was used as a loading control. One representative experiment out of 3 is shown. (B) Densitometric analysis of OXPHOS complex subunits (mean ± SD, n=3). *P < 0.05; multiple t-test.*

Discussion

1. WES general results

- **1.1. WES metrics comparison**

The whole cohort considered in this study satisfied the standard sequencing quality, assessed through FastQC software, depth of coverage, and covered target percentage requirements for WES. Deviation in coverage values between samples is wider for Illumina and IDT workflows, because samples were sequenced in multiple runs with different plexity (from 8-plex to 12-plex), so producing more reads per sample when fewer samples were pooled together. Moreover, there is a striking difference in performance of different library preparation and enrichment kits used, with Illumina workflow showing the lowest mean coverage and coverage uniformity. This result is explained by Illumina's enzymatic library preparation via tagmentation, compared to other workflows' mechanic DNA fragmentation, and by different probe hybridization strategy, repeated two times instead of a single hybridization in other workflows.
Different WES preparation kits were used in order to test the better performing solution in our laboratory, so we finally set to the DT workflow that had a good mean coverage of target and a results consistent between samples. This workflow was later updated by the company with a v2 probe design, that further improved the performance.

- **1.2. Diagnostic yield in study cohorts**

In the whole cohort of 106 patients, 29 were considered solved for a diagnostic rate of 27%, while additional 10 VUS and 5 GUS cases bring a total of 42% of WES with some positive result, including the ones requiring further confirmation. However, the cohort here analysed is not fully representative of all optic neuropathies genetically investigated at our Institute, since mtDNA and *OPA1* gene are usually screened previously to WES, thus excluding two major causes of HON from solved WES cases. So, we also calculated diagnostic yield in a more uniform subset of the total cohort, including 62 ON and sON cases, only negative for *OPA1* screening. The solved rate here was 23%, with 37% of cases with positive results if we add VUS and GUS cases. This subset cohort even allowed to compare the yield between analysis of only HON specific gene panel and analysis of all WES data: the solved ON cases increase from 13% with panel to 19% with WES, and more strikingly solved sON increase from 20% to 33%.

Diagnostic yield here reported is an underestimate of real WES power, since inclusion criteria of the cohort are not uniform and it is therefore enriched in samples negative for the most common HON gene, *OPA1*. Indeed, in the study cohort we solved only 3 patients by finding variants in *OPA1* (3% of cases), while in our in-house database 308 HON patients screened for *OPA1* the positive rate is of 23%. Thus, we should expect a minimum yield of WES on a uniformly recruited cohort of at least 23% (solved cases in *OPA1*-negative WES) of the 77% of samples that are negative for *OPA1*, that should reach a value close to 40%.

Our study provides a first estimate of WES diagnostic yield for a cohort characterized by optic atrophy, in both isolated and syndromic form. Comparable results, specific for optic atrophy cases, are not present in literature, where target gene panels have usually been the most diffuse approach to ON diagnosis. For example, a recent work on a large ON cohort reported a diagnostic yield of 22% after targeted NGS sequencing of only 22 known and candidate genes (225). Instead, a few WES studies exist for wide cohorts of putative mitochondrial diseases patients, also summarized in a recent review (140). Since many hereditary optic neuropathies are due to mitochondrial dysfunction, these works represent a good comparison to ours, especially for the sON cohort that includes variable mitochondrial presentations. In those studies, a wide variation in diagnostic yield is reported (35% to 70%), but this is generally slightly higher than 27% yield in present study. The theoretical yield of ~40% proposed for our cohort should however better match the published values.

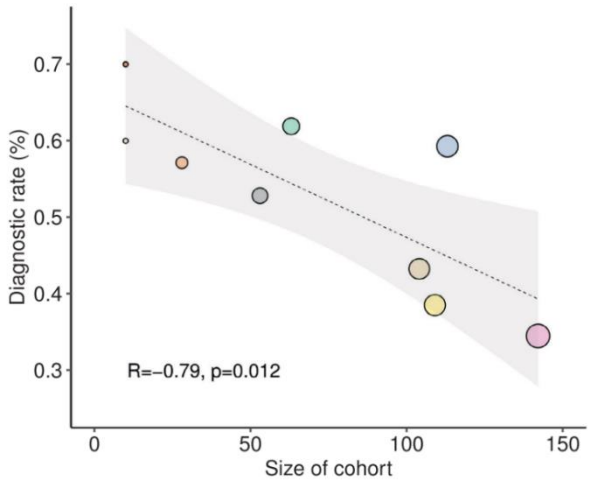

Figure 50. *Diagnostic rate of WES from 9 studies on suspected mitochondrial disease with linear regression, taken from (140).*

Inclusion criteria in study cohort, like molecular analysis performed before WES or precise clinical phenotyping, greatly influence final yield results. This is also visible from the trend of reduced diagnostic rate with increasing study size in published works (**Fig. 50**), because larger

cohorts mean more heterogenous patients, possibly not even with genetic etiology of disease. Moreover, WES studies on mitochondrial diseases with sample numerosity comparable to ours only include pediatric patients with severe presentations (226–228), while our HON cohort consist of both childhood- and adult-onset case. Clinical phenotype is generally mild, especially for ON cases, and further complicates the gathering of a precise medical history of proband and family members without thorough examination by clinicians.

The ON subgroup has 5% less total solved cases compared to sON subgroup, an expected result given that AD cases are more numerous in ON and are also harder to solve through WES, if variants are not found in classic DOA genes. The difference is more striking for VUS and GUS cases, more numerous in sON cohort, accounting together for 31% of patients, and thus represented equally to solved cases. A similar trend is seen in the subset of *OPA1*-only negative cases, where still 33% of sON patients are classified as VUS, compared to only 9% of VUS/GUS cases for ON patients. This result is possibly explained by more complex phenotypes of sON cases, that are sometimes hard to precisely match to known disease phenotypes, resulting in their categorization as VUS or GUS.

In conclusion, diagnostic yield from WES only in optic neuropathies is sufficient to support this technique as primary molecular diagnostic analysis, preferred to target gene panels as in other rare diseases with heterogenous genetic cause. This new analysis also allowed us to solved a couple of cases that went undetected through old HON target gene panel, because bioinformatic pipeline was less efficient in calling of indels.

There is, however, a relevant portion of still unsolved cases that should be periodically re-analysed to stay updated with novel gene discoveries. WES data can be further analysed for detection of copy number variants (CNVs) through specific bioinformatic pipelines. Moreover, different molecular approaches can be applied, like WGS (also on long-reads platforms) or RNAseq, in order to detect non-coding variants and aberrant gene expression or splicing products. Recent works also demonstrated diagnostic potential of an integrative omic approach for rare diseases, combining transcriptomics, proteomics, and metabolomics (229).

- **1.3. Inheritance in WES with positive results**

Different modes of inheritance are not uniformly represented in ON and sON cohorts. The prevalence of AD cases in solved ON (53%) is mainly due to two common DOA genes, *OPA1* and

ACO2, while most of solved sON (80%) show AR inheritance. In VUS and GUS categories all ON have AD inheritance, and again sON have instead mostly AR inheritance (70% of VUS+GUS).
For a few mitochondrial diseases , heterozygous variants in a gene usually cause a milder, isolate form, but also rare biallelic forms exist and show more severe, syndromic phenotypes (e.g., *OPA1*, *OPA3*, *MFN2*, *WFS1*, *SDHA*). This is the case for example in our cohort with 3 *WFS1* AD cases with isolated ON and one AR case with syndromic ON. Besides, a more general paradigm of milder presentation for AD cases and complex phenotype for AR cases, could at least partially explain their different distribution in ON and sON cohorts.

- **1.4. Mitochondrial cases in study cohort**

More than 80% of solved cases in ON and sON cohorts can be attributed to a mitochondrial form of optic atrophy, confirming this pathway as the most relevant in pathophysiology of HON. Instead, non-mitochondrial cellular functions are putatively involved in the majority of VUS and GUS cases. Thus, optic atrophy could be a novel or underestimated hallmark of already described genetic diseases, like the ones known for candidate genes in VUS samples. Moreover, since many mitochondrial disease genes are already well characterized, gene discovery for HON is more likely to uncover alternative mechanisms leading to this phenotype. Indeed, the GUS here presented are involved in nuclear pore transport (*NUTF2*), axonal guidance in neuronal development (*EPHB2*), and vesicles/autophagosomes formation (*SNF8*, *WDR45*).

2. Solved ON and sON cases

- **2.1. Mitochondrial ON with AD inheritance**

In all solved AD cases for ON cohort the DOA phenotype was associated with mitochondrial dysfunction, in particular with genes involved in energy metabolism/TCA cycle (*ACO2*, *SDHA*), mitochondrial dynamics (*OPA1*) and mtDNA maintenance (*SSBP1*).
After some initial report of biallelic *ACO2* variants causing isolated or syndromic optic atrophy (69), heterozygous pathogenic variants in multiple DOA patients were identified (71,72). Aconitase dysfunction is now seen as one of the most common cause of DOA, and our results agree with these findings, with 4 positive cases in ON cohort (ON_1-4). Of these variants illustrated in **Fig. 51**, one disrupts a canonical splice site (c.1761+1G>A), so being a loss-of-function allele, while others are missense variants. While variant p.Arg671Trp is recurrent in

multiple families, the remaining missense changes are novel (p.Phe165Ser, p.Asn480Asp), and all will be soon characterized in their pathological role through yeast modelling.

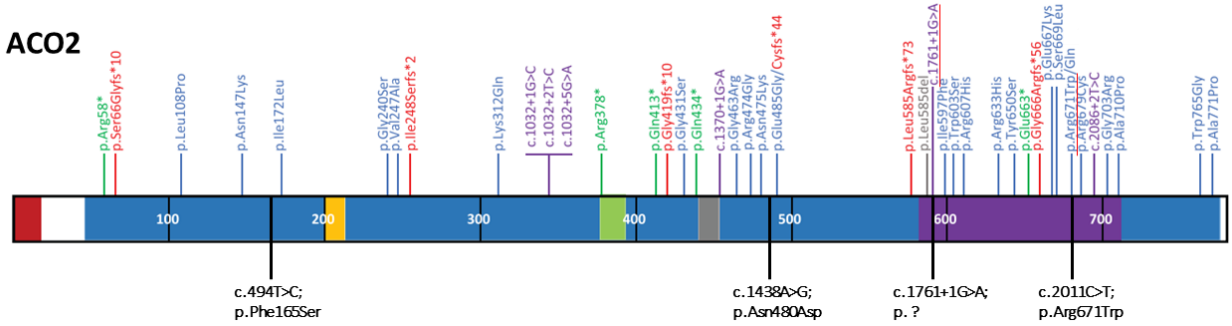

Figure 51. *Aconitase protein sequence with described dominant pathogenic variants (blue=missense, green=nonsense, red=frameshift, purple=splice) plus variants discovered in ON cohort (below), image modified from (72).*

As for aconitase, mutation of succinate-dehydrogenase subunits like SDHA impairs TCA cycle, but also the electron transport chain, generating an energetic defect in mitochondria. The *SDHA* variant found in ON_9 (p.Arg451Cys) is already described in two dominant pedigrees (179,180) where clinical presentation was more complex, with ataxia and cardiomyopathy. The isolated optic atrophy in our case, coupled with incomplete penetrance, is another example of great phenotypic variation in mitochondrial disorders.

The other most frequent gene mutated in ON cohort is *OPA1*. Given its the great prevalence in DOA patients, the majority of isolated ON patients were screened for *OPA1* variants (often also for copy number variants, CNVs, using MLPA) before WES. Nonetheless, 4 cases (ON_5-8) harboured pathogenic or likely pathogenic variants in this gene, all predicted to generate a null allele. Only one of these cases had never been screened for *OPA1* and was found with p.Arg905Ter variant. For the other 3, the variants were either not identified through Sanger sequencing for alignment issues (p.Ile313ValfsTer10) or identified but not correctly classified as pathogenic (c.1212+5G>A, c.1212+6T>G). Limited automation in Sanger sequencing analysis can increase human error, especially frequent during manual examination of a long target as *OPA1* complete sequence. The splice region variants were instead discarded because predicted as mildly affecting splicing, but they were however re-evaluated after WES proved inconclusive for any other variant compatible with DOA. Sequencing of cDNA from ON_7 then confirmed the alteration of splicing due to c.1212+5G>A, with exon 12 skipping, and it is predicted to happen also with newly described mutation of adjacent nucleotide c.1212+6T>G in ON_8.

Finally, the *SSBP1* variant p.Lys51Glu in ON_10 is novel and thus classified as VUS (P), but the case is treated as solved because DOA phenotype is well documented in *SSBP1* patients, the variant is absent from control population, and it segregates in affected family members.

- **2.2. Mitochondrial ON with AR/XLR inheritance**

Most of AR cases in ON cohort are also associated with a mitochondrial form of optic atrophy, caused by impairment of respiratory complex I (*DNAJC30*, *NDUFV2*), MAMs functions (*WFS1*), and fatty acids metabolism (*MECR*).

Interestingly, isolated ON cases positive to both *DNAJC30* and *NDUFV2* showed a LHON-like optic atrophy with subacute onset. A defect in CI activity is common to these cases, even though DNAJC30 protein is a chaperone involved in CI turnover, while NDUFV2 is a CI core subunit. The 3 cases (ON_11, ON_12, ON_13) homozygous for the recurrent *DNAJC30* variant p.Tyr51Cys have eastern European origins, compatible with proposed founder effect occurred in this geographic region (10). The overall European frequency of this variant in GnomAD (MAF: 1.457E-3) is ten times higher compared to Southern European frequency (MAF: 1.734E-4). So, even if relevant in our cohort, probably in Italian population *DNAJC30* must be a rarer cause of optic atrophy.

The ON_15 case harbouring compound heterozygous variants in *NDUFV2* (p.Phe55Val and p.Cys225Tyr) is a first report of LHON presentation for this gene mutation. In first reports loss-of-function variants in this gene were associated with Leigh syndrome, hypertrophic cardiomyopathy and encephalopathy. A more recent report describes also two cavitating leukoencephalopathy pedigrees with homozygous or compound heterozygous missense variants (**Fig. 52**) (46,230–232). Thus, functional validation is ongoing on ON_15 fibroblast cell line to better understand the mild clinical manifestation in our patient.

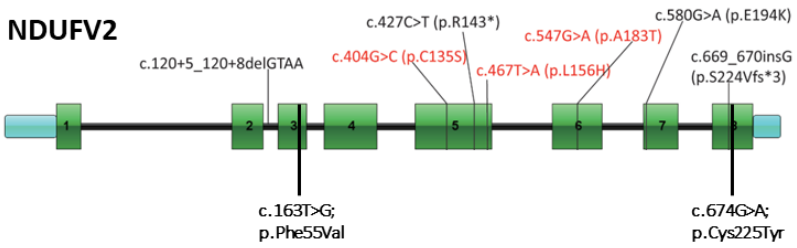

Figure 52. *NDUFV2 protein sequence with described pathogenic variants (red=newly described in ref.46) plus variants discovered in ON_15 (below), modified from (46).*

We can speculate that *NDUFV2* gene may behave in a fashion similar to *DNAJC30*, for which also one patient with Leigh syndrome is described (10), and *NDUFS2*, with multiple published Leigh cases and one family having LHON phenotype (11,12). Moreover, there are also rare reports of Leigh syndrome associated with common LHON mtDNA variants like m.11778A>G/*MT-ND4*, so that a paradigm is emerging for which the two clinical presentations can be different outcomes of similar molecular defects (233–236).

Another frequent gene in AR cases is *WFS1*, with Wolframin protein involved in MAMs functions such as Ca^{2+} homeostasis, then possibly leading to secondary mitochondrial impairment. In ON cohort 2 patients were found with compound heterozygous variants (ON_16 and ON_17) and one a homozygous variant (ON_18), confirming its role as cause of isolated optic atrophy besides Wolfram syndrome. Indeed, the phenotypic spectrum of *WFS1* mutation is supported by observation in our ON cases of variants already described in a typical recessive presentation of Wolfram syndrome, namely p.Arg732Cys and p.Pro533Ser (181,182). Other variants are reported as population ultra-rare alleles (p.Ala738Asp) or are newly described (p.Ile561ArgfsTer53 and p.Cys505_Val509del), so contributing to widen the list of pathogenic variants in *WFS1* gene.

One last case presented with isolated ON and mild hearing loss, arising from a homozygous pathogenic variant in *MECR* gene (p.Arg258Trp). Pathogenic mechanism of MECR dysfunction is mainly attributed to energetic defect caused by metabolic enzymes not correctly lipoylated after lipoic acid deficiency. Variant p.Arg258Trp is relatively common in the few cases reported in literature with childhood-onset dystonia and optic atrophy, but always in compound heterozygous state with other variants (90,91,184). The milder phenotype in ON_14 case, also identical in the proband's sister, is however translated into a very strong growth defect in yeast model of p.Arg258Trp variant. The mutant yeast strain, moreover, is more sensitive to oxidative stress produced by H_2O_2 and supplementation of lipoic acid that is lacking in mutant allows the rescue of survival rate after H_2O_2. A recent report of a *MECR* patient with typical sings of dystonia and basal ganglia abnormalities, but without optic atrophy, describes lipoic acid supplementation as therapeutic approach, even if results in this case are unclear (92).

- **2.3. Non-mitochondrial ON cases**

A single case in ON cohort, ON_19, has an optic atrophy form due to calcium flux imbalance causing alteration of retinal and optic nerve electrochemical signal, and not of mitochondrial

origin. This patient harbours stop-gain variant (p.Arg680Ter) in *CACNA1F* gene, associated in multiple pedigrees with X-linked optic atrophy and congenital stationary night blindness (185,186). Our case shows this known specific phenotype, also present in the affected maternal grandfather that carries the pathogenic variant.

- **2.4. Mitochondrial sON with AD inheritance**

The only AD solved case in sON cohort, sON_1, shows a syndromic manifestation of mitochondrial disease caused by *AFG3L2* mutation. AFG3L2 protein dysfunction leads to impairment in OPA1 processing, with mitochondrial network morphology fragmentation. The identified heterozygous variant (p.Thr355Met) occurred here *de novo* and is already reported in one AD pedigree with overlapping symptoms (37). Besides, this variant is located in the ATPase domain where most of *AFG3L2* variants linked to DOA/DOA plus are clustered.

- **2.5. Mitochondrial sON with AR/XLR inheritance**

The majority of AR/XLR solved sON cases derive from mitochondrial dysfunction, as well. Specifically, the syndromic phenotypes observed in our cohort are due to alterations in complex I activity (*NDUFAF2*, *NDUFB11*), MAMs functions (*WFS1*, *C19orf12*), mitochondrial translation (*MTFMT*), Fe-S cluster biosynthesis (*FDXR*), and CoQ10 biosynthesis (*PDSS1*).

Childhood-onset complex phenotypes, mostly ascribed to Leigh syndrome, are usually linked to CI deficiency. However, in our cohort of syndromic optic atrophies we identified 2 cases with less severe phenotypes, due to mutation in *NDUFAF2* and *NDUFB11* genes. Disease linked to CI assembly factor NDUFAF2 was firstly reported in a case of progressive encephalopathy (237) and few other cases were then described harbouring homozygous null alleles, leading to Leigh-like presentation often with lethal outcome in the first years of life (238). The here described sON_6 patient, together with equally affected brother, represents the first compound heterozygote case for *NDUFAF2* gene (p.[(Tyr32Cys)];[(Arg50GlufsTer3)]). The phenotype is milder and not infantile-lethal, prominently showing optic atrophy, hearing impairment, and sensory axonal neuropathy, while MRI findings of cerebral calcification are also less severe compared to published cases (239). The distinctive phenotype observed in sON_10 of sideroblastic anemia with optic atrophy is, instead, well described for mutation of CI subunit *NDUFB11*, although pathogenic variants in the same gene are linked to severe pediatric manifestation as well (210). The identified in-frame deletion (p.Phe93del) is a recurrent

pathogenic variant associated with X-linked pure or syndromic sideroblastic anemia and, like in sON_10, often arises as *de novo* mutation.

Mutation of *WFS1* was found here as cause of 3 isolated ON cases, but is also responsible for a single complex case, sON_9, presenting with the main hallmarks of Wolfram syndrome (optic atrophy, diabetes mellitus, hearing impairment, brainstem degeneration). Two damaging variants, p.Ala677Thr and p.Gly736Ser, were detected in compound heterozygous state, of which the latter already known for Wolfram syndrome cases (205,206). A better clinical characterization of the proband's daughters then allowed to uncover a semidominant effect of these variants, since the one who inherited the p.Ala677Thr allele shows hearing impairment, while the one with p.Gly736Ser allele isolated optic atrophy. Like Wolframin, C19orf12 protein is mainly located in MAMs compartment and probably regulates the MAMs processes of lipid transfer, calcium metabolism and autophagosome formation by mitochondrial damage sensing (193). The clinical phenotype of *C19orf12* patients is, however, primarily a neurodegeneration with brain iron accumulation (MPAN/NBIA4) with childhood-onset. The case identified in sON cohort, sON_2, harbours a homozygous variant in *C19orf12* (p.Gly58Ser) already described in one case with overlapping symptoms of optic atrophy, brain iron accumulation, mild cognitive impairment, and movement disorders (192).

A wide phenotypic spectrum is also known for *MTFMT*-linked genetic disease, due to dysfunction of the mitochondrial methionyl-tRNA formyltransferase required for correct protein synthesis. Patients described in literature usually show early encephalomyopathic phenotype, compatible to Leigh syndrome, often with lactic acidosis, basal ganglia lesions, psychomotor retardation, optic atrophy, ataxia, and cardiomyopathy (240). The phenotype is frequently rather mild for Leigh syndrome and a considerable percentage of patients survive to adulthood with some preserved neurological functions (110). In the pedigree of sON_5 the 3 affected siblings have highly variable presentation going from a Leigh-like phenotype to only hypogonadism and hearing loss in the female. A variant never described as pathogenic was detected in homozygous state (p.Thr173Ile) in the proband and its pathogenic effect confirmed by yeast studies, that also support impairment mostly in CIV stability and activity as previously reported in *MTFMT* mouse model (241). The homozygous variant p.Thr173Ile is carried by all the affected individuals, thus making this one of the most extreme examples of phenotypic variation associated with the same pathogenic variant in MTFMT gene. Moreover, the sister of

the proband can have the mildest phenotype reported for the disease and research for a possible genetic or biochemical explanation for the variable expressivity observed is underway.

The biosynthesis of Fe-S clusters also take place in mitochondrial matrix, and its impairment produce a secondary defect in OXPHOS complexes, that rely on Fe-S clusters for electron transport. Clinical manifestation of FDXR mutation is variable (88), but the recurrent symptoms of optic atrophy, hearing impairment, and movement disorder are present in sON_3 case. Two variants in compound heterozygous state were here identified (p.Met1? and p.Asp368Asn) and are described in different combinations in literature for *FDXR* patients (**Fig. 53**) (194,195).

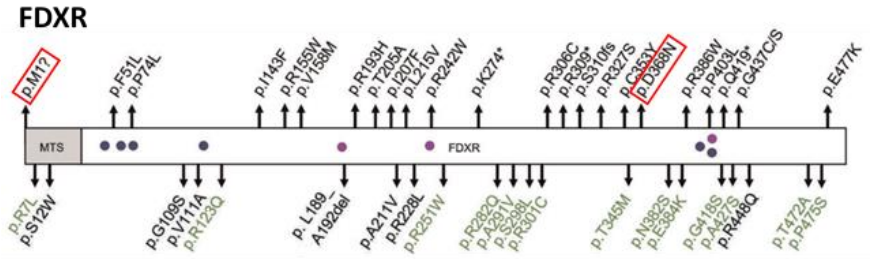

Figure 53. *FDXR protein sequence with described pathogenic variants (black) plus putative benign variants reported as homozygous in GnomAD database (green), the variants found in sON_3 are in red box , modified from (88).*

Finally, mitochondrial dysfunction is also secondary to ubiquinone deficiency due to *PDSS1* mutation, until now reported for only two families (201,202). In sON_7 and the affected sister we identified a homozygous variant (p.Gln245His) in *PDSS1*, that represents the third case described of such CoQ10 deficiency (200). Moreover, clinical manifestation with deafness, optic atrophy, mental retardation, and movement disorder matches to the first published family's phenotype.

- **2.6. Non-mitochondrial sON cases**

Two cases in the solved sON category are caused by genes not directly involved in mitochondrial function by current knowledge, *LYST* and *SLC52A2*.

In sON_4 a homozygous stop-gain variant (p.Ser1099Ter) was detected in *LYST*, encoding a regulator of lysosomes formation with reported pathogenic variants causing a lysosomial syndrome (Chediak Higashi, CHS). In our case the most prominent clinical features are movement disorder, hearing impairment and optic atrophy, and thus not matching a typical early-onset a more severe CHS. Rare cases have been described were CHS has adult-onset, milder phenotype with mainly motor function deterioration and no ocular albinism seen in

pediatric cases. Moreover, optic neuropathy is well characterized in one adult CHS pedigree, also carrying *LYST* homozygous null alleles, further supporting our case diagnosis (197,242).

The other non-mitochondrial solved case is sON_8, presenting with optic atrophy plus sensory and axonal neuropathy. This phenotype is compatible with Brown-Vialetto-Van Laere syndrome, caused by riboflavin deficiency, here after *SLC52A2* mutation. Two compound heterozygous variants (p.Gly415Ala and p.Gly419Ser) were identified in the gene, of which the second already described as pathogenic (204). Though not properly considered a mitochondrial form of ON, there is evidence that at least part of the phenotype in Brown-Vialetto-Van Laere syndrome could be dependent on secondarily altered mitochondrial function and morphology (127). The symptoms of BVVL syndrome can benefit from by riboflavin supplementation, recently started as treatment in our patient, so it is particularly valuable to have rapid molecular diagnosis of such cases.

3. VUS ON and sON cases

- **3.1. Mitochondrial VUS cases**

The 3 cases classified as VUS carry variants of uncertain significance in genes well characterized for their role in mitochondrial optic neuropathies (*OPA1*, *SDHA*, and *WFS1*).

One case, ON_20, is peculiar in harbouring both a synonym variant predicted to affect splicing in *OPA1* (Lys505=), and a predicted damaging missense variant in *WFS1* (p.Lys768Gln), that should equally be compatible with isolated optic atrophy observed. While is not possible to obtain information about variants' effect from their segregation with the phenotype in family members, only some functional study can ascertain where the pathogenic defect originates. A first experiment planned will analyse cDNA of *OPA1* transcript from patient's blood, in order to find an aberrant splicing product possibly showing the skipping of exon 15.

The remaining 2 cases are both linked to VUS in *SDHA* gene, but with very different clinical presentation and possible experimental strategies to validate a pathogenic role of the variants. The ON_21 case shows only optic atrophy plus retinal dystrophy and carries a de novo missense variant never described (p.Thr626Asn). Only two pathogenic variants with dominant effect are known for *SDHA*, namely p.Arg451Cys and p.Arg662Cys (74,179,180), that are predicted to impair FAD cofactor normal activity, but they do not directly interact with Thr626 residue. Therefore, yeast modelling is ongoing to assess the effect and putative inheritance mode of this

variant. The second case sON_ 14 shows instead a syndromic phenotype of optic atrophy with dystonia, basal ganglia anomalies and hearing impairment. Another heterozygous novel variant was here identified (p.Leu376Pro), compatible with CII defect. However, since the variant is carried by the unaffected mother, in depth functional studies on yeast, muscle biopsy, and fibroblast cell line are being performed, with all results discussed in following Chapter 5.

- **3.2. Non-mitochondrial VUS cases**

An indirect or not yet demonstrated link to mitochondrial function characterizes the majority of genes identified in VUS cases, also more abundant in sON cohort. Thus, cellular processes involved are diverse but mainly linked to neural specific functions (*CACNA1A*, *GFAP*, *USH2A*, *KIF1A*), then to ubiquitin-proteasome system (*UCHL1*), or vitamin metabolism (*BTD*).

Both VUS cases ON_22 and ON_23 with isolated optic atrophy and possible AD inheritance carry heterozygous novel missense variants in *UCHL1* gene (c.586-2A>C and p.Leu95Arg, respectively). The variants segregate in multiple affected family members of ON__22 and at least in the affected mother of ON_23, but still the dominant behaviour needs to be verified as never reported before for *UCHL1* disease. For ON_22 the splice defect has been confirmed and the available fibroblast cell line from proband's mother is undergoing other functional characterization experiments, better discussed in Chapter 6. For p.Leu95Arg of sON_23 the deleterious effect could be produced by alteration of the active site, with catalytic Cys90 closely located to the mutant residue. Functional validation is however required being another putative novel dominant variant. Since biallelic pedigrees have been reported presenting with Behr syndrome-like phenotype (188–190) caused by *UCHL1* mutation, the cases here identified are classified as VUS pending demonstration that an autosomal dominant mode of inheritance also exists for *UCHL1*-associated disease. Indeed, an isolated ON pathogenic phenotype due to heterozygous variant, compared to more severe recessive syndromic presentation, is known for some classic mitochondrial genes linked to DOA, including *OPA1*, *OPA3*, or *DNM1L*. In this respect, a possible involvement of mitochondrial dysfunction has been proposed, since *in vitro* studies point to direct regulation of MFN2 by deubiquitinase activity of UCH-L1, but still this mechanism is not demonstrated for pathogenic reported variants (55).

The first of syndromic cases with AD inheritance, sON_11, present with a cognitive impairment, cerebellar atrophy, and optic atrophy and carries a novel predicted damaging variant (p.Phe1794Ser) in *CACNA1A* gene. This voltage-dependent calcium channel is key to

neurotransmitter release in the nervous system and particularly in the cerebellar Purkinje cells. Different AD transmission diseases have been described in *CACNA1A* patients: familial hemiplegic migraine (FHM1, MIM#141500), developmental and epileptic encephalopathy (DEE42, MIM#617106), episodic ataxia (EA2, MIM# 108500), and spinocerebellar ataxia 6 (SCA6, MIM#183086). Given the cerebellar involvement showed by our case, an atypical SCA6 phenotype cannot be ruled out for a deleterious variant found in this well recognized disease-gene. The ON presentation is however not common, a single report in fact describes optic nerve atrophy in a rare biallelic *CACNA1A* case, condition with severe symptoms (125). Until evidence from functional validation, this case has an atypical phenotype associated with a VUS in a pathogenic but highly polymorphic gene with alternative transcripts, so it is not possible to be considered solved.

Specific of nervous system is also GFAP, an abundant intermediate filament protein specific of mature astrocytes. Mutation of *GFAP* gene is associated with Alexander diseases, a neurodegenerative condition where early-onset patients typically present with seizures, megalencephaly, developmental delay, and spasticity, while adult-onset forms are milder, mostly with bulbar or pseudobulbar symptoms and spasticity (213,243). In case sON_12 we detected a novel heterozygous variant p.Lys356Asn in *GFAP* that could account for the parkinsonism, cerebral atrophy, and sleep disturbance. A variant affecting a close residue (p.Leu359Phe) is already reported in one Italian patient with adult form of Alexander disease mainly characterized by spasticity and bulbar signs (244). While segregation studies and histopathology positive for the characteristic Rosenthal fibres in astrocytes could confirm pathogenic role of the *GFAP* variant, there is still to uncover a link between this disease and optic atrophy observed in this patient, if no other stronger genetic cause will be found.

The case sON_13 then was found positive for VUS in *KIF1A* gene, encoding a kinesin specific of neurons where it is involved in anterograde axonal vesicle transport. Disease associated with *KIF1A* variants is a PEHO form typically characterized by spasticity, cerebellar atrophy, and often skeletal abnormalities and optic atrophy (NESCAV syndrome or spastic paraplegia 30) (214), symptoms present also in sON_13 and her brother. The heterozygous variant identified in both affected siblings (c.3749+7G>A) is in a splice region and is reported in one allele from GnomAD database, so requires validation of effect on the transcript and further segregation studies in more family members.

Two more sON cases in VUS category show AR inheritance for disease not related to mitochondrial function. In sON_15 two damaging variants were detected in *BTD* gene, encoding the enzyme biotinidase involved in biotin recycling pathway. The clinical presentation of biotinidase deficiency can range from early-onset severe neuromuscular disease forms to milder late-onset cases, the latter usually developing with optic neuropathy and spastic paraparesis in adolescence (217). Our case harbour one already described pathogenic variant (p.Cys33PhefsTer36) (216) plus a novel missense one (p.Ser319Tyr), and has a typical late-onset BTD presentation. VUS classification of the case was assigned pending demonstration of the two variants being *in trans*. Biotin supplementation has already been suggested to clinicians, since it is usually very effective in treating the main symptoms.

The last VUS case is sON_16, presenting with muscle weakness, lactic acidosis, hearing loss and optic atrophy, where two compound heterozygous variants in *USH2A* gene were identified. Usher syndrome type 2, associated with USH2A mutation, is a ciliopathy characterized by sensorineural hearing impairment and retinitis pigmentosa (245). Conflicting reports of pathogenicity exist for both variants here found (p.Ala1953Gly and p.Arg3205His), moreover the clinical phenotype of the patient is more suggestive of a mitochondrial disease and is more complex than classic Usher syndrome. Therefore, this case is not considered fully solved, but the USH2A variants can contribute to final manifestation and assessing their pathogenic relevance demands for functional studies.

4. GUS ON and sON cases

- **4.1. Non-mitochondrial GUS cases**

A total of 5 cases with 4 candidate genes (*NUTF2*, *EPHB2*, *SNF8*, and *WDR45*) are included in GUS category and all do not directly participate in mitochondrial functions.

The single GUS case from ON cohort shows putative AD inheritance and the presentation of optic atrophy with glaucoma has been attributed to a VUS in *NUTF2* gene (p.Ala122Val). This gene encodes the nuclear transport factor 2 (NTF2), that mediates nuclear transport of GTPase Ran involved in translocation of several targets into nucleus (246). No pathogenic variant is published in literature for this gene, but it was prioritized in our analysis since we identified a VUS in the same gene in the DOA pedigree where OPA8 locus was found through linkage analysis (191). The exact way NTF2 defect can lead to DOA is not clear because of the multiple

targets and pathways linked to this protein activity, but in depth functional studies are ongoing to establish the pathogenic mechanism.

Another gene of uncertain significance, *EPHB2*, was identified in sON_17 case presenting with macular dystrophy, thin corpus callosum, and congenital nystagmus and optic atrophy. EPHB2 protein is an ephrin tyrosine kinase receptor involved in axonal guidance during brain development, with a role in excitatory synapse formation and strengthening in particular for commissural axons and RGCs' axons (247). Thus, the observed thin corpus callosum and optic nerve hypoplasia could be explained by this neurodevelopment defect. Particularly interesting is observation in our patient of an important abnormal fear-related behaviour, mainly expressed as a "constant fear of death", that could be indicative of amygdala functions impairment, for which *EPHB2* is a key player in mouse (248,249). After finding of the compound heterozygous missense variants (p.Val427Met and p.Pro796Leu) in sON_17, more cases were gathered from other Institutes with comparable neurological disease. The ongoing experiments on fibroblast cell lines of the patients will address the pathogenic mechanism of neurological phenotype, as well as try to explain why a very different disorder of coagulation is associated with other *EPHB2* variants (221).

Finally, the last two genes (*SNF8* and *WDR45*) of uncertain significance from sON cohort are components of the autophagic machinery, and the optic atrophy phenotype could therefore derive from a secondary mitochondrial defect caused by inefficient autophagy/mitophagy. While for *SNF8* no pathogenic variants are described, *WDR45* is a well-established genetic cause of neurodegeneration with brain iron accumulation (BPAN/NBIA5), but here presenting with milder X-linked recessive phenotype that is still undescribed.

For *SNF8*, sON_18 and sON_19 cases harbour VUS in compound heterozygous state, with a shared missense variant p.Val102Ile i*n trans* with a predicted null allele (p.Asp225TrpfsTer99 and c.423-1G>C, respectively). The phenotype is similar with optic atrophy plus mild cognitive impairment and minor brain anomalies at MRI. We then added our patients to other 3 pedigrees from different research groups, presenting with severe leukoencephalopathy. Since the two Italian patients show a milder phenotype, the common missense p.Val102Ile could have a possible hypomorphic role. The defect in autophagy due to ESCRT-II complex impairment will be assessed in fibroblast cell lines from patients and disease will be modelled in zebrafish. It would be particularly interesting to study mitochondrial function in these models,

since optic nerve degeneration is suggestive of mitochondrial impairment, possibly explained by mitophagy alterations.

Then, a *WDR45* hemizygous novel variant (p.Met56Val) identified in sON_20 is compatible to complex clinical findings of developmental delay, gait ataxia, limb apraxia, and optic atrophy after brain iron accumulation. Also compatible to X-linked disease is the presence of one affected brother and one unaffected sister, as well as inheritance of *WDR45* variant from the mother. Segregation of the variant, however, is still lacking for the siblings of proband. Male *WDR45* patients are usually reported with really severe, often infantile-lethal, phenotype (223). This case can represent a first male patient with milder symptoms, similar to an OA plus, and thus experimental evidence is needed for confirmation of the pathogenic variant.

5. Validation studies of *SDHA* variants

Patient sON_15 was found to carry a novel p.Leu376Pro variants in *SDHA* gene, that is however inherited from the unaffected mother. To gain insight into possible pathogenic mechanism for this variant, functional studies were performed on yeast models and patient's muscle biopsy and fibroblast line. The experiments included also parallel validation of p.Arg451Cys variant found in ON_10, to have comparison with a known dominant pathogenic mutation and possibly explain incomplete penetrance in our pedigree.

- **5.1. Yeast modelling studies**

Yeast strains were produced harbouring *SDHA* equivalent variants in yeast Sdh1: L367P for human L376P and R444C for human R451C. A strong respiration deficient phenotype was observed for R444C mutant, replicating the findings from literature (250). A milder defect on growth, respiration rate and CII activity was only evident at non-permissive temperature of 37 °C for L367P mutant. Moreover, yeast Sdh1 gene is not haploinsufficient, but R444C cause the mutant phenotype even in single allele on a diploid strain, thus acting as dominant negative. This result is further supported by respiration defect also deriving from overexpression of the mutant allele. The milder phenotype of L367P is not seen when present in single copy in the diploid strain, showing a putative recessive behaviour. So, yeast modelling supports the known AD inheritance for p.Arg451Cys variant in ON_10 sample, but not for novel p.Leu376Pro in sON_15.

- **5.2. Studies on skeletal muscle and fibroblasts**

Biochemical activity of respiratory complexes was assayed in skeletal muscle available for sON_15 and his mother. A decreased activity of mitochondrial CI, CIV and especially CII was detected in the proband only. The result was also consistent with Western blot from the same samples, in which a reduction of CII subunits SDHA and SDHB was significant for the proband. Moreover, an increase in CI subunit NDUFB8 and CIV subunit COXII in both proband and the mother may indicate a compensatory mechanism acting on respiratory chain with impaired CII.

Fibroblast cell lines were available for both sON_15 and ON_10 as well as for the unaffected carrier mothers, so Western blot was performed also in this model. The reduction in SDHA and SDHB was again confirmed in sON_15 cells only, but without any other statistically significant variation in protein levels. Noteworthy, the carriers of p.Arg451Cys were both comparable in OXPHOS subunits levels to controls, as already described in literature (179,180). Through native electrophoresis, we then observed impaired CII assembly in sON_15 fibroblasts only and so non-assembled SDH subunits are probably at least in part degraded.

Experiments on patient's tissues thus confirm that p.Arg451Cys is not affecting protein stability nor CII assembly, and defect is exclusively seen in biochemical activity in published cases. The incomplete penetrance of this variant in our case is confirmed by the lack of relevant findings from WES and from Western blot on OXPHOS complexes comparing the proband and the unaffected mother. An exact mechanism for incomplete penetrance remains to be elucidated, and more untargeted analysis like transcriptomics and proteomics could reveal some involved pathways.

For p.Leu376Pro the pathogenic potential was confirmed by yeast modelling, though pointing to a recessive mode of inheritance. Given the striking difference in OXPHOS activity in muscle, as well as CII assembly and subunits abundance in fibroblast, more evidence is building against isolated effect on this variant. The severe phenotypic presentation of sON_15 is also more suggestive of recessive *SDHA* disease, usually overlapping a Leigh syndrome (73). More genetic defects in CII subunits or assembly factors are not evident in WES, also looking at variants not inherited from the mother. Besides, the father is not available for sampling and trio analysis could not be performed. A final molecular diagnosis of this case will require different techniques like WGS or transcriptomics, as p.Leu376Pro could act *in trans* with another mutant allele in *SDHA* that remains to be identified.

6. Validation studies of *UCHL1* variant

A novel variant in *UCHL1* gene (c.586-2A>C) was identified in patient ON_22, with putative dominant effect since it segregates with optic atrophy in 4 family members (Fig. xx). The fibroblast cell line derived from proband's mother was studied to confirm the effect on gene transcript and protein product. *UCHL1* is normally expressed in brain tissue at high levels but is also detectable in cultivated primary fibroblast. Indeed, after cDNA sequencing, we confirmed that the canonical splice site of last exon was lost in the mutant allele with a new splice acceptor site forming in the 3' UTR.

- **6.1. Studies on fibroblasts protein levels**

Western blot assay on protein lysate from fibroblasts revealed a significant decrease in UCH-L1 protein level and no additional band that could originate from aberrant transcript translation. All the main key enzymes for mitochondrial function were then checked to confirm a link between UCHL1 and these frequently altered processes in optic atrophy. While indicators of mitochondrial mass and dynamics were normal, reduced levels of OXPHOS complexes' subunits were detected, especially for CI and CIV. This result can suggest mitochondrial impairment is in fact caused by *UCHL1* mutation but is still unclear through which pathway. Moreover, whole mtDNA the sequencing of the proband's mother did not identify possible deleterious variants that could impact respiratory complexes.

So, some preliminary evidence here presented does not reproduce what has been recently described in *UCHL1*-silenced cells, that is a mitochondrial network morphology alteration after ubiquitinated MFN2 degradation (55). However, the cited work used a tumoral nervous cell line for experiments (neuroblastoma SH-SY5Y) and shRNA silencing, that could not precisely match what fibroblasts from a patient show. The exact primary targets of UCH-L1 are also not completely identified and MFN2 can be just one of many secondarily impaired enzymes driving mitochondrial dysfunction. An omic approach could be very informative to uncover more intracellular processes influenced by UCH-L1 activity and could confirm the recessive or dominant effect of different variants reported.

Conclusions

This study specifically investigated a cohort of isolated and syndromic optic neuropathies through whole exome sequencing analysis. The isolated ON cases (ON, *n*=74) were more abundant than syndromic ON (sON, *n*=32) in the total cohort of 106 patients included in the study.

Total diagnostic rate of 27% is a satisfactory result given that included samples were usually already screened for the most common ON genes (mtDNA, *OPA1*) and some also for target gene panel. An even higher diagnostic yield is expected from WES analysis in HON cohorts never screened for target genes, a preliminary test that in our study had a confounding effect on solved rate calculation. With addition of cases harbouring variants of uncertain significance in disease-genes, or variants only partially matching the clinical phenotype, a positive result was obtained for 42% of cases. The percentage of solved and positive samples is higher in sON cohort, which is expected because it includes more recessive cases than sporadic or dominant ones, usually leading to better results at WES analysis. A better diagnostic rate in a more uniform subset of our cohort is achieved through analysis of WES than of HON genes panel (23% vs 15%), confirming the improvement brought by WES also in the molecular diagnosis pipeline of optic atrophy cases.

Further analysis of WES data will be performed in unsolved cases to evaluate presence of CNVs, while for patients with available muscle biopsy or fibroblast cell line more information can be acquired through RNAseq. RNAseq could identify aberrantly expressed or spliced transcripts deriving from non-coding genetic defects in unsolved WES cases, as well as validate predicted splice defects in both canonical sites and splice regions discovered through WES. WGS can also enhance detection of CNVs and allow analysis of structural variants, especially if obtained through long-reads sequencing technology.

A mitochondria-related gene was found in most solved cases of ON and sON cohorts, but the proportion of non-mitochondrial genes increase in VUS group and genes of GUS samples are all non-mitochondrial. Indeed, GUS category is composed of genes with undefined function or lacking clear pathogenic mechanism for optic atrophy, while many mitochondrial genes are already well characterized.

The most common genes identified in solved ON cases with AD inheritance are *ACO2* and *OPA1*, while *DNAJC30* and *WFS1* are prevalent in AR cases. More mitochondrial genes were found in

ON cases, namely *SDHA* and *SSBP1* with AD variants, and *MECR* and *NDUFV2* with AR variants. A single X-linked case was due to a non-mitochondrial gene, *CACNA1F*.

No recurrent genes were detected in solved sON cases, that have in fact very variable clinical manifestations. Among these, *AFG3L2* with AD inheritance, as well as *C19orf12*, *FDXR*, *MTFMT*, *NDUFAF2*, *PDSS1, and WFS1* with AR inheritance, and the single X-linked *NDUFB11* all cause optic atrophy through mitochondrial impairment. Only cases with AR variants in *LYST* and *SLC52A2* genes are here considered non-mitochondrial.

Genes like *ACO2* for ON, or *WFS1* for both isolated and syndromic ON, are expected as they are already reported in several cases with a great number of pathogenic variants. Other genes are instead rarer in literature and known from just a few families with linked disease, such as *MECR*, *NDUFAF2* and *PDSS1*. Then, a very interesting finding in solved cases involves *DNAJC30*, for which our 3 patients are part of the study that establish it as a recurrent cause of autosomal recessive LHON. Finally, even if DOA cases with *SSBP1* pathogenic variants have only recently been described, the new pedigree here identified suggest this gene could acquire greater relevance in HON diagnosis after inclusion in future gene panels.

For the genes included in VUS (*CACNA1A*, *GFAP*, *KIF1A*, *BTD*, *UCHL1*, *USH2A*) and GUS (*EPHB2*, *NUTF2*, *SNF8*) categories, more research is required to assess the exact pathogenic potential of the identified variants and establish the yet unknown pathogenic mechanism responsible for optic atrophy. Noteworthy, pathogenic variants leading to neurological disease have not already been described for genes *EPHB2*, *NUTF2* and *SNF8*, thus representing a major discovery in this cohort and requiring more extensive functional studies.

Mitochondrial complex I is a hotspot for HON pathogenesis. Indeed, genes encoding subunits or assembly factors of CI are well represented here and, interestingly, two out of four are identified in patients with LHON-like phenotype (*DNAJC30* and *NDUFV2*), while another one in a syndromic case, though definitely milder than reported cases (*NDUFAF2*).

A few of solved and VUS cases in our cohort show an unexpected clinical presentation, such as a milder phenotype compared to severe childhood disease found in literature (*MECR*, *WDR45*), or a late-onset form of disease with an atypical clinical spectrum still poorly described (*BTD*, *GFAP*, *LYST*). This phenotypic heterogeneity is especially challenging for molecular diagnosis, and an untargeted approach like WES is best suited to such pathologies.

This study underlines the importance of introducing into the genetic diagnostic pipeline for rare diseases a step of functional validation for candidate pathogenic variants. The use of an

inexpensive and versatile model organism such as yeast was particularly suitable in our case, also allowing the rapid evaluation of mitochondrial function. Thus, we managed to support the pathogenic role of variants found in *MECR*, also assessing therapeutic effect of lipoic acid supplementation, as well as in *MTFMT* and *SDHA* genes.

For *SDHA*, however, these experiments do not confirm a dominant effect for the novel variant from patient sON_15. Other genetic factors remain to be identified to completely explain the severe reduction in abundance and activity of CII seen in skeletal muscle biopsy and fibroblast cell lines from the proband.

Finally, the expression levels of some key mitochondrial proteins were evaluated in fibroblasts from a carrier of novel *UCHL1* variant discovered, for which we propose for the first time an AD mode of inheritance linked to a mild non-syndromic phenotype of ON. Recent work on cell line models suggests a secondary defect in mitochondrial dynamics after UCH-L1 downregulation. In fibroblasts we do observe possible mitochondrial impairment only from the reduction in subunits of respiratory complexes I and IV. However, we were unable to find evidence for involvement of mitochondrial dynamics machinery. Thus, further research is needed to better characterize the exact pathogenic mechanism in *UCHL1* patients, even considering that this protein could have tissue specific functions, being mostly expressed *in vivo* in neurons.

In conclusion, this thesis provides an overall expansion of the genetic landscape for inherited optic neuropathies, confirming the paramount importance of mitochondrial function for retinal ganglion cell development, functioning and survival. The establishment of a solid understanding of the genetic basis and pathogenic mechanism for inherited optic neuropathies is the prerequisite to elaborate therapeutic strategies, which in some cases already emerged in this study, such as lipoic acid for MECR defects, or biotin supplementation.

References

1. Maresca A, Carelli V. Molecular mechanisms behind inherited neurodegeneration of the optic nerve. Biomolecules. 2021;11(4):1–32.
2. Lenaers G, Neutzner A, Le Dantec Y, Jüschke C, Xiao T, Decembrini S, et al. Dominant optic atrophy: Culprit mitochondria in the optic nerve. Prog Retin Eye Res. 2021 Jul;83:100935.
3. Carelli V, La Morgia C, Valentino ML, Barboni P, Ross-Cisneros FN, Sadun AA. Retinal ganglion cell neurodegeneration in mitochondrial inherited disorders. Biochim Biophys Acta. 2009 May;1787(5):518–28.
4. Carelli V, Ross-Cisneros FN, Sadun AA. Mitochondrial dysfunction as a cause of optic neuropathies. Prog Retin Eye Res. 2004;23:53–89.
5. Wallace DC, Singh G, Lott MT, Hodge JA, Schurr TG, Lezza AM, et al. Mitochondrial DNA mutation associated with Leber's hereditary optic neuropathy. Science (80-). 1988 Dec;242(4884):1427–30.
6. Yu-Wai-Man P, Griffiths PG, Brown DT, Howell N, Turnbull DM, Chinnery PF. The epidemiology of Leber hereditary optic neuropathy in the North East of England. Am J Hum Genet. 2003 Feb;72(2):333–9.
7. Achilli A, Iommarini L, Olivieri A, Pala M, Hooshiar Kashani B, Reynier P, et al. Rare primary mitochondrial DNA mutations and probable synergistic variants in Leber's hereditary optic neuropathy. PLoS One. 2012;7(8):e42242.
8. Caporali L, Iommarini L, La Morgia C, Olivieri A, Achilli A, Maresca A, et al. Peculiar combinations of individually non-pathogenic missense mitochondrial DNA variants cause low penetrance Leber's hereditary optic neuropathy. PLoS Genet. 2018 Feb;14(2):e1007210.
9. Caporali L, Maresca A, Capristo M, Del Dotto V, Tagliavini F, Valentino ML, et al. Incomplete penetrance in mitochondrial optic neuropathies. Mitochondrion. 2017 Sep;36:130–7.
10. Stenton SL, Sheremet NL, Catarino CB, Andreeva NA, Assouline Z, Barboni P, et al. Impaired complex I repair causes recessive Leber's hereditary optic neuropathy. J Clin Invest. 2021 Mar;131(6).
11. Loeffen J, Elpeleg O, Smeitink J, Smeets R, Stöckler-Ipsiroglu S, Mandel H, et al. Mutations in the complex I NDUFS2 gene of patients with cardiomyopathy and encephalomyopathy. Ann Neurol. 2001 Feb;49(2):195–201.
12. Gerber S, Ding MG, Gérard X, Zwicker K, Zanlonghi X, Rio M, et al. Compound heterozygosity for severe and hypomorphic NDUFS2 mutations cause non-syndromic LHON-like optic neuropathy. J Med Genet. 2017 May;54(5):346–56.
13. Zhang L, Joshi AK, Smith S. Cloning, expression, characterization, and interaction of two components of a human mitochondrial fatty acid synthase. Malonyltransferase and acyl carrier protein. J Biol Chem. 2003 Oct;278(41):40067–74.
14. Li H, Yuan S, Minegishi Y, Suga A, Yoshitake K, Sheng X, et al. Novel mutations in malonyl-CoA-acyl carrier protein transacylase provoke autosomal recessive optic neuropathy. Hum Mol Genet. 2020 Feb;29(3):444–58.
15. Gerber S, Orssaud C, Kaplan J, Johansson C, Rozet J-M. MCAT Mutations Cause Nuclear LHON-like Optic Neuropathy. Vol. 12, Genes. 2021.
16. Yu-Wai-Man P, Griffiths PG, Chinnery PF. Mitochondrial optic neuropathies – Disease mechanisms and therapeutic strategies. Prog Retin Eye Res. 2011 Mar 1;30(2):81–114.
17. Kjerl B, Eiberg H, Kjer P, Rosenberg T. Dominant optic atrophy mapped to chromosome 3q region 11. Clinical and epidemiological aspects. Sci Sect Acta Ophthalmol Scand. 1996;74:3–7.
18. Yu-Wai-Man P, Chinnery PF. Dominant optic atrophy: novel OPA1 mutations and revised prevalence estimates. Ophthalmology. 2013 Aug;120(8):1712-1712.e1.
19. Delettre C, Lenaers G, Griffoin JM, Gigarel N, Lorenzo C, Belenguer P, et al. Nuclear gene OPA1, encoding a mitochondrial dynamin-related protein, is mutated in dominant optic atrophy. Nat Genet. 2000 Oct;26(2):207–10.
20. Alexander C, Votruba M, Pesch UE, Thiselton DL, Mayer S, Moore A, et al. OPA1, encoding a dynamin-related GTPase, is mutated in autosomal dominant optic atrophy linked to chromosome 3q28. Nat Genet. 2000 Oct;26(2):211–5.
21. Yu-Wai-Man P, Griffiths PG, Burke A, Sellar PW, Clarke MP, Gnanaraj L, et al. The prevalence and natural history of dominant optic atrophy due to OPA1 mutations. Ophthalmology. 2010 Aug;117(8):1538–46, 1546.e1.
22. Ferré M, Bonneau D, Milea D, Chevrollier A, Verny C, Dollfus H, et al. Molecular screening of 980 cases of suspected hereditary optic neuropathy with a report on 77 novel OPA1 mutations. Hum Mutat. 2009

Jul;30(7):E692-705.
23. Anand R, Wai T, Baker MJ, Kladt N, Schauss AC, Rugarli E, et al. The i-AAA protease YME1L and OMA1 cleave OPA1 to balance mitochondrial fusion and fission. J Cell Biol. 2014;204(6):919–29.
24. Le Roux B, Lenaers G, Zanlonghi X, Amati-Bonneau P, Chabrun F, Foulonneau T, et al. OPA1: 516 unique variants and 831 patients registered in an updated centralized Variome database. Orphanet J Rare Dis. 2019 Sep;14(1):214.
25. Xu X, Wang P, Jia X, Sun W, Li S, Xiao X, et al. Pathogenicity evaluation and the genotype–phenotype analysis of OPA1 variants. Mol Genet Genomics 2021 2964. 2021 Apr;296(4):845–62.
26. Yu-Wai-Man P, Griffiths PG, Gorman GS, Lourenco CM, Wright AF, Auer-Grumbach M, et al. Multi-system neurological disease is common in patients with OPA1 mutations. Brain. 2010 Mar;133(Pt 3):771–86.
27. Del Dotto V, Fogazza M, Musiani F, Maresca A, Aleo SJ, Caporali L, et al. Deciphering OPA1 mutations pathogenicity by combined analysis of human, mouse and yeast cell models. Biochim Biophys Acta - Mol Basis Dis. 2018 Oct 1;1864(10):3496–514.
28. Schaaf CP, Blazo M, Lewis RA, Tonini RE, Takei H, Wang J, et al. Early-onset severe neuromuscular phenotype associated with compound heterozygosity for OPA1 mutations. Mol Genet Metab. 2011 Aug;103(4):383–7.
29. Spiegel R, Pines O, Ta-Shma A, Burak E, Shaag A, Halvardson J, et al. Infantile cerebellar-retinal degeneration associated with a mutation in mitochondrial aconitase, ACO2. Am J Hum Genet. 2012 Mar;90(3):518–23.
30. Nasca A, Rizza T, Doimo M, Legati A, Ciolfi A, Diodato D, et al. Not only dominant, not only optic atrophy: expanding the clinical spectrum associated with OPA1 mutations. Orphanet J Rare Dis. 2017 May;12(1):89.
31. Navaratnarajah T, Anand R, Reichert AS, Distelmaier F. The relevance of mitochondrial morphology for human disease. Int J Biochem Cell Biol. 2021 May;134:105951.
32. Hartmann B, Wai T, Hu H, MacVicar T, Musante L, Fischer-Zirnsak B, et al. Homozygous YME1L1 mutation causes mitochondriopathy with optic atrophy and mitochondrial network fragmentation. Elife. 2016 Aug;5.
33. Patron M, Sprenger H-G, Langer T. m-AAA proteases, mitochondrial calcium homeostasis and neurodegeneration. Cell Res. 2018 Mar;28(3):296–306.
34. Klebe S, Depienne C, Gerber S, Challe G, Anheim M, Charles P, et al. Spastic paraplegia gene 7 in patients with spasticity and/or optic neuropathy. Brain. 2012 Oct;135(Pt 10):2980–93.
35. Charif M, Roubertie A, Salime S, Mamouni S, Goizet C, Hamel CP, et al. A novel mutation of AFG3L2 might cause dominant optic atrophy in patients with mild intellectual disability. Front Genet. 2015;6:311.
36. Charif M, Chevrollier A, Gueguen N, Bris C, Goudenège D, Desquiret-Dumas V, et al. Mutations in the m-AAA proteases AFG3L2 and SPG7 are causing isolated dominant optic atrophy. Neurol Genet. 2020 Jun;6(3):e428.
37. Caporali L, Magri S, Legati A, Del Dotto V, Tagliavini F, Balistreri F, et al. ATPase Domain AFG3L2 Mutations Alter OPA1 Processing and Cause Optic Neuropathy. Ann Neurol. 2020 Jul 1;88(1):18–32.
38. Züchner S, Mersiyanova I V, Muglia M, Bissar-Tadmouri N, Rochelle J, Dadali EL, et al. Mutations in the mitochondrial GTPase mitofusin 2 cause Charcot-Marie-Tooth neuropathy type 2A. Nat Genet. 2004 May;36(5):449–51.
39. Nicholson GA, Magdelaine C, Zhu D, Grew S, Ryan MM, Sturtz F, et al. Severe early-onset axonal neuropathy with homozygous and compound heterozygous MFN2 mutations. Neurology. 2008 May;70(19):1678–81.
40. Züchner S, De Jonghe P, Jordanova A, Claeys KG, Guergueltcheva V, Cherninkova S, et al. Axonal neuropathy with optic atrophy is caused by mutations in mitofusin 2. Ann Neurol. 2006 Feb;59(2):276–81.
41. Pareyson D, Saveri P, Sagnelli A, Piscosquito G. Mitochondrial dynamics and inherited peripheral nerve diseases. Neurosci Lett. 2015 Jun;596:66–77.
42. Bernard-Marissal N, Van Hameren G, Juneja M, Pellegrino C, Louhivuori L, Bartesaghi L, et al. Altered interplay between endoplasmic reticulum and mitochondria in Charcot-Marie-Tooth type 2A neuropathy. Proc Natl Acad Sci U S A. 2019;116(6):2328–37.
43. Friedman JR, Lackner LL, West M, DiBenedetto JR, Nunnari J, Voeltz GK. ER tubules mark sites of mitochondrial division. Science (80-). 2011;334(6054):358–62.
44. Losó n OC, Song Z, Chen H, Chan DC. Fis1, Mff, MiD49, and MiD51 mediate Drp1 recruitment in mitochondrial fission. Mol Biol Cell. 2013;24(5):659–67.
45. Waterham HR, Koster J, van Roermund CWT, Mooyer PAW, Wanders RJA, Leonard J V. A Lethal Defect of Mitochondrial and Peroxisomal Fission. N Engl J Med. 2007;356(17):1736–41.
46. Liu Z, Zhang L, Ren C, Xu M, Li S, Ban R, et al. Whole genome and exome sequencing identify NDUFV2 mutations as a new cause of progressive cavitating leukoencephalopathy. J Med Genet. 2021 Apr;0:1–7.

47. Gerber S, Charif M, Chevrollier A, Chaumette T, Angebault C, Kane MS, et al. Mutations in DNM1L, as in OPA1, result indominant optic atrophy despite opposite effectson mitochondrial fusion and fission. Brain. 2017;140(10):2586–96.
48. Koch J, Feichtinger RG, Freisinger P, Pies M, Schrödl F, Iuso A, et al. Disturbed mitochondrial and peroxisomal dynamics due to loss of MFF causes Leigh-like encephalopathy, optic atrophy and peripheral neuropathy. J Med Genet. 2016;53(4):270–8.
49. Charif M, Wong YC, Kim S, Guichet A, Vignal C, Zanlonghi X, et al. Dominant mutations in MIEF1 affect mitochondrial dynamics and cause a singular late onset optic neuropathy. Mol Neurodegener. 2021;16(1):1–9.
50. Claramunt R, Pedrola L, Sevilla T, López De Munain A, Berciano J, Cuesta A, et al. Genetics of Charcot-Marie-Tooth disease type 4A: Mutations, inheritance, phenotypic variability, and founder effect. J Med Genet. 2005;42(4):358–65.
51. Wu R, Lv H, Wang H, Wang Z, Yuan Y. The Pathological Features of Common Hereditary Mitochondrial Dynamics Neuropathy. Front Neurosci. 2021;15(July):1–7.
52. Rzepnikowska W, Kochański A. A role for the GDAP1 gene in the molecular pathogenesis of Charcot-Marie-Tooth disease. Acta Neurobiol Exp (Wars). 2018;78(1):1–13.
53. Perrone M, Caroccia N, Genovese I, Missiroli S, Modesti L, Pedriali G, et al. The role of mitochondria-associated membranes in cellular homeostasis and diseases. Int Rev Cell Mol Biol. 2020;350:119–96.
54. De Brito OM, Scorrano L. Mitofusin 2 tethers endoplasmic reticulum to mitochondria. Nature. 2008;456(7222):605–10.
55. Cerqueira FM, von Stockum S, Giacomello M, Goliand I, Kakimoto P, Marchesan E, et al. A new target for an old DUB: UCH-L1 regulates mitofusin-2 levels, altering mitochondrial morphology, function and calcium uptake. Redox Biol. 2020 Oct;37:101676.
56. Leroy E, Boyer R, Auburger G, Leube B, Ulm G, Mezey E, et al. The ubiquitin pathway in Parkinson's disease. Vol. 395, Nature. England; 1998. p. 451–2.
57. Lincoln S, Vaughan J, Wood N, Baker M, Adamson J, Gwinn-Hardy K, et al. Low frequency of pathogenic mutations in the ubiquitin carboxy-terminal hydrolase gene in familial Parkinson's disease. Neuroreport. 1999 Feb;10(2):427–9.
58. Saini P, Rudakou U, Yu E, Ruskey JA, Asayesh F, Laurent SB, et al. Association study of DNAJC13, UCHL1, HTRA2, GIGYF2, and EIF4G1 with Parkinson's disease. Neurobiol Aging. 2021 Apr;100:119.e7-119.e13.
59. McMacken G, Lochmüller H, Bansagi B, Pyle A, Lochmüller A, Chinnery PF, et al. Behr syndrome and hypertrophic cardiomyopathy in a family with a novel UCHL1 deletion. J Neurol. 2020 Dec 1;267(12):3643–9.
60. Charif M, Nasca A, Thompson K, Gerber S, Makowski C, Mazaheri N, et al. Neurologic phenotypes associated with mutations in RTN4IP1 (OPA10) in children and young adults. JAMA Neurol. 2018;75(1):105–13.
61. Meunier I, Bocquet B, Charif M, Dhaenens C-M, Manes G, Amati-Bonneau P, et al. A rod-cone dystrophy is systematically associated to the RTN4IP1 recessive optic atrophy. Retina. 2020 Dec;41(8):1771–9.
62. Rajabian F, Manitto MP, Palombo F, Caporali L, Grazioli A, Starace V, et al. Combined Optic Atrophy and Rod-Cone Dystrophy Expands the RTN4IP1 (Optic Atrophy 10) Phenotype. J neuro-ophthalmology Off J North Am Neuro-Ophthalmology Soc. 2020 Oct;
63. Inoue H, Tanizawa Y, Wasson J, Behn P, Kalidas K, Bernal-Mizrachi E, et al. A gene encoding a transmembrane protein is mutated in patients with diabetes mellitus and optic atrophy (Wolfram syndrome). Nat Genet. 1998 Oct;20(2):143–8.
64. Pallotta MT, Tascini G, Crispoldi R, Orabona C, Mondanelli G, Grohmann U, et al. Wolfram syndrome, a rare neurodegenerative disease: from pathogenesis to future treatment perspectives. J Transl Med. 2019 Jul;17(1):238.
65. Eiberg H, Hansen L, Kjer B, Hansen T, Pedersen O, Bille M, et al. Autosomal dominant optic atrophy associated with hearing impairment and impaired glucose regulation caused by a missense mutation in the WFS1 gene. J Med Genet. 2006 May;43(5):435–40.
66. Abu-El-Haija A, McGowan C, Vanderveen D, Bodamer O. Autosomal-dominant WFS1-related disorder—Report of a novel WFS1 variant and review of the phenotypic spectrum of autosomal recessive and dominant forms. Am J Med Genet Part A. 2021;185(2):528–33.
67. Grenier J, Meunier I, Daien V, Baudoin C, Halloy F, Bocquet B, et al. WFS1 in Optic Neuropathies: Mutation Findings in Nonsyndromic Optic Atrophy and Assessment of Clinical Severity. Ophthalmology. 2016 Sep;123(9):1989–98.
68. Delprat B, Maurice T, Delettre C. Wolfram syndrome: MAMs' connection? Cell Death Dis. 2018;9(3).

69. Metodiev MD, Gerber S, Hubert L, Delahodde A, Chretien D, Gérard X, et al. Mutations in the tricarboxylic acid cycle enzyme, aconitase 2, cause either isolated or syndromic optic neuropathy with encephalopathy and cerebellar atrophy. J Med Genet. 2014 Dec;51(12):834–8.
70. Blackburn PR, Schultz MJ, Lahner CA, Li D, Bhoj E, Fisher LJ, et al. Expanding the clinical and phenotypic heterogeneity associated with biallelic variants in ACO2. Ann Clin Transl Neurol. 2020 Jun;7(6):1013–28.
71. Neumann MA-C, Grossmann D, Schimpf-Linzenbold S, Dayan D, Stingl K, Ben-Menachem R, et al. Haploinsufficiency due to a novel ACO2 deletion causes mitochondrial dysfunction in fibroblasts from a patient with dominant optic nerve atrophy. Sci Rep. 2020 Oct;10(1):16736.
72. Charif M, Gueguen N, Ferré M, Elkarhat Z, Khiati S, LeMao M, et al. Dominant ACO2 mutations are a frequent cause of isolated optic atrophy. Brain Commun. 2021;3(2):fcab063.
73. Fullerton M, McFarland R, Taylor RW, Alston CL. The genetic basis of isolated mitochondrial complex II deficiency. Mol Genet Metab. 2020;131(1–2):53–65.
74. Zehavi Y, Saada A, Jabaly-Habib H, Dessau M, Shaag A, Elpeleg O, et al. A novel de novo heterozygous pathogenic variant in the SDHA gene results in childhood onset bilateral optic atrophy and cognitive impairment. Metab Brain Dis. 2021 Apr;36(4):581–8.
75. Rahman S, Thorburn D. Nuclear Gene-Encoded Leigh Syndrome Spectrum Overview. In: Adam MP, Ardinger HH, Pagon RA, Wallace SE, Bean LJH, Mirzaa G, et al., editors. GeneReviews. Seattle (WA); 2015.
76. Pagniez-Mammeri H, Loublier S, Legrand A, Bénit P, Rustin P, Slama A. Mitochondrial complex I deficiency of nuclear origin. I. Structural genes. Mol Genet Metab. 2012;105(2):163–72.
77. Pagniez-Mammeri H, Rak M, Legrand A, Bénit P, Rustin P, Slama A. Mitochondrial complex I deficiency of nuclear origin. II. Non-structural genes. Mol Genet Metab. 2012;105(2):173–9.
78. Formosa LE, Reljic B, Sharpe AJ, Hock DH, Muellner-Wong L, Stroud DA, et al. Optic atrophy-associated TMEM126A is an assembly factor for the ND4-module of mitochondrial complex I. Proc Natl Acad Sci U S A. 2021 Apr;118(17).
79. D'Angelo L, Astro E, De Luise M, Kurelac I, Umesh-Ganesh N, Ding S, et al. NDUFS3 depletion permits complex I maturation and reveals TMEM126A/OPA7 as an assembly factor binding the ND4-module intermediate. Cell Rep. 2021 Apr;35(3):109002.
80. Hanein S, Perrault I, Roche O, Gerber S, Khadom N, Rio M, et al. TMEM126A, encoding a mitochondrial protein, is mutated in autosomal-recessive nonsyndromic optic atrophy. Am J Hum Genet. 2009 Apr;84(4):493–8.
81. Kloth K, Synofzik M, Kernstock C, Schimpf-Linzenbold S, Schuettauf F, Neu A, et al. Novel likely pathogenic variants in TMEM126A identified in non-syndromic autosomal recessive optic atrophy: two case reports. BMC Med Genet. 2019 Apr;20(1):62.
82. La Morgia C, Caporali L, Tagliavini F, Palombo F, Carbonelli M, Liguori R, et al. First TMEM126A missense mutation in an Italian proband with optic atrophy and deafness. Neurol Genet. 2019 Jun;5(3):e329.
83. Collet M, Assouline Z, Bonnet D, Rio M, Iserin F, Sidi D, et al. High incidence and variable clinical outcome of cardiac hypertrophy due to ACAD9 mutations in childhood. Eur J Hum Genet. 2016 Aug;24(8):1112–6.
84. Repp BM, Mastantuono E, Alston CL, Schiff M, Haack TB, Rötig A, et al. Clinical, biochemical and genetic spectrum of 70 patients with ACAD9 deficiency: is riboflavin supplementation effective? Orphanet J Rare Dis. 2018 Jul;13(1):120.
85. Gueguen N, Piarroux J, Sarzi E, Benkirane M, Manes G, Delettre C, et al. Optic neuropathy linked to ACAD9 pathogenic variants: A potentially riboflavin-responsive disorder? Mitochondrion. 2021 Jul;59:169–74.
86. Cook A, Giunti P. Friedreich's ataxia: clinical features, pathogenesis and management. Br Med Bull. 2017 Dec;124(1):19–30.
87. Paul A, Drecourt A, Petit F, Deguine DD, Vasnier C, Oufadem M, et al. FDXR Mutations Cause Sensorial Neuropathies and Expand the Spectrum of Mitochondrial Fe-S-Synthesis Diseases. Am J Hum Genet. 2017 Oct;101(4):630–7.
88. Stenton SL, Piekutowska-Abramczuk D, Kulterer L, Kopajtich R, Claeys KG, Ciara E, et al. Expanding the clinical and genetic spectrum of FDXR deficiency by functional validation of variants of uncertain significance. Hum Mutat. 2021 Mar;42(3):310–9.
89. Wachnowsky C, Fidai I, Cowan JA. Iron-sulfur cluster biosynthesis and trafficking-impact on human disease conditions. Metallomics. 2018;10(1):9–29.
90. Heimer G, Kerätär JM, Riley LG, Balasubramaniam S, Eyal E, Pietikäinen LP, et al. MECR Mutations Cause Childhood-Onset Dystonia and Optic Atrophy, a Mitochondrial Fatty Acid Synthesis Disorder. Am J Hum Genet. 2016 Dec;99(6):1229–44.
91. Gorukmez O, Gorukmez O, Havalı C. Novel MECR Mutation in Childhood-Onset Dystonia, Optic Atrophy, and Basal Ganglia Signal Abnormalities. Neuropediatrics. 2019 Oct;50(5):336–7.

92. Liu Z, Shimura M, Zhang L, Zhang W, Wang J, Ogawa-Tominaga M, et al. Whole exome sequencing identifies a novel homozygous MECR mutation in a Chinese patient with childhood-onset dystonia and basal ganglia abnormalities, without optic atrophy. Mitochondrion. 2021 Mar;57:222–9.
93. Janer A, Prudent J, Paupe V, Fahiminiya S, Majewski J, Sgarioto N, et al. SLC 25A46 is required for mitochondrial lipid homeostasis and cristae maintenance and is responsible for Leigh syndrome. EMBO Mol Med. 2016;8(9):1019–38.
94. Abrams AJ, Fontanesi F, Tan NBL, Buglo E, Campeanu IJ, Rebelo AP, et al. Insights into the genotype-phenotype correlation and molecular function of SLC25A46. Hum Mutat. 2018 Dec;39(12):1995–2007.
95. Wells T, Davies JR, Guschina IA, Ball DJ, Davies JS, Davies VJ, et al. Opa3, a novel regulator of mitochondrial function, controls thermogenesis and abdominal fat mass in a mouse model for Costeff syndrome. Hum Mol Genet. 2012 Nov;21(22):4836–44.
96. Anikster Y, Kleta R, Shaag A, Gahl WA, Elpeleg O. Type III 3-methylglutaconic aciduria (optic atrophy plus syndrome, or Costeff optic atrophy syndrome): identification of the OPA3 gene and its founder mutation in Iraqi Jews. Am J Hum Genet. 2001 Dec;69(6):1218–24.
97. Reynier P, Amati-Bonneau P, Verny C, Olichon A, Simard G, Guichet A, et al. OPA3 gene mutations responsible for autosomal dominant optic atrophy and cataract. J Med Genet. 2004;41(9):1–6.
98. Zeharia A, Friedman JR, Tobar A, Saada A, Konen O, Fellig Y, et al. Mitochondrial hepato-encephalopathy due to deficiency of QIL1/MIC13 (C19orf70), a MICOS complex subunit. Eur J Hum Genet. 2016 Dec;24(12):1778–82.
99. He J, Mao C-C, Reyes A, Sembongi H, Di Re M, Granycome C, et al. The AAA+ protein ATAD3 has displacement loop binding properties and is involved in mitochondrial nucleoid organization. J Cell Biol. 2007 Jan;176(2):141–6.
100. Gilquin B, Taillebourg E, Cherradi N, Hubstenberger A, Gay O, Merle N, et al. The AAA+ ATPase ATAD3A controls mitochondrial dynamics at the interface of the inner and outer membranes. Mol Cell Biol. 2010 Apr;30(8):1984–96.
101. Harel T, Yoon WH, Garone C, Gu S, Coban-Akdemir Z, Eldomery MK, et al. Recurrent De Novo and Biallelic Variation of ATAD3A, Encoding a Mitochondrial Membrane Protein, Results in Distinct Neurological Syndromes. Am J Hum Genet. 2016 Oct;99(4):831–45.
102. Vedrenne V, Gowher A, De Lonlay P, Nitschke P, Serre V, Boddaert N, et al. Mutation in PNPT1, which encodes a polyribonucleotide nucleotidyltransferase, impairs RNA import into mitochondria and causes respiratory-chain deficiency. Am J Hum Genet. 2012 Nov;91(5):912–8.
103. Rius R, Van Bergen NJ, Compton AG, Riley LG, Kava MP, Balasubramaniam S, et al. Clinical Spectrum and Functional Consequences Associated with Bi-Allelic Pathogenic PNPT1 Variants. J Clin Med. 2019 Nov;8(11).
104. Ahola S, Isohanni P, Euro L, Brilhante V, Palotie A, Pihko H, et al. Mitochondrial EFTs defects in juvenile-onset Leigh disease, ataxia, neuropathy, and optic atrophy. Neurology. 2014 Aug;83(8):743–51.
105. Antonicka H, Ostergaard E, Sasarman F, Weraarpachai W, Wibrand F, Pedersen AMB, et al. Mutations in C12orf65 in patients with encephalomyopathy and a mitochondrial translation defect. Am J Hum Genet. 2010 Jul;87(1):115–22.
106. Shimazaki H, Takiyama Y, Ishiura H, Sakai C, Matsushima Y, Hatakeyama H, et al. A homozygous mutation of C12orf65 causes spastic paraplegia with optic atrophy and neuropathy (SPG55). J Med Genet. 2012 Dec;49(12):777–84.
107. Ghezzi D, Baruffini E, Haack TB, Invernizzi F, Melchionda L, Dallabona C, et al. Mutations of the mitochondrial-tRNA modifier MTO1 cause hypertrophic cardiomyopathy and lactic acidosis. Am J Hum Genet. 2012 Jun;90(6):1079–87.
108. O'Byrne JJ, Tarailo-Graovac M, Ghani A, Champion M, Deshpande C, Dursun A, et al. The genotypic and phenotypic spectrum of MTO1 deficiency. Mol Genet Metab. 2018 Jan;123(1):28–42.
109. Tucker EJ, Hershman SG, Köhrer C, Belcher-Timme CA, Patel J, Goldberger OA, et al. Mutations in MTFMT underlie a human disorder of formylation causing impaired mitochondrial translation. Cell Metab. 2011 Sep;14(3):428–34.
110. Hayhurst H, de Coo IFM, Piekutowska-Abramczuk D, Alston CL, Sharma S, Thompson K, et al. Leigh syndrome caused by mutations in MTFMT is associated with a better prognosis. Ann Clin Transl Neurol. 2019 Mar;6(3):515–24.
111. Ramón J, Vila-Julià F, Molina-Granada D, Molina-Berenguer M, Melià MJ, García-Arumí E, et al. Therapy prospects for mitochondrial dna maintenance disorders. Int J Mol Sci. 2021;22(12).
112. Jurkute N, Leu C, Pogoda HM, Arno G, Robson AG, Nürnberg G, et al. SSBP1 mutations in dominant optic atrophy with variable retinal degeneration. Ann Neurol. 2019;86(3):368–83.

113. Del Dotto V, Ullah F, Di Meo I, Magini P, Gusic M, Maresca A, et al. SSBP1 mutations cause mtDNA depletion underlying a complex optic atrophy disorder. J Clin Invest. 2020;130(1):108–25.
114. Piro-Mégy C, Sarzi E, Tarrés-Solé A, Péquignot M, Hensen F, Quilès M, et al. Dominant mutations in mtDNA maintenance gene SSBP1 cause optic atrophy and foveopathy. J Clin Invest. 2020;130(1):143–56.
115. Bosch DGM, Boonstra FN, Gonzaga-Jauregui C, Xu M, de Ligt J, Jhangiani S, et al. NR2F1 mutations cause optic atrophy with intellectual disability. Am J Hum Genet. 2014 Feb;94(2):303–9.
116. Martín-Hernández E, Rodríguez-García ME, Chen C-A, Cotrina-Vinagre FJ, Carnicero-Rodríguez P, Bellusci M, et al. Mitochondrial involvement in a Bosch-Boonstra-Schaaf optic atrophy syndrome patient with a novel de novo NR2F1 gene mutation. J Hum Genet. 2018 Apr;63(4):525–8.
117. Hayflick SJ, Kurian MA, Hogarth P. Neurodegeneration with brain iron accumulation. Handb Clin Neurol. 2018;147:293–305.
118. Wang Z-B, Liu J-Y, Xu X-J, Mao X-Y, Zhang W, Zhou H-H, et al. Neurodegeneration with brain iron accumulation: Insights into the mitochondria dysregulation. Biomed Pharmacother. 2019 Oct;118:109068.
119. Hinarejos I, Machuca-Arellano C, Sancho P, Espinós C. Mitochondrial Dysfunction, Oxidative Stress and Neuroinflammation in Neurodegeneration with Brain Iron Accumulation (NBIA). Antioxidants (Basel, Switzerland). 2020 Oct;9(10).
120. Hedera P. Hereditary Spastic Paraplegia Overview. In: Adam MP, Ardinger HH, Pagon RA, Wallace SE, Bean LJH, Mirzaa G, et al., editors. GeneReviews. Seattle (WA); 2000.
121. de Freitas JL, Rezende Filho FM, Sallum JMF, França MCJ, Pedroso JL, Barsottini OGP. Ophthalmological changes in hereditary spastic paraplegia and other genetic diseases with spastic paraplegia. J Neurol Sci. 2020 Feb;409:116620.
122. Sabaie H, Ahangar NK, Ghafouri-Fard S, Taheri M, Rezazadeh M. Clinical and genetic features of PEHO and PEHO-Like syndromes: A scoping review. Biomed Pharmacother. 2020 Nov;131:110793.
123. Nakamura M, Ito S, Piao C-H, Terasaki H, Miyake Y. Retinal and optic disc atrophy associated with a CACNA1F mutation in a Japanese family. Arch Ophthalmol (Chicago, Ill 1960). 2003 Jul;121(7):1028–33.
124. Leahy KE, Wright T, Grudzinska Pechhacker MK, Audo I, Tumber A, Tavares E, et al. Optic atrophy and inner retinal thinning in CACNA1F-related congenital stationary night blindness. Genes (Basel). 2021;12(3):1–22.
125. Reinson K, Õiglane-Shlik E, Talvik I, Vaher U, Õunapuu A, Ennok M, et al. Biallelic CACNA1A mutations cause early onset epileptic encephalopathy with progressive cerebral, cerebellar, and optic nerve atrophy. Am J Med Genet A. 2016 Aug;170(8):2173–6.
126. Kutkowska-Kaźmierczak A, Rydzanicz M, Chlebowski A, Kłosowska-Kosicka K, Mika A, Gruchota J, et al. Dominant ELOVL1 mutation causes neurological disorder with ichthyotic keratoderma, spasticity, hypomyelination and dysmorphic features. J Med Genet. 2018;55(6):408–14.
127. Manole A, Jaunmuktane Z, Hargreaves I, Ludtmann MHR, Salpietro V, Bello OD, et al. Clinical, pathological and functional characterization of riboflavin-responsive neuropathy. Brain. 2017 Nov;140(11):2820–37.
128. Procter M, Wolf B, Crockett DK, Mao R. The Biotinidase Gene Variants Registry: A Paradigm Public Database. G3 (Bethesda). 2013 Apr;3(4):727–31.
129. Kim H-J, Sohn K-M, Shy ME, Krajewski KM, Hwang M, Park J-H, et al. Mutations in PRPS1, which encodes the phosphoribosyl pyrophosphate synthetase enzyme critical for nucleotide biosynthesis, cause hereditary peripheral neuropathy with hearing loss and optic neuropathy (cmtx5). Am J Hum Genet. 2007 Sep;81(3):552–8.
130. Fenzl CR, Teramoto K, Moshirfar M. Ocular manifestations and management recommendations of lysosomal storage disorders I: Mucopolysaccharidoses. Clin Ophthalmol. 2015;9:1633–44.
131. Jones DE, Klacking E, Ryan RO. Inborn errors of metabolism associated with 3-methylglutaconic aciduria. Clin Chim Acta. 2021 Aug;
132. Fernandez-Marmiesse A, Gouveia S, Couce ML. NGS Technologies as a Turning Point in Rare Disease Research, Diagnosis and Treatment. Curr Med Chem. 2018 Jan;25(3):404–32.
133. Bamshad MJ, Nickerson DA, Chong JX. Mendelian Gene Discovery: Fast and Furious with No End in Sight. Am J Hum Genet. 2019 Sep;105(3):448–55.
134. Li H, Handsaker B, Wysoker A, Fennell T, Ruan J, Homer N, et al. The Sequence Alignment/Map format and SAMtools. Bioinformatics. 2009 Aug;25(16):2078–9.
135. Danecek P, Auton A, Abecasis G, Albers CA, Banks E, DePristo MA, et al. The variant call format and VCFtools. Bioinformatics. 2011 Aug;27(15):2156–8.
136. Poplin R, Ruano-Rubio V, DePristo MA, Fennell TJ, Carneiro MO, Van der Auwera GA, et al. Scaling accurate genetic variant discovery to tens of thousands of samples. bioRxiv. 2017;1–22.
137. Yohe S, Thyagarajan B. Review of Clinical Next-Generation Sequencing. Arch Pathol Lab Med. 2017 Nov;141(11):1544–57.

138. Rehm HL, Bale SJ, Bayrak-Toydemir P, Berg JS, Brown KK, Deignan JL, et al. ACMG clinical laboratory standards for next-generation sequencing. Genet Med. 2013 Sep;15(9):733–47.
139. McInerney-Leo AM, Duncan EL. Massively Parallel Sequencing for Rare Genetic Disorders: Potential and Pitfalls. Front Endocrinol (Lausanne). 2020;11:628946.
140. Stenton SL, Prokisch H. Genetics of mitochondrial diseases: Identifying mutations to help diagnosis. EBioMedicine. 2020 Jun;56:102784.
141. Walter K, Min JL, Huang J, Crooks L, Memari Y, McCarthy S, et al. The UK10K project identifies rare variants in health and disease. Nature. 2015 Oct;526(7571):82–90.
142. Sobreira N, Schiettecatte F, Valle D, Hamosh A. GeneMatcher: a matching tool for connecting investigators with an interest in the same gene. Hum Mutat. 2015 Oct;36(10):928–30.
143. Bamshad MJ, Ng SB, Bigham AW, Tabor HK, Emond MJ, Nickerson DA, et al. Exome sequencing as a tool for Mendelian disease gene discovery. Nat Rev Genet. 2011 Sep;12(11):745–55.
144. Karczewski KJ, Francioli LC, Tiao G, Cummings BB, Alföldi J, Wang Q, et al. The mutational constraint spectrum quantified from variation in 141,456 humans. Nature. 2020 May;581(7809):434–43.
145. Adzhubei IA, Schmidt S, Peshkin L, Ramensky VE, Gerasimova A, Bork P, et al. A method and server for predicting damaging missense mutations. Vol. 7, Nature methods. 2010. p. 248–9.
146. Sim N-L, Kumar P, Hu J, Henikoff S, Schneider G, Ng PC. SIFT web server: predicting effects of amino acid substitutions on proteins. Nucleic Acids Res. 2012 Jul;40(Web Server issue):W452-7.
147. Schwarz JM, Rödelsperger C, Schuelke M, Seelow D. MutationTaster evaluates disease-causing potential of sequence alterations. Vol. 7, Nature methods. United States; 2010. p. 575–6.
148. Kircher M, Witten DM, Jain P, O'Roak BJ, Cooper GM, Shendure J. A general framework for estimating the relative pathogenicity of human genetic variants. Nat Genet. 2014 Mar;46(3):310–5.
149. Ioannidis NM, Rothstein JH, Pejaver V, Middha S, McDonnell SK, Baheti S, et al. REVEL: An Ensemble Method for Predicting the Pathogenicity of Rare Missense Variants. Am J Hum Genet. 2016 Oct;99(4):877–85.
150. Ghosh R, Oak N, Plon SE. Evaluation of in silico algorithms for use with ACMG/AMP clinical variant interpretation guidelines. Genome Biol. 2017 Nov;18(1):225.
151. Li J, Zhao T, Zhang Y, Zhang K, Shi L, Chen Y, et al. Performance evaluation of pathogenicity-computation methods for missense variants. Nucleic Acids Res. 2018 Sep;46(15):7793–804.
152. Amberger JS, Bocchini CA, Scott AF, Hamosh A. OMIM.org: Leveraging knowledge across phenotype-gene relationships. Nucleic Acids Res. 2019;47(D1):D1038–43.
153. Landrum MJ, Lee JM, Riley GR, Jang W, Rubinstein WS, Church DM, et al. ClinVar: public archive of relationships among sequence variation and human phenotype. Nucleic Acids Res. 2014 Jan;42(Database issue):D980-5.
154. Stenson PD, Ball E V, Mort M, Phillips AD, Shiel JA, Thomas NST, et al. Human Gene Mutation Database (HGMD): 2003 update. Hum Mutat. 2003 Jun;21(6):577–81.
155. Richards S, Aziz N, Bale S, Bick D, Das S, Gastier-Foster J, et al. Standards and guidelines for the interpretation of sequence variants: a joint consensus recommendation of the American College of Medical Genetics and Genomics and the Association for Molecular Pathology. Genet Med. 2015 May;17(5):405–24.
156. Kopanos C, Tsiolkas V, Kouris A, Chapple CE, Albarca Aguilera M, Meyer R, et al. VarSome: the human genomic variant search engine. Bioinformatics. 2019 Jun;35(11):1978–80.
157. Miller DT, Lee K, Chung WK, Gordon AS, Herman GE, Klein TE, et al. ACMG SF v3.0 list for reporting of secondary findings in clinical exome and genome sequencing: a policy statement of the American College of Medical Genetics and Genomics (ACMG). Genet Med. 2021 Aug;23(8):1381–90.
158. Köhler S, Gargano M, Matentzoglu N, Carmody LC, Lewis-Smith D, Vasilevsky NA, et al. The Human Phenotype Ontology in 2021. Nucleic Acids Res. 2021 Jan;49(D1):D1207–17.
159. Robinson PN, Köhler S, Oellrich A, Wang K, Mungall CJ, Lewis SE, et al. Improved exome prioritization of disease genes through cross-species phenotype comparison. Genome Res. 2014 Feb;24(2):340–8.
160. Smedley D, Jacobsen JOB, Jäger M, Köhler S, Holtgrewe M, Schubach M, et al. Next-generation diagnostics and disease-gene discovery with the Exomiser. Nat Protoc. 2015 Dec;10(12):2004–15.
161. Hombach D, Schuelke M, Knierim E, Ehmke N, Schwarz JM, Fischer-Zirnsak B, et al. MutationDistiller: user-driven identification of pathogenic DNA variants. Nucleic Acids Res. 2019 Jul;47(W1):W114–20.
162. Zemojtel T, Köhler S, Mackenroth L, Jäger M, Hecht J, Krawitz P, et al. Effective diagnosis of genetic disease by computational phenotype analysis of the disease-associated genome. Sci Transl Med. 2014 Sep;6(252):252ra123.
163. Ji J, Shen L, Bootwalla M, Quindipan C, Tatarinova T, Maglinte DT, et al. A semiautomated whole-exome

sequencing workflow leads to increased diagnostic yield and identification of novel candidate variants. Cold Spring Harb Mol case Stud. 2019 Apr;5(2).
164. Cipriani V, Pontikos N, Arno G, Sergouniotis PI, Lenassi E, Thawong P, et al. An Improved Phenotype-Driven Tool for Rare Mendelian Variant Prioritization: Benchmarking Exomiser on Real Patient Whole-Exome Data. Genes (Basel). 2020 Apr;11(4).
165. Pesch UE, Leo-Kottler B, Mayer S, Jurklies B, Kellner U, Apfelstedt-Sylla E, et al. OPA1 mutations in patients with autosomal dominant optic atrophy and evidence for semi-dominant inheritance. Hum Mol Genet. 2001 Jun;10(13):1359–68.
166. DePristo MA, Banks E, Poplin R, Garimella K V, Maguire JR, Hartl C, et al. A framework for variation discovery and genotyping using next-generation DNA sequencing data. Nat Genet. 2011 May;43(5):491–8.
167. Li H. Aligning sequence reads, clone sequences and assembly contigs with BWA-MEM. 2013;00(00):1–3. Available from: http://arxiv.org/abs/1303.3997
168. Danecek P, Bonfield JK, Liddle J, Marshall J, Ohan V, Pollard MO, et al. Twelve years of SAMtools and BCFtools. Gigascience. 2021 Feb;10(2).
169. Van der Auwera GA, O'Connor BD. Genomics in the Cloud. In: Genomics in the Cloud. O'Reilly Media, Inc.; 2020.
170. Paila U, Chapman BA, Kirchner R, Quinlan AR. GEMINI: integrative exploration of genetic variation and genome annotations. PLoS Comput Biol. 2013;9(7):e1003153.
171. Rath S, Sharma R, Gupta R, Ast T, Chan C, Durham TJ, et al. MitoCarta3.0: an updated mitochondrial proteome now with sub-organelle localization and pathway annotations. Nucleic Acids Res. 2021 Jan;49(D1):D1541–7.
172. Rimmer A, Phan H, Mathieson I, Iqbal Z, Twigg SRF, Wilkie AOM, et al. Integrating mapping-, assembly- and haplotype-based approaches for calling variants in clinical sequencing applications. Nat Genet. 2014 Aug;46(8):912–8.
173. Wang K, Li M, Hakonarson H. ANNOVAR: functional annotation of genetic variants from high-throughput sequencing data. Nucleic Acids Res. 2010 Sep;38(16):e164.
174. Magi A, Tattini L, Palombo F, Benelli M, Gialluisi A, Giusti B, et al. H3M2: detection of runs of homozygosity from whole-exome sequencing data. Bioinformatics. 2014 Oct;30(20):2852–9.
175. Robinson JT, Thorvaldsdóttir H, Winckler W, Guttman M, Lander ES, Getz G, et al. Integrative genomics viewer. Vol. 29, Nature biotechnology. 2011. p. 24–6.
176. Robinson JT, Thorvaldsdóttir H, Wenger AM, Zehir A, Mesirov JP. Variant Review with the Integrative Genomics Viewer. Cancer Res. 2017 Nov;77(21):e31–4.
177. den Dunnen JT, Dalgleish R, Maglott DR, Hart RK, Greenblatt MS, McGowan-Jordan J, et al. HGVS Recommendations for the Description of Sequence Variants: 2016 Update. Hum Mutat. 2016 Jun;37(6):564–9.
178. Schimpf S, Fuhrmann N, Schaich S, Wissinger B. Comprehensive cDNA study and quantitative transcript analysis of mutant OPA1 transcripts containing premature termination codons. Hum Mutat. 2008 Jan;29(1):106–12.
179. Birch-Machin MA, Taylor RW, Cochran B, Ackrell BA, Turnbull DM. Late-onset optic atrophy, ataxia, and myopathy associated with a mutation of a complex II gene. Ann Neurol. 2000 Sep;48(3):330–5.
180. Courage C, Jackson CB, Hahn D, Euro L, Nuoffer J-M, Gallati S, et al. SDHA mutation with dominant transmission results in complex II deficiency with ocular, cardiac, and neurologic involvement. Am J Med Genet A. 2017 Jan;173(1):225–30.
181. La Morgia C, Maresca A, Amore G, Gramegna LL, Carbonelli M, Scimonelli E, et al. Calcium mishandling in absence of primary mitochondrial dysfunction drives cellular pathology in Wolfram Syndrome. Sci Rep. 2020 Mar;10(1):4785.
182. Majander A, Bitner-Glindzicz M, Chan CM, Duncan HJ, Chinnery PF, Subash M, et al. Lamination of the Outer Plexiform Layer in Optic Atrophy Caused by Dominant WFS1 Mutations. Ophthalmology. 2016 Jul;123(7):1624–6.
183. Astuti D, Sabir A, Fulton P, Zatyka M, Williams D, Hardy C, et al. Monogenic diabetes syndromes: Locus-specific databases for Alström, Wolfram, and Thiamine-responsive megaloblastic anemia. Hum Mutat. 2017 Jul;38(7):764–77.
184. Riley LG, Cowley MJ, Gayevskiy V, Minoche AE, Puttick C, Thorburn DR, et al. The diagnostic utility of genome sequencing in a pediatric cohort with suspected mitochondrial disease. Genet Med. 2020 Jul;22(7):1254–61.
185. Zeitz C, Minotti R, Feil S, Mátyás G, Cremers FPM, Hoyng CB, et al. Novel mutations in CACNA1F and NYX in Dutch families with X-linked congenital stationary night blindness. Mol Vis. 2005 Mar;11:179–83.

186. Bijveld MMC, Florijn RJ, Bergen AAB, van den Born LI, Kamermans M, Prick L, et al. Genotype and phenotype of 101 dutch patients with congenital stationary night blindness. Ophthalmology. 2013 Oct;120(10):2072–81.
187. Matuszczak E, Tylicka M, Komarowska MD, Debek W, Hermanowicz A. Ubiquitin carboxy-terminal hydrolase L1 - physiology and pathology. Cell Biochem Funct. 2020 Jul;38(5):533–40.
188. Bilguvar K, Tyagi NK, Ozkara C, Tuysuz B, Bakircioglu M, Choi M, et al. Recessive loss of function of the neuronal ubiquitin hydrolase UCHL1 leads to early-onset progressive neurodegeneration. Proc Natl Acad Sci U S A. 2013;110(9):3489–94.
189. Das Bhowmik A, Patil SJ, Deshpande DV, Bhat V, Dalal A. Novel splice-site variant of UCHL1 in an Indian family with autosomal recessive spastic paraplegia-79. J Hum Genet. 2018 Aug;63(8):927–33.
190. McMacken G, Lochmüller H, Bansagi B, Pyle A, Lochmüller A, Chinnery PF, et al. Behr syndrome and hypertrophic cardiomyopathy in a family with a novel UCHL1 deletion. J Neurol. 2020 Dec;267(12):3643–9.
191. Carelli V, Schimpf S, Fuhrmann N, Valentino ML, Zanna C, Iommarini L, et al. A clinically complex form of dominant optic atrophy (OPA8) maps on chromosome 16. Hum Mol Genet. 2011 May;20(10):1893–905.
192. Panteghini C, Zorzi G, Venco P, Dusi S, Reale C, Brunetti D, et al. C19orf12 and FA2H mutations are rare in Italian patients with neurodegeneration with brain iron accumulation. Semin Pediatr Neurol. 2012 Jun;19(2):75–81.
193. Venco P, Bonora M, Giorgi C, Papaleo E, Iuso A, Prokisch H, et al. Mutations of C19orf12, coding for a transmembrane glycine zipper containing mitochondrial protein, cause mis-localization of the protein, inability to respond to oxidative stress and increased mitochondrial Ca^{2+}. Front Genet. 2015;6:185.
194. Slone J, Peng Y, Chamberlin A, Harris B, Kaylor J, McDonald MT, et al. Biallelic mutations in FDXR cause neurodegeneration associated with inflammation. J Hum Genet. 2018 Dec;63(12):1211–22.
195. Peng Y, Shinde DN, Valencia CA, Mo J-S, Rosenfeld J, Truitt Cho M, et al. Biallelic mutations in the ferredoxin reductase gene cause novel mitochondriopathy with optic atrophy. Hum Mol Genet. 2017 Dec;26(24):4937–50.
196. Toro C, Nicoli E-R, Malicdan MC, Adams DR, Introne WJ. Chediak-Higashi Syndrome. In: Adam MP, Ardinger HH, Pagon RA, Wallace SE, Bean LJH, Mirzaa G, et al., editors. GeneReviews. Seattle (WA); 2009.
197. Weisfeld-Adams JD, Mehta L, Rucker JC, Dembitzer FR, Szporn A, Lublin FD, et al. Atypical Chédiak-Higashi syndrome with attenuated phenotype: three adult siblings homozygous for a novel LYST deletion and with neurodegenerative disease. Orphanet J Rare Dis. 2013 Mar;8:46.
198. Yarnell DS, Roney JC, Teixeira C, Freitas MI, Cipriano A, Leuschner P, et al. Diagnosis of Chediak Higashi disease in a 67-year old woman. Vol. 182, American journal of medical genetics. Part A. United States; 2020. p. 3007–13.
199. Herzer M, Koch J, Prokisch H, Rodenburg R, Rauscher C, Radauer W, et al. Leigh disease with brainstem involvement in complex I deficiency due to assembly factor NDUFAF2 defect. Neuropediatrics. 2010 Feb;41(1):30–4.
200. Nardecchia F, De Giorgi A, Palombo F, Fiorini C, De Negri AM, Carelli V, et al. Missense PDSS1 mutations in CoenzymeQ10 synthesis cause optic atrophy and sensorineural deafness. Ann Clin Transl Neurol. 2021 Jan;8(1):247–51.
201. Mollet J, Giurgea I, Schlemmer D, Dallner G, Chretien D, Delahodde A, et al. Prenyldiphosphate synthase, subunit 1 (PDSS1) and OH-benzoate polyprenyltransferase (COQ2) mutations in ubiquinone deficiency and oxidative phosphorylation disorders. J Clin Invest. 2007 Mar;117(3):765–72.
202. Vasta V, Merritt JL 2nd, Saneto RP, Hahn SH. Next-generation sequencing for mitochondrial diseases: a wide diagnostic spectrum. Pediatr Int. 2012 Oct;54(5):585–601.
203. Retterer K, Juusola J, Cho MT, Vitazka P, Millan F, Gibellini F, et al. Clinical application of whole-exome sequencing across clinical indications. Genet Med. 2016 Jul;18(7):696–704.
204. Ciccolella M, Corti S, Catteruccia M, Petrini S, Tozzi G, Rizza T, et al. Riboflavin transporter 3 involvement in infantile Brown-Vialetto-Van Laere disease: two novel mutations. J Med Genet. 2013 Feb;50(2):104–7.
205. Giuliano F, Bannwarth S, Monnot S, Cano A, Chabrol B, Vialettes B, et al. Wolfram syndrome in French population: characterization of novel mutations and polymorphisms in the WFS1 gene. Hum Mutat. 2005 Jan;25(1):99–100.
206. Hardy C, Khanim F, Torres R, Scott-Brown M, Seller A, Poulton J, et al. Clinical and molecular genetic analysis of 19 Wolfram syndrome kindreds demonstrating a wide spectrum of mutations in WFS1. Am J Hum Genet. 1999 Nov;65(5):1279–90.
207. Domènech E, Gómez-Zaera M, Nunes V. Study of the WFS1 gene and mitochondrial DNA in Spanish Wolfram syndrome families. Clin Genet. 2004 Jun;65(6):463–9.
208. Matsunaga K, Tanabe K, Inoue H, Okuya S, Ohta Y, Akiyama M, et al. Wolfram syndrome in the Japanese

population; molecular analysis of WFS1 gene and characterization of clinical features. PLoS One. 2014;9(9):e106906.
209. Indrieri A, Franco B. Linear skin defects with multiple congenital anomalies (LSDMCA): An unconventional mitochondrial disorder. Genes (Basel). 2021;12(2):1–14.
210. Reinson K, Kovacs-Nagy R, Õiglane-Shlik E, Pajusalu S, Nõukas M, Wintjes LT, et al. Diverse phenotype in patients with complex I deficiency due to mutations in NDUFB11. Eur J Med Genet. 2019 Nov;62(11):103572.
211. Torraco A, Bianchi M, Verrigni D, Gelmetti V, Riley L, Niceta M, et al. A novel mutation in NDUFB11 unveils a new clinical phenotype associated with lactic acidosis and sideroblastic anemia. Clin Genet. 2017 Mar;91(3):441–7.
212. Lichtenstein DA, Crispin AW, Sendamarai AK, Campagna DR, Schmitz-Abe K, Sousa CM, et al. A recurring mutation in the respiratory complex 1 protein NDUFB11 is responsible for a novel form of X-linked sideroblastic anemia. Blood. 2016 Oct;128(15):1913–7.
213. Srivastava S, Waldman A, Naidu S. Alexander Disease. In: Adam MP, Ardinger HH, Pagon RA, Wallace SE, Bean LJH, Stephens K, et al., editors. GeneReviews. Seattle (WA); 2002.
214. Okamoto N, Miya F, Tsunoda T, Yanagihara K, Kato M, Saitoh S, et al. KIF1A mutation in a patient with progressive neurodegeneration. J Hum Genet. 2014 Nov;59(11):639–41.
215. Langlois S, Tarailo-Graovac M, Sayson B, Drögemöller B, Swenerton A, Ross CJ, et al. De novo dominant variants affecting the motor domain of KIF1A are a cause of PEHO syndrome. Eur J Hum Genet. 2016 Jun;24(6):949–53.
216. Pomponio RJ, Reynolds TR, Cole H, Buck GA, Wolf B. Mutational hotspot in the human biotinidase gene causes profound biotinidase deficiency. Nat Genet. 1995 Sep;11(1):96–8.
217. Wolf B. Biotinidase Deficiency. In: Adam MP, Ardinger HH, Pagon RA, Wallace SE, Bean LJH, Mirzaa G, et al., editors. GeneReviews. Seattle (WA); 2016.
218. Clark GR, Crowe P, Muszynska D, O'Prey D, O'Neill J, Alexander S, et al. Development of a diagnostic genetic test for simplex and autosomal recessive retinitis pigmentosa. Ophthalmology. 2010 Nov;117(11):2169-77.e3.
219. McGee TL, Seyedahmadi BJ, Sweeney MO, Dryja TP, Berson EL. Novel mutations in the long isoform of the USH2A gene in patients with Usher syndrome type II or non-syndromic retinitis pigmentosa. J Med Genet. 2010 Jul;47(7):499–506.
220. Vietri M, Radulovic M, Stenmark H. The many functions of ESCRTs. Nat Rev Mol Cell Biol. 2020 Jan;21(1):25–42.
221. Berrou E, Soukaseum C, Favier R, Adam F, Elaib Z, Kauskot A, et al. A mutation of the human EPHB2 gene leads to a major platelet functional defect. Blood. 2018 Nov;132(19):2067–77.
222. Haack TB, Hogarth P, Kruer MC, Gregory A, Wieland T, Schwarzmayr T, et al. Exome sequencing reveals de novo WDR45 mutations causing a phenotypically distinct, X-linked dominant form of NBIA. Am J Hum Genet. 2012 Dec;91(6):1144–9.
223. Cong Y, So V, Tijssen MAJ, Verbeek DS, Reggiori F, Mauthe M. WDR45, one gene associated with multiple neurodevelopmental disorders. Autophagy. 2021 Apr;1–16.
224. Bannon AE, Kent J, Forquer I, Town A, Klug LR, McCann K, et al. Biochemical, Molecular, and Clinical Characterization of Succinate Dehydrogenase Subunit A Variants of Unknown Significance. Clin Cancer Res. 2017 Nov;23(21):6733–43.
225. Charif M, Bris C, Goudenège D, Desquiret-Dumas V, Colin E, Ziegler A, et al. Use of Next-Generation Sequencing for the Molecular Diagnosis of 1,102 Patients With a Autosomal Optic Neuropathy. Front Neurol. 2021;12:602979.
226. Ohtake A, Murayama K, Mori M, Harashima H, Yamazaki T, Tamaru S, et al. Diagnosis and molecular basis of mitochondrial respiratory chain disorders: exome sequencing for disease gene identification. Biochim Biophys Acta. 2014 Apr;1840(4):1355–9.
227. Wortmann SB, Koolen DA, Smeitink JA, van den Heuvel L, Rodenburg RJ. Whole exome sequencing of suspected mitochondrial patients in clinical practice. J Inherit Metab Dis. 2015 May;38(3):437–43.
228. Pronicka E, Piekutowska-Abramczuk D, Ciara E, Trubicka J, Rokicki D, Karkucińska-Więckowska A, et al. New perspective in diagnostics of mitochondrial disorders: two years' experience with whole-exome sequencing at a national paediatric centre. J Transl Med. 2016 Jun;14(1):174.
229. Stenton SL, Kremer LS, Kopajtich R, Ludwig C, Prokisch H. The diagnosis of inborn errors of metabolism by an integrative "multi-omics" approach: A perspective encompassing genomics, transcriptomics, and proteomics. J Inherit Metab Dis. 2020;43(1):25–35.
230. Bénit P, Beugnot R, Chretien D, Giurgea I, De Lonlay-Debeney P, Issartel J-P, et al. Mutant NDUFV2 subunit

of mitochondrial complex I causes early onset hypertrophic cardiomyopathy and encephalopathy. Hum Mutat. 2003 Jun;21(6):582–6.
231. Cameron JM, MacKay N, Feigenbaum A, Tarnopolsky M, Blaser S, Robinson BH, et al. Exome sequencing identifies complex I NDUFV2 mutations as a novel cause of Leigh syndrome. Eur J Paediatr Neurol. 2015 Sep;19(5):525–32.
232. Ogawa E, Shimura M, Fushimi T, Tajika M, Ichimoto K, Matsunaga A, et al. Clinical validity of biochemical and molecular analysis in diagnosing Leigh syndrome: a study of 106 Japanese patients. J Inherit Metab Dis. 2017 Sep;40(5):685–93.
233. McFarland R, Chinnery PF, Blakely EL, Schaefer AM, Morris AAM, Foster SM, et al. Homoplasmy, heteroplasmy, and mitochondrial dystonia. Neurology. 2007 Aug;69(9):911–6.
234. Fruhman G, Landsverk ML, Lotze TE, Hunter J V, Wangler MF, Adesina AM, et al. Atypical presentation of Leigh syndrome associated with a Leber hereditary optic neuropathy primary mitochondrial DNA mutation. Mol Genet Metab. 2011 Jun;103(2):153–60.
235. Chen Y-T, Chen W-L, Chen S-N, Liu C-S. Brain stem lesion in mitochondrial DNA G11778A mutation of Leber's hereditary optic neuropathy. J Formos Med Assoc. 2015 Jul;114(7):668–9.
236. Miyaue N, Yamanishi Y, Tada S, Ando R, Yabe H, Nagai M, et al. Repetitive brainstem lesions in mitochondrial DNA 11778G>A mutation of Leber hereditary optic neuropathy. Vol. 14, eNeurologicalSci. 2019. p. 74–6.
237. Ogilvie I, Kennaway NG, Shoubridge EA. A molecular chaperone for mitochondrial complex I assembly is mutated in a progressive encephalopathy. J Clin Invest. 2005 Oct;115(10):2784–92.
238. Kahlhöfer F, Gansen M, Zickermann V. Accessory Subunits of the Matrix Arm of Mitochondrial Complex I with a Focus on Subunit NDUFS4 and Its Role in Complex I Function and Assembly. Life (Basel, Switzerland). 2021 May;11(5).
239. Barghuti F, Elian K, Gomori JM, Shaag A, Edvardson S, Saada A, et al. The unique neuroradiology of complex I deficiency due to NDUFA12L defect. Mol Genet Metab. 2008 May;94(1):78–82.
240. Haack TB, Gorza M, Danhauser K, Mayr JA, Haberberger B, Wieland T, et al. Phenotypic spectrum of eleven patients and five novel MTFMT mutations identified by exome sequencing and candidate gene screening. Mol Genet Metab. 2014 Mar;111(3):342–52.
241. Arguello T, Köhrer C, RajBhandary UL, Moraes CT. Mitochondrial methionyl N-formylation affects steady-state levels of oxidative phosphorylation complexes and their organization into supercomplexes. J Biol Chem. 2018 Sep;293(39):15021–32.
242. Desai N, Weisfeld-Adams JD, Brodie SE, Cho C, Curcio CA, Lublin F, et al. Optic neuropathy in late-onset neurodegenerative Chédiak-Higashi syndrome. Br J Ophthalmol. 2016 May;100(5):704–7.
243. Stumpf E, Masson H, Duquette A, Berthelet F, McNabb J, Lortie A, et al. Adult Alexander disease with autosomal dominant transmission: a distinct entity caused by mutation in the glial fibrillary acid protein gene. Arch Neurol. 2003 Sep;60(9):1307–12.
244. Caroli F, Biancheri R, Seri M, Rossi A, Pessagno A, Bugiani M, et al. GFAP mutations and polymorphisms in 13 unrelated Italian patients affected by Alexander disease. Clin Genet. 2007 Nov;72(5):427–33.
245. Toualbi L, Toms M, Moosajee M. USH2A-retinopathy: From genetics to therapeutics. Exp Eye Res. 2020 Dec;201:108330.
246. Smith A, Brownawell A, Macara IG. Nuclear import of Ran is mediated by the transport factor NTF2. Curr Biol. 1998 Dec;8(25):1403–6.
247. Liu Z, Thakar A, Santoro SW, Pratt KG. Presenilin Regulates Retinotectal Synapse Formation through EphB2 Receptor Processing. Dev Neurobiol. 2018 Dec;78(12):1171–90.
248. Zhu X-N, Liu X-D, Zhuang H, Henkemeyer M, Yang J-Y, Xu N-J. Amygdala EphB2 Signaling Regulates Glutamatergic Neuron Maturation and Innate Fear. J Neurosci. 2016 Sep;36(39):10151–62.
249. Zhang J-T, Liu Y, Li L-X, Li K, Chen J-G, Wang F. Activation of EphB2 in the basolateral amygdala promotes stress vulnerability of mice by increasing NMDA-dependent synaptic function. Neuropharmacology. 2020 May;167:107934.
250. Bannon AE, Kent J, Forquer I, Town A, Klug LR, McCann K, et al. Biochemical, molecular, and clinical characterization of succinate dehydrogenase subunit A variants of unknown significance. Clin Cancer Res. 2017;23(21):6733–43.
251. Boycott KM, Vanstone MR, Bulman DE, MacKenzie AE. Rare-disease genetics in the era of next-generation sequencing: discovery to translation. Nat Rev Genet. 2013 Oct;14(10):681–91.

Appendix

Table 1. *Complete cohort with WES sequencing workflow used and basic metrics (mean and median depth of coverage, percentage of bases covered at least 10x or 20x).*

Sample	Mean coverage	Median coverage	Bases >10x	Bases >20x	WES target	Sample	Mean coverage	Median coverage	Bases >10x	Bases >20x	WES target
ON_1	199.6	184	99.7	99.5	IDT	**ON_54**	103.7	102	99	98.3	Twist
ON_2	206.9	191	99.9	99.7	IDT	**ON_55**	107.4	105	99	98.3	Twist
ON_3	120.0	105	99.7	98.9	IDT	**ON_56**	101.0	99	98.7	98	Twist
ON_4	163.1	154	99.1	98.8	IDT v2	**ON_57**	173.1	165	98.9	98.7	IDT v2
ON_5	68.6	59	99.1	94.6	IDT	**ON_58**	154.3	146	99.1	98.8	IDT v2
ON_6	123.9	107	99.5	99	IDT	**ON_59**	140.3	133	99.1	98.7	IDT v2
ON_7	118.2	103	99.6	99	IDT	**ON_60**	189.1	179	98.9	98.7	IDT v2
ON_8	106.2	95	99.7	99	IDT	**ON_61**	185.2	176	99.1	98.9	IDT v2
ON_9	126.1	111	99.6	99.1	IDT	**ON_62**	184.1	171	98.8	98.2	IDT v2
ON_10	206.2	190	99.7	99.5	IDT	**ON_63**	138.0	132	99	98.6	IDT v2
ON_11	102.6	93	97.4	94.5	Illumina	**ON_64**	182.0	169	98.8	98.3	IDT v2
ON_12	96.2	86	97	93.5	Illumina	**ON_65**	187.9	176	99.1	98.8	IDT v2
ON_13	96.2	87	97	93.8	Illumina	**ON_66**	188.1	179	99.1	98.9	IDT v2
ON_14	78.8	72	98.2	95.8	Illumina	**ON_67**	165.7	155	99.1	98.7	IDT v2
ON_15	100.7	98	98.9	98.1	Twist	**ON_68**	165.5	154	99.1	98.5	IDT v2
ON_16	63.6	57	92.6	86.3	Illumina	**ON_69**	162.3	154	99.1	98.9	IDT v2
ON_17	151.4	142	99	98.7	IDT v2	**ON_70**	126.7	121	99.1	98.7	IDT v2
ON_18	186.0	177	98.9	98.7	IDT v2	**ON_71**	210.4	196	98.9	98.6	IDT v2
ON_19	58.1	51	96.1	89	Illumina	**ON_72**	206.1	196	99.1	99	IDT v2
ON_20	144.1	138	98.9	98.6	IDT v2	**ON_73**	162.9	155	99.1	98.9	IDT v2
ON_21	131.8	125	98.8	98.4	IDT v2	**ON_74**	138.0	172	99.1	98.7	IDT v2
ON_22	61.1	52	92.1	84.8	Illumina	**sON_1**	173.6	165	99.1	98.9	IDT v2
ON_23	107.3	93	99.5	98.6	IDT	**sON_2**	106.0	93	99.5	98.6	IDT
ON_24	151.0	131	99.5	99.1	IDT	**sON_3**	86.5	76	98.1	95.7	Illumina
ON_25	105.8	97	97.2	94.5	Illumina	**sON_4**	220.2	202	99.7	99.6	IDT
ON_26	86.1	78	96.3	92.3	Illumina	**sON_5**	87.4	79	96.8	92.9	Illumina
ON_27	115.6	102	98.2	96.9	Illumina	**sON_6**	112.1	102	97.2	94.8	Illumina
ON_28	86.6	77	98	95.4	Illumina	**sON_7**	100.8	83	95.6	91	Illumina
ON_29	86.8	78	98.3	95.8	Illumina	**sON_8**	100.7	89	98.4	96.7	Illumina
ON_30	61.9	54	92.4	85.5	Illumina	**sON_9**	80.8	70	99.4	97.1	IDT
ON_31	65.6	56	92.6	86.2	Illumina	**sON_10**	64.1	55	96.8	90.6	Illumina
ON_32	69.2	60	93	87.3	Illumina	**sON_11**	107.6	105	98.8	98.1	Twist
ON_33	67.8	59	93.2	87.4	Illumina	**sON_12**	197.2	181	99.9	99.7	IDT
ON_34	104.4	89	96.3	92.3	Illumina	**sON_13**	105.2	92	99.5	98.7	IDT
ON_35	93.9	78	95.8	90.9	Illumina	**sON_14**	78.6	66	95.4	89.4	Illumina
ON_36	208.4	191	99.8	99.7	IDT	**sON_15**	99.6	87	99.6	98.4	IDT
ON_37	201.4	186	99.7	99.5	IDT	**sON_16**	113.8	93	97.1	93.6	Illumina
ON_38	216.0	198	99.8	99.7	IDT	**sON_17**	66.3	57	92.9	86.5	Illumina
ON_39	205.6	188	99.8	99.7	IDT	**sON_18**	91.1	83	98.3	96.4	Illumina
ON_40	109.9	98	99.7	99	IDT	**sON_19**	123.2	112	96.1	92.4	Illumina
ON_41	102.9	91	99.5	98.7	IDT	**sON_20**	69.1	59	96	89.6	Illumina
ON_42	115.3	100	99.7	98.9	IDT	**sON_21**	115.7	104	98.3	97	Illumina
ON_43	85.6	75	99.3	97.8	IDT	**sON_22**	70.8	61	93.5	87.8	Illumina
ON_44	124.8	108	99.7	99.1	IDT	**sON_23**	65.9	57	92.9	86.7	Illumina
ON_45	134.3	116	99.8	99.2	IDT	**sON_24**	66.9	58	92.7	86.4	Illumina
ON_46	138.4	119	99.6	99.1	IDT	**sON_25**	82.1	71	94.3	89.9	Illumina
ON_47	108.4	92	99.7	98.6	IDT	**sON_26**	97.1	84	99.4	97.7	IDT
ON_48	156.7	138	99.6	99.3	IDT	**sON_27**	116.5	100	99.5	98.8	IDT
ON_49	150.3	132	99.8	99.5	IDT	**sON_28**	113.6	100	99.5	98.9	IDT
ON_50	132.1	116	99.6	99.1	IDT	**sON_29**	108.6	106	98.8	98.1	Twist
ON_51	112.9	110	98.9	98.3	Twist	**sON_30**	159.2	148	99.1	98.8	IDT v2
ON_52	105.3	103	99	98.3	Twist	**sON_31**	164.1	156	98.9	98.6	IDT v2
ON_53	105.6	103	98.8	98.2	Twist	**sON_32**	164.0	156	99.1	98.9	IDT v2

Table 2. *Screened ON cohort with sex, age of onset and sampling, negative previous genetic screening, inheritance of available pedigree, HPO terms for phenotype, gene for solved, VUS and GUS samples, alleles present in DNA and predicted protein products. O, OPA1 gene; L, LHON common mutations; mt, mtDNA whole sequencing; P, NGS panel for target ON genes. HPO:0000648-Optic atrophy is common to all samples and not reported.*

Sample	Sex	Age of onset	Age at sampling	Negative screening	Pedigree inheritance	HPO Term Identifier	HPO Term Name	Gene	Genotype alleles	Protein alleles
ON_1	F	13 y	56 y	O, L	Sporadic	HP:0000646 HP:0001135 HP:0000821 HP:0007906	Amblyopia Chorioretinal dystrophy Hypothyroidism Increased intraocular pressure	*ACO2*	NM_001098.3: c.[2011C>T];[2011=]	NP_001089.1: p.[(Arg671Trp)];[(Arg671=)]
ON_2	M	6 y	9 y	L	Sporadic	HP:0001952	Abnormal glucose tolerance	*ACO2*	NM_001098.3: c.[1761+1G>A];[1761+1=]	NP_001089.1:p.?
ON_3	M	7 y	17 y	O, L	AD	-	-	*ACO2*	NM_001098.3: c.[1438A>G];[1438=]	NP_001089.1: p.[(Asn480Asp)];[(Asn480=)]
ON_4	M	10 y	18 y	O, L	Sporadic	-	-	*ACO2*	NM_001098.3: c.[494T>C];[494=]	NP_001089.1: p.[(Phe165Ser)];[(Phe165=)]
ON_5	M	NA	24 y	L, mt	Sporadic	-	-	*OPA1*	NM_015560.3: c.[2713C>T];[2713=]	NP_056375.2: p.[(Arg905Ter)];[(Arg905=)]
ON_6	F	NA	28 y	O	AD	-	-	*OPA1*	NM_015560.3: c.[893_936dup];[893_936=]	NP_056375.2: p.[(Ile313ValfsTer10)];[(Ile313=)]
ON_7	M	Child	30 y	O, L	AD	-	-	*OPA1*	NM_015560.3: c.[1212+5G>A];[1212+5=]	NP_056375.2: p.[Thr381_Asn404del];[Thr381_Asn404=]
ON_8	M	9 y	9 y	O, L, P	AD	-	-	*OPA1*	NM_015560.3: c.[1212+6T>G];[1212+6=]	NP_056375.2:p.?
ON_9	M	14 y	14 y	O, L, P	Sporadic	HP:0011347	Abnormality of ocular abduction	*SDHA*	NM_004168.4: c.[1351C>T];[1351=]	NP_004159.2: p.[(Arg451Cys)];[(Arg451=)]
ON_10	F	16 y	72 y	O, L	AD	HP:0000822	Hypertension	*SSBP1*	NM_001256512.1: c.[151A>G];[151=]	NP_001243441.1: p.[(Lys51Glu)];[(Lys51=)]
ON_11	M	17 y	17 y	P	Sporadic	HP:0004901	Exercise-induced lactic acidemia	*DNAJC30*	NM_032317.3: c.[152A>G];[152A>G]	NP_115693.2: p.[(Tyr51Cys)];[(Tyr51Cys)]
ON_12	M	16 y	16 y	L, P	Sporadic	HP:0004901 HP:0000739	Exercise-induced lactic acidemia Anxiety	*DNAJC30*	NM_032317.3: c.[152A>G];[152A>G]	NP_115693.2: p.[(Tyr51Cys)];[(Tyr51Cys)]
ON_13	M	15 y	15 y	L, mt	Sporadic	-	-	*DNAJC30*	NM_032317.3: c.[152A>G];[152A>G]	NP_115693.2: p.[(Tyr51Cys)];[(Tyr51Cys)]
ON_14	F	26 y	45 y	P	AR	HP:0000407	Sensorineural hearing impairment	*MECR*	NM_016011.5: c.[772C>T];[772C>T]	NP_057095.4: p.[(Arg258Trp)];[(Arg258Trp)]
ON_15	M	16 y	16 y	L, mt	Sporadic	-	-	*NDUFV2*	NM_021074.5: c.[163T>G];[674G>A]	NP_066552.2: p.[(Phe55Val)];[(Cys225Tyr)]

ON_16	F	33 y	32 y	O, L, P	AR	-	-	*WFS1*	NM_006005.3: c.[2194C>T];[1656_1680dup]	NP_005996.2: p.[(Arg732Cys)];[(Ile561ArgfsTer53)]
ON_17	M	7 y	20 y	-	Sporadic	-	-	*WFS1*	NM_006005.3: c.[2213C>A];[1514_1528del]	NP_005996.2: p.[(Ala738Asp)];[(Cys505_Val509del)]
ON_18	F	43 y	58 y	O, L	Sporadic	HP:0000020 HP:0002076	Urinary incontinence Migraine	*WFS1*	NM_006005.3: c.[1597C>T];[1597C>T]	NP_005996.2: p.[(Pro533Ser)];[(Pro533Ser)]
ON_19	M	4 y	5 y	O, L, mt, P	XL	HP:0007642 HP:0000556	Congenital stationary night blindness Retinal dystrophy	*CACNA1F*	NM_001256789.3: c.[2038C>T];[0]	NP_001243718.1: p.[(Arg680Ter)];[(0)]
ON_20	F	NA	69 y	O, L, mt	Sporadic	-	-	*OPA1* *WFS1*	NM_015560.3: c.[1515A>G];[1515=] NM_006005.3: c.[2302A>C];[2302=]	NP_056375.2: p.[(Lys505=)];[(Lys505=)] NP_005996.2: p.[(Lys768Gln)];[(Lys768=)]
ON_21	F	Birth	2 y	-	Sporadic	HP:0000556 HP:0006934	Retinal dystrophy Congenital nystagmus	*SDHA*	NM_004168.4: c.[1877C>A];[1877=]	NP_004159.2: p.[(Thr626Asn)];[(Thr626?)]
ON_22	M	12 y	14 y	O, P	AD	-	-	*UCHL1*	NM_004181.5: c.[586-2A>C];[586-2=]	NP_004172.2:p.?
ON_23	F	23? y	26 y	O	AD?	-	-	*UCHL1*	NM_004181.5: c.[284T>G];[284=]	NP_004172.2: p.[(Leu95Arg)];[(Leu95=)]
ON_24	F	Child	39 y	O	AD	HP:0000501	Glaucoma	*NUTF2*	NM_005796.3: c.[365C>T];[365=]	NP_005787.1: p.[(Ala122Val)];[(Ala122?)]
ON_25	F	Adult	48 y	O, P	AD	HP:0003124 HP:0002155 HP:0001875	Hypercholesterolemia Hypertriglyceridemia Neutropenia			
ON_26	F	Adult	37 y	L, P	AR?	-	-			
ON_27	F	21 y	24 y	O, L, P	AD	HP:0200026	Ocular pain			
ON_28	M	2 y	5 y	P	Sporadic	-	-			
ON_29	M	11 y	14 y	P	Sporadic	-	-			
ON_30	M	NA y	42 y	P	AD	-	-			
ON_31	F	48 y	54 y	P	Sporadic	HP:0003124	Hypercholesterolemia			
ON_32	F	13 y	14 y	O, L, P	Sporadic	-	-			
ON_33	M	14 y	19 y	O, P	Sporadic	-	-			
ON_34	M	Child	48 y	O, P	AD	-	-			
ON_35	F	47 y	44 y	O, mt, P	AD	HP:0002077 HP:0030880 HP:0030890 HP:0012683 HP:0011003	Migraine with aura Raynaud phenomenon Hyperintensity of cerebral white matter on MRI Pineal cyst Severe Myopia			
ON_36	M	4 y	4 y	O	Sporadic	-	-			

ON_37	F	26 y	26 y	L	Sporadic	HP:0100653 HP:0030890 HP:0002315	Optic neuritis Hyperintensity of cerebral white matter on MRI Headache
ON_38	M	10 y	27 y	O, L	Sporadic	-	-
ON_39	M	19 y	39 y	O, L	AD	-	-
ON_40	M	24 y	24 y	O, L, P	Sporadic	-	-
ON_41	F	4 y	35 y	-	AD	-	-
ON_42	M	Child	52 y	O, L, P	Sporadic	HP:0000646 HP:0000518 HP:0100507	Amblyopia Cataract Folate deficiency
ON_43	F	39 y	48 y	O, L	Sporadic	HP:0000501 HP:0011003	Glaucoma Severe Myopia
ON_44	M	NA	40 y	-	NA	-	-
ON_45	M	10 y	60 y	O	NA	-	-
ON_46	F	14 y	19 y	O	AD?	-	-
ON_47	M	NA	10 y	O	NA	-	-
ON_48	F	11 y	24 y	O	AD	-	-
ON_49	M	12 y	15 y	O, L	AD	-	-
ON_50	F	50 y	62 y	O, L	AD	HP:0001677 HP:0001658 HP:0004936 HP:0003256	Coronary artery disease Myocardial infarction Venous thrombosis Abnormality of the coagulation cascade
ON_51	F	NA	25 y	O	NA	-	-
ON_52	M	NA	54 y	O	NA	-	-
ON_53	F	NA	37 y	L	NA	HP:0002315	Headache
ON_54	M	14 y	14 y	O, L	AD	-	-
ON_55	M	15 y	24 y	O, L	Sporadic	-	-
ON_56	F	27 y	26 y	L	AR	HP:0040087	Abnormality of folate in blood
ON_57	F	45 y	45 y	O, P	Sporadic	-	-
ON_58	M	53 y	54 y	O, L, mt, P	Sporadic	HP:0003124	Hypercholesterolemia
ON_59	M	9 y	33 y	-	XL	-	-
ON_60	F	6 y	13 y	O	AR	-	-
ON_61	M	NA	10 y	L, mt	NA	-	-
ON_62	F	y	54 y	O, L	NA	-	-
ON_63	M	NA	64 y	-	NA	-	-
ON_64	F	NA	5 y	-	NA	HP:0006934	Congenital nystagmus

ON_65	M	Birth	33 y	O	AD	HP:0006934	Congenital nystagmus
ON_66	M	43 y	62 y	O, L	AR	-	-
ON_67	M	41 y	43 y	-	Sporadic	-	-
ON_68	M	NA	23 y	O	NA	-	-
ON_69	M	23 y	41 y	O, L	Sporadic	HP:0000822	Hypertension
ON_70	M	NA	36 y	-	NA	HP:0000822 HP:0007352 HP:0002315	Hypertension Cerebellar calcifications Headache
ON_71	F	36 y	38 y	O, L	Sporadic	HP:0002076	Migraine
ON_72	M	NA	18 y	-	NA	-	-
ON_73	M	46 y	59 y	-	Sporadic	HP:0033748 HP:0011109 HP:0004901 HP:0002315 HP:0003737	Hypoesthesia Chronic sinusitis Exercise-induced lactic acidemia Headache Mitochondrial myopathy
ON_74	M	44 y	48 y	O, L, P	AR	HP:0003688	Cytochrome C oxidase-negative muscle fibers

Table 3. *Screened sON cohort with sex, age of onset and sampling, negative previous genetic screening, inheritance of available pedigree, HPO terms for phenotype, gene for solved, VUS and GUS samples, alleles present in DNA and predicted protein products. O, OPA1 gene; L, LHON common mutations; mt, mtDNA whole sequencing; P, NGS panel for target ON genes. HPO:0000648-Optic atrophy is common to all samples and not reported.*

Sample	Sex	Age of onset	Age at sampling	Negative screening	Pedigree inheritance	HPO Term Identifier	HPO Term Name	Gene	Genotype alleles	Protein alleles
sON_1	M	Child	10 y	O, L	Sporadic	HP:0001249 HP:0002650 HP:0001760 HP:0002174 HP:0002345 HP:0002451 HP:0007256	Intellectual disability Scoliosis Abnormality of the foot Postural tremor Action tremor Limb dystonia Abnormal pyramidal signs	*AFG3L2*	NM_006796.3: c.[1064C>T];[1064=]	NP_006787.2: p.[(Thr355Met)];[(Thr355=)]
sON_2	F	Child	19 y	O, L	NA	HP:0001251 HP:0001256 HP:0001300 HP:0002180 HP:0012675	Ataxia Intellectual disability, mild Parkinsonism Neurodegeneration Iron accumulation in brain	*C19orf12*	NM_001031726.3: c.[172G>A];[172G>A]	NP_001026896.2: p.[(Gly58Ser)];[(Gly58Ser)]
sON_3	M	Child	24 y	P	Sporadic	HP:0002131 HP:0000708 HP:0000407 HP:0011712 HP:0003477 HP:0000639 HP:0007687 HP:0001290 HP:0002460 HP:0001284 HP:0002066 HP:0001761	Episodic ataxia Behavioral abnormality Sensorineural hearing impairment Right bundle branch block Peripheral axonal neuropathy Nystagmus Unilateral ptosis Generalized hypotonia Distal muscle weakness Areflexia Gait ataxia Pes cavus	*FDXR*	NM_024417.5: c.[1A>G];[1102G>A]	NP_077728.3: p.[(Met1?)];[(Asp368Asn)]

sON_4	F	25 y	32 y	-	Sporadic	HP:0001251 HP:0003477 HP:0002360 HP:0001388 HP:0000407 HP:0001171 HP:0003202 HP:0001324 HP:0007256 HP:0001336 HP:0001310	Ataxia Peripheral axonal neuropathy Sleep disturbance Joint laxity Sensorineural hearing impairment Split hand Skeletal muscle atrophy Muscle weakness Abnormal pyramidal signs Myoclonus Dysmetria	*LYST*	NM_000081.4: c.[3296C>A];[3296C>A]	NP_000072.2: p.[(Ser1099Ter)];[(Ser1099Ter)]
sON_5	M	Child	29 y	P	AR	HP:0004901 HP:0002075 HP:0002403 HP:0030891 HP:0003390 HP:0002076 HP:0100507	Exercise-induced lactic acidemia Dysdiadochokinesis Positive Romberg sign Periventricular white matter hyperdensities Sensory axonal neuropathy Migraine Folate deficiency	*MTFMT*	NM_139242.4: c.[518C>T];[518C>T]	NP_640335.2: p.[(Thr173Ile)];[(Thr173Ile)]
sON_6	F	Child	38 y	O, L, P	AR	HP:0008587 HP:0003390 HP:0003128 HP:0002514 HP:0002624 HP:0100502	Mild neurosensory hearing impairment Sensory axonal neuropathy Lactic acidosis Cerebral calcification Venous abnormality Vitamin B deficiency	*NDUFAF2*	NM_174889.5: c.[95A>G];[148del]	NP_777549.1: p.[(Tyr32Cys)];[(Arg50GlufsTer3)]
sON_7	M	9 y	14 y	O, P	AR	HP:0000407 HP:0001256 HP:0001324	Sensorineural hearing impairment Intellectual disability, mild Muscle weakness	*PDSS1*	NM_014317.5: c.[735G>T];[735G>T]	NP_055132.2: p.[(Gln245His)];[(Gln245His)]

sON_8	F	4 y	20 y	O, P	Sporadic	HP:0008587 HP:0003477 HP:0003390 HP:0007002 HP:0001649 HP:0100507 HP:0003710	Mild neurosensory hearing impairment Peripheral axonal neuropathy Sensory axonal neuropathy Motor axonal neuropathy Tachycardia Folate deficiency Exercise-induced muscle cramps	*SLC52A2*	NM_024531.5: c.[1244G>C];[1255G>A]	NP_078807.1: p.[(Gly415Ala)];[(Gly419Ser)]
sON_9	M	26 y	69 y	O	AD	HP:0002120 HP:0001272 HP:0007366 HP:0000819 HP:0000407	Cerebral cortical atrophy Cerebellar atrophy Atrophy/Degeneration affecting the brainstem Diabetes mellitus Sensorineural hearing impairment	*WFS1*	NM_006005.3: c.[2029G>A];[2206G>A]	NP_005996.2: p.[(Ala677Thr)];[(Gly736Ser)]
sON_10	M	Birth	23 y	-	Sporadic	HP:0001889 HP:0100507 HP:0005264	Megaloblastic anemia Folate deficiency Abnormality of the gallbladder	*NDUFB11*	NM_019056.7: c.[276_278del];[0]	NP_061929.2: p.[(Phe93del)];[0]
sON_11	F	NA	45 y	O, L	Sporadic	HP:0001256 HP:0001272 HP:0000508	Intellectual disability, mild Cerebellar atrophy Ptosis	*CACNA1A*	NM_023035.3: c.[5381T>C];[5381T=]	NP_075461.2: p.[(Phe1794Ser)];[(Phe1794=)]
sON_12	M	60 y	72 y	O	AD	HP:0004944 HP:0000726 HP:0001300 HP:0002134 HP:0030891 HP:0002120 HP:0000011 HP:0002360	Cerebral aneurysm Dementia Parkinsonism Abnormality of the basal ganglia Periventricular white matter hyperdensities Cerebral cortical atrophy Neurogenic bladder Sleep disturbance	*GFAP*	NM_002055.5: c.[1068G>C];[1068=]	NP_002046.1: p.[(Lys356Asn)];[(Lys356=)]
sON_13	F	Birth	50 y	O, L	AR/AD	HP:0001258 HP:0000924	Spastic paraplegia Abnormality of the skeletal system	*KIF1A*	NM_001244008.2: c.[3749+7G>A];[3749+7=]	NP_001230937.1:p.?

sON_14	M	3 y	21 y	O, L, P	Sporadic	HP:0001332 HP:0002174 HP:0002134 HP:0001249 HP:0000407 HP:0031931 HP:0000639	Dystonia Postural tremor Abnormality of the basal ganglia Intellectual disability Sensorineural hearing impairment Ocular flutter Nystagmus	*SDHA*	NM_004168.4: c.[1127T>C];[?]	NP_004159.2: p.[(Leu376Pro)];[?]
sON_15	M	17 y	17 y	L, mt	Sporadic	HP:0001251 HP:0001324 HP:0007351	Ataxia Muscle weakness Upper limb postural tremor	*BTD*	NM_001370658.1: c.956C>A(;)98_104delinsTCC	NP_001357587.1: p.Ser319Tyr(;)Cys33PhefsTer36
sON_16	M	2 y	44 y	O	Sporadic	HP:0000486 HP:0000639 HP:0000407 HP:0003690 HP:0003124 HP:0025379 HP:0004901 HP:0006827 HP:0100561	Strabismus Nystagmus Sensorineural hearing impairment Limb muscle weakness Hypercholesterolemia Anti-thyroid peroxidase antibody positivity Exercise-induced lactic acidemia Atrophy of the spinal cord Spinal cord lesion	*USH2A*	NM_206933.4: c.[5858C>G];[9614G>A]	NP_996816.3: p.[(Ala1953Gly)];[(Arg3205His)]
sON_17	M	Birth	46 y	L, P	Sporadic	HP:0006934 HP:0000708 HP:0012433 HP:0000563 HP:0007754 HP:0033725	Congenital nystagmus Behavioral abnormality Abnormal social behavior Keratoconus Macular dystrophy Thin corpus callosum	*EPHB2*	NM_004442.7: c.[1279G>A];[2387C>T]	NP_004433.2: p.[(Val427Met)];[(Pro796Leu)]
sON_18	M	6 y	11 y	P	AR/XL	HP:0001249 HP:0000708 HP:0000609 HP:0025163 HP:0002079	Intellectual disability Behavioral abnormality Optic nerve hypoplasia Abnormality of optic chiasm morphology Hypoplasia of the corpus callosum	*SNF8*	NM_007241.4: c.[304G>A];[673_683delinsTGGA]	NP_009172.2: p.[(Val102Ile)];[(Asp225TrpfsTer99)]

sON_19	M	4 y	10 y	mt, P	Sporadic	HP:0011342 HP:0001272 HP:0003458 HP:0001260 HP:0012043 HP:0020036 HP:0001348	Mild global developmental delay Cerebellar atrophy EMG: myopathic abnormalities Dysarthria Pendular nystagmus Upper limb dysmetria Brisk reflexes	*SNF8*	NM_007241.4: c.[304G>A];[423-1G>C]	NP_009172.2: p.[(Val102Ile)];?
sON_20	M	17 y	17 y	O, L, P	AR/XLR	HP:0011342 HP:0001249 HP:0002079 HP:0000639 HP:0002066 HP:0030217	Mild global developmental delay Intellectual disability Hypoplasia of the corpus callosum Nystagmus Gait ataxia Limb apraxia	*WDR45*	NM_007075.4: c.[166A>G];[0]	NP_009006.2: p.[(Met56Val)];[0]
sON_21	M	3 y	9 y	P	Sporadic	HP:0000750 HP:0001273	Delayed speech and language development Abnormal corpus callosum morphology			
sON_22	M	Birth	6 y	O, L, mt, P	Sporadic	HP:0001263 HP:0001511 HP:0003128 HP:0031481 HP:0001256 HP:0011185 HP:0000609	Global developmental delay Intrauterine growth retardation Lactic acidosis Abnormal mitral valve physiology Intellectual disability, mild EEG with focal epileptiform discharges Optic nerve hypoplasia			
sON_23	F	13 y	50 y	O, P	AD	HP:0002313 HP:0001271 HP:0000407 HP:0002083 HP:0001716	Spastic paraparesis Polyneuropathy Sensorineural hearing impairment Migraine without aura Wolff-Parkinson-White syndrome			

sON_24	F	20 y	54 y	O, L, mt, P	Sporadic	HP:0002099 HP:0009726 HP:0002315 HP:0000822 HP:0001298	Asthma Renal neoplasm Headache Hypertension Encephalopathy
sON_25	F	32 y	55 y	O, P	Sporadic	HP:0003002 HP:0000563 HP:0011505	Breast carcinoma Keratoconus Cystoid macular edema
sON_26	F	26 y	70 y	-	Sporadic	HP:0000407 HP:0003390 HP:0001251 HP:0001272 HP:0002059 HP:0012675 HP:0002313 HP:0001260	Sensorineural hearing impairment Sensory axonal neuropathy Ataxia Cerebellar atrophy Cerebral atrophy Iron accumulation in brain Spastic paraparesis Dysarthria
sON_27	F	8 y	49 y	-	AR	HP:0001250 HP:0002514	Seizures Cerebral calcification
sON_28	F	5 y	16 y	O, L, P	NA	HP:0000609 HP:0001935 HP:0000147 HP:0001510 HP:0000639 HP:0000556 HP:0030799 HP:0025163 HP:0002076	Optic nerve hypoplasia Microcytic anemia Polycystic ovaries Growth delay Nystagmus Retinal dystrophy Scaphocephaly Abnormality of optic chiasm morphology Migraine
sON_29	F	5 y	5 y	O, L	AD?	HP:0001256 HP:0000365	Intellectual disability, mild Hearing impairment

sON_30	M	2 y	19 y	O, P	NA	HP:0007030	Nonprogressive encephalopathy
						HP:0001263	Global developmental delay
						HP:0002313	Spastic paraparesis
						HP:0000639	Nystagmus
						HP:0000722	Obsessive-compulsive behavior
						HP:0007256	Abnormal pyramidal signs
sON_31	F	20 y	65 y	-	AR?	HP:0007325	Generalized dystonia
						HP:0002858	Meningioma
						HP:0000407	Sensorineural hearing impairment
						HP:0000716	Depression
						HP:0000726	Dementia
						HP:0003737	Mitochondrial myopathy
sON_32	M	27 y	33 y	-	Sporadic	HP:0012758	Optic nerve hypoplasia
						HP:0002059	Neurodevelopmental delay
						HP:0000609	Cerebral atrophy
						HP:0002079	Hypoplasia of the corpus callosum
						HP:0001263	Global developmental delay
						HP:0003737	Mitochondrial myopathy